EXPERIMENTAL ACTINIDE ELEMENT PARTITIONING BETWEEN WHITLOCKITE, APATITE, DIOPSIDIC CLINOPYROXENE, AND ANHYDROUS MELT AT ONE BAR AND 20 KILOBARS PRESSURE

Thesis by

Timothy Miller Benjamin

In Partial Fulfillment of the Requirements

for the Degree of

Doctor of Philosophy

California Institute of Technology

Pasadena, California

1980

(Submitted December 3, 1979)

ACKNOWLEDGEMENTS

This work would not have been possible without aid and cooperation from Don Burnett, P. M. Bell, B. O. Mysen, M. G. Seitz, and many students and staff of both the California Institute of Technology and the Carnegie Geophysical Laboratory. Special thanks to I. D. MacGregor for helping me get in and to Lou Ann Cordell for helping me get out. Funding from NASA grant NSG 7202, NSF Energy Fellowship 7610626, and the Geophysical Lab is gratefully acknowledged.

ABSTRACT

Fission and alpha track radiography techniques have been used to measure partition coefficients (D) at trace (ppm) concentration levels for the actinide elements Th, U, and Pu between synthetic diopsidic clinopyroxene, whitlockite (β-$Ca_3(PO_4)_2$), apatite, and coexisting "haplobasaltic" silicate liquid at 1 bar and 20 kilobars pressure at oxygen fugacities from $10^{-8.6}$ to $10^{-0.7}$ bars. Equilibrium (Rayleigh) partitioning at the crystal-liquid interface is assumed and corrections for actinide zoning and relative alpha and fission fragment ranges have been applied to the measured D values. Reproducibility for both actinide and minor element D values is carefully examined as a criterion for crystal-liquid interface equilibrium. The data are mostly compatible with interface equilibrium except at high cooling rates ($\geq$30 deg/hr).

Pu is much more readily incorporated into crystalline phases than is U or Th, under reducing conditions ($fO_2=10^{-8.6}$), because Pu is most likely trivalent whereas U and Th are tetravalent. The effect of changing pressure and liquidus temperature is small where direct comparisons can be made. Definitive valence state assignments cannot be made, but our best estimates of corrected partition coefficients for Pu^{+3}, Pu^{+4}, Th^{+4}, U^{+4}, and U^{+6} are, for whitlockite: 3.6 / 0.58 / 1.2 / 0.5 / 0.002; for chloro-oxy-apatites: -- / -- / 1.22 / 1.69 / --; and for diopsidic clinopyroxene: 0.06 / -- / 0.002 / 0.002 / -- respectively in P-bearing systems.

Strong compositional effects are seen on the addition of P and, to a lesser extent, U. The D_{cpx} for Th and U are a factor of 10, and

D_{cpx} for Pu^{+3} a factor of three higher in P-free systems relative to P-bearing systems. This is interpreted as a result of actinide stabilization in the melt, possibly by complex formation with PO_4^{-3} groups.

Actinide substitution in these phases is most likely into the Ca site as this site is the largest in each phase and the magnitude of the relative D values, between phases, corresponds to the relative range of Ca site sizes. However experiments run with percent concentrations of UO_2 added to the whitlockite-producing compositions suggest that substitution of UO_4^{-4} for PO_4^{-3} is a possibility.

Preliminary results on Sm partitioning at 1 bar pressure and published lanthanide partition coefficients place the partitioning behavior of Pu^{+3} amongst the light rare earth elements with Nd having a factor of two greater D_{whit} than Pu^{+3}. These results support the use of Pu/Nd chronology for meteorites provided chemical fractionation effects, which could result in a 60 m.y. error, are assessed.

These results have application in evaluating actinide-actinide and actinide-lanthanide fractionations in natural materials utilized in addressing problems in geochronology, cosmochronology, and petrogenesis. Additionally, these data define a 'bracketing theorem' for selection of unfractionated materials for use in the aforementioned disciplines. This bracketing theorem, based on the sequence of relative crystal/liquid partition coefficients: $D_{Nd}>D_{Pu}>D_{Th}\geq D_U$, predicts that a sample with unfractionated (relative to solar-system abundances) lanthanide and Th-U abundances will also have a solar-system Pu abundance. Further use of this type of experimentation has clear application to the current problem of radioactive waste disposal.

TABLE OF CONTENTS

I. INTRODUCTION

The discovery of a xenon component in meteorites having a fissiogenic distribution of isotopes, yet unlike the xenon isotopic spectrum of any known spontaneous fission nuclide (Rowe and Kuroda, 1965) suggested the presence of a, now extinct, spontaneously fissioning nuclide at some time prior to the formation of that meteorite, and by inference, prior to the formation of the solar system. This curious and exciting result was given much greater significance by the proof that the fissioning transuranic isotope had decayed *in situ* (Cantalaube *et al.*, 1967; Wasserburg *et al.*, 1969a). The work of Alexander *et al.* (1971) demonstrated, conclusively, that the xenon spectrum was that of spontaneously fissioning ^{244}Pu ($t_{\frac{1}{2}}$ = 82 m.y.). The record provided by the xenon could now be given time significance, both in terms of cosmochronology and geochronology, rather than merely recording a product of an ancient, but unexplained, nucleosynthetic event.

The discovery of *in situ* decaying ^{244}Pu not only added another geologic clock to the well known ^{87}Rb, ^{232}Th, ^{235}U, ^{238}U, ^{40}K, and ^{129}I (Reynolds, 1960) clocks, but also encouraged research into other extinct radionuclides, such as ^{26}Al (Gray and Compston, 1974; Lee and Papanstassiou, 1974; Lee *et al.*, 1976), and motivated searches for general isotopic anomalies.

The enthusiasm generated by the prospect of ^{244}Pu utilization was tempered by the lack of a stable or even longer-lived isotope of Pu for normalization of the observed ^{244}Pu abundances. By default, another element must be chosen for normalization. A reasonable choice would be U, and this was originally used. However, in fact, one of the light lanthanides may be a better choice

(Lugmair and Marti, 1977; Wasserburg et al., 1977; Boynton, 1978). The following sections present some of the current problems that benefit from application of experimentally determined actinide-actinide and actinide-lanthanide fractionation factors.

Areas of Application of Experimental Actinide-Lanthanide Fractionation Factors

A. Meteorite/Lunar Chronology

The ability to determine the age of formation, metamorphism, or, more specifically, the time of 'freezing in' of the elemental and isotopic composition of a particular sample is essential in deciphering the origin, evolution, and relationships of materials of geologic interest. The standard chronometers, Rb-Sr, U-Th-Pb, K-Ar, and Sm-Nd, are based on measurements of the present isotopic abundances which are corrected for non-radiogenic components and then extrapolated back in time, under model assumptions, until all of the radiogenic daughter(s) are accounted for by decay of the radioactive parent nuclide over that time interval. The absolute age errors must increase as the extrapolation is extended back in time.

The formal errors (precision) in ages for meteorites and lunar rocks, have been reduced to 5-50 m.y. for 4600 m.y. age dates (Wetherill, 1975). For many, if not most applications, an error of this magnitude can be tolerated; however, a more precise measurement of relative ages of ancient materials can, in principle, be obtained from a comparison of the normalized abundance of ^{244}Pu in a sample to that of a reference sample. Any difference can, ideally, be ascribed solely to the decay of ^{244}Pu. The short half-life, geologi-

cally, ($t_{\frac{1}{2}}$=82 m.y.) would permit comparatively fine resolution of relative ages.

If ^{244}Pu abundances are normalized to ^{238}U, then the time interval between the sample of interest and the reference object is given by:

$$(1) \qquad t_r = (1/(\lambda_{238}-\lambda_{244}))\ln((N_{244}/N_{238})_s/(N_{244}/N_{238})_r)$$

where t_r is the relative age, λ_{238} and λ_{244} are the decay constants of ^{238}U and ^{244}Pu respectively, $(N_{244}/N_{238})_s$ is the ratio of the number of atoms of ^{244}Pu and ^{238}U in the sample, and $(N_{244}/N_{238})_r$ is the corresponding ratio for the reference object.

If ^{244}Pu is normalized to a stable nuclide then the equation is, using the above definition of terms:

$$(2) \qquad t_r = (-1/\lambda_{244})\ln((N_{244}/N_{stable})_s/(N_{244}/N_{stable})_r)$$

The useful interval for Pu chronometry is 0-600 m.y. starting at 4600 m.y. ago.

The assumptions that are made in the above are: 1) there is no chemical fractionation between Pu and the reference nuclide during the processes that formed both the sample and reference object, and 2) the reservoirs from which the objects of interest were formed (and presumably the entire solar system) were isotopically homogeneous. Unfortunately neither of these assumptions is rigorously true. (The problem of inaccurate Pu abundances due to loss of fissiogenic Xe may be important, but will not be discussed here).

Clear-cut evidence for initial isotopic heterogeneities in refractory elements in early solar system materials now exists, (see, for example, McCulloch and Wasserburg, 1978 a, b; Papanastassiou and Wasserburg, 1978; Lugmair et al., 1978; and references therein). The observed variations are, percentagewise, small (parts in 10^4) and may not invalidate the assumption, for all practical purposes, of uniform initial isotopic abundances, provided that the solar system $^{244}Pu/^{238}U$ is of the order of 10^{-2} (Podosek, 1972; Ganapathy and Grossman, 1976; Drozd et al., 1977; Jones and Burnett, 1979). A similar conclusion can be drawn from reported U isotopic variations (Unruh et al., 1979) although larger U inhomogeneities were observed by Arden (1977). The U isotopic composition measurements require further documentation to confidently assess their precise effect on the geochronological use of ^{244}Pu abundances.

Evidence of large chemical fractionation effects between the actinides has been obtained from meteorites. Wasserburg et al. (1969) measured a relatively high $^{244}Pu/^{238}U$ value of 0.03 in a separate of whitlockite (β-$Ca_3(PO_4)_2$) from the St. Severin chondrite compared to the whole rock St. Severin $^{244}Pu/^{238}U$ value of 0.015 reported by Podosek (1970a, b, 1972). Additionally, Crozaz (1974) obtained a Th/U value of 10 for a St. Severin whitlockite separate, a value clearly distinct and anomalous from the well known, impressively constant, solar-system Th/U value of 3.8 (Morgan and Lovering, 1968; Toksoz and Johnston, 1977). Exploratory experimental work of Seitz et al. (1974) demonstrated large actinide fractionations, expecially for Pu.

Based on semi-theoretical arguments, Boynton (1978) proposed normalization of Pu abundances to the lanthanide Pr. This suggestion

has received empirical support with the measurement of near constant $^{244}Pu/Nd$ values in meteorites (Lugmair and Marti, 1977; Wasserburg et al., 1977). These measurements reveal that the clinopyroxene and whitlockite from Angra dos Reis have the same Pu/Nd value suggesting a chemical coherence between Pu and the light lanthanides, a result with obvious attractiveness for geochronology. Marti et al. (1977) also obtained the same Pu/Nd value for Juvinas (whole rock) and for mellilite from an Allende coarse-grained inclusion.

The concurrence of the Pu/Nd values between different objects and different minerals in a single object does not prove a lack of chemical fractionation although this is a simple and therefore attractive idea. For example, the alternative of a relatively constant ratio of fractionation factors for Pu and Nd must be considered. Thus, the problem, experimentally, shifts from actinide-actinide to actinide-lanthanide fractionation.

Clearly, for ^{244}Pu abundances to be used successfully to calculate precise relative ages, the magnitude and conditions of actinide fractionation must be quantitatively understood for the phases pertinent to meteorites and lunar samples. Because Pu no longer exists in nature at readily measureable levels, the only choice is to follow the lead of Seitz et al. (1974) in applying the techniques of experimental petrology to address and hopefully solve the problem of chemical fractionation of the actinides during geologic processes.

Given a solution to the actinide fractionation problem, the precise relative ages obtained will not only yield temporal relationships between related samples of a particular rock suite, but also may provide insights to and resolution of problems currently encountered with

different radiometric techniques yielding distinct and inconsistent relative ages of ancient objects (Gray et al., 1973; Wetherill, 1975).

As discussed in Gray et al. (1973), the initial $^{87}Sr/^{86}Sr$ condensation time scale represented by the interval from BABI to ALL is 8-15 m.y. and is extended to 80 m.y. when equilibrated chondrites are included. In contrast, the $^{129}I/^{127}I$ time scale, including equilibrated chondrites, is 14 m.y. (Podosek, 1970 a). This "sharp isochronism" does not include the basaltic achondrites which, at least for Petersburg, appear by this chronometer to be 27 m.y. younger (relative to Bjurböle) (Wetherill, 1975). Wetherill (1975) also tabulates $^{244}Pu/^{238}U$ values that if interpreted solely as time, not fractionation, differences yield a spread of 350 m.y. from BABI to ALL (although the Allende inclusion mixture studied by Podosek and Lewis (1972) is very likely chemically enhanced in Pu relative to U). As a further example, the data presented by Huneke et al. (1977) on four basalt clasts from Kapoeta show widely varying ^{39}Ar-^{40}Ar and Rb-Sr ages and inconsistent concentrations of ^{129}Xe and fissiogenic ^{136}Xe. The models that attempt to order this data in terms of retentive sites, thermal metamorphism, and cooling rates can be further constrained by the Pu data provided the geochemical behavior of Pu can be quantified.

B. Cosmochronology

The time dependence of r-process nucleosynthesis is constrained by the relative abundances of the r-process nuclides: $^{244}Pu/^{238}U/^{235}U/^{232}Th/^{129}I/^{127}I$ at the time of solar system isolation (see, for example, Schramm and Wasserburg, 1970). The discovery of ^{26}Al (Lee et al., 1976) and probably ^{107}Pd (Kelly and Wasserburg, 1978)

as in situ decaying nuclides has changed the nucleosynthesis picture. At stake are the questions of whether or not the solar-system originated from the products of continuous nucleosynthesis or whether there were one or more spikes of nucleosynthetic material injected just prior to, or even initiating, the collapse of the proto-stellar nebula, and the question of the time scale between the beginning of nebular collapse (and isolation from further nucleosynthetic reservoirs) and the formation of 'cold' solid objects.

The simplest interpretation seems to be one of assigning the aforementioned radionuclides to two discrete nucleosynthetic periods. The earlier period, to which the Pu,U,Th, and perhaps part of the ^{129}I are assigned, would occur $\gtrsim 10^{7}$ years prior to condensation. Whether or not this period contained a spike in addition to contributions from uniform nucleosynthesis is discussed further below. The recently postulated second period is probably an event (spike) that is responsible for the ^{26}Al, ^{107}Pd, and at least some (possible all) of the ^{129}I (Kelly and Wasserburg, 1978), and occurred within 3×10^{6} years prior to formation of Allende white inclusions.

The necessity of postulating at least two distinct nucleosynthetic periods follows from the relative abundances and half-lives of these nuclides. Briefly, ^{244}Pu ($t_{1/2}$=82 m.y.) has an abundance, relative to ^{238}U, of approximately 0.01 whereas ^{26}Al ($t_{1/2}$=0.72 m.y.) has an abundance, relative to ^{27}Al, of about 5×10^{-5} (see, for example, Esat et al., 1979 and references therein), ^{107}Pd ($t_{1/2}$=6.5 m.y.) relative to ^{110}Pd is about 2×10^{-5} (Kelly and Wasserburg, 1978), and ^{129}I ($t_{1/2}$=17 m.y.) relative to ^{127}I is about 1×10^{-4} (Hohenberg et al., 1967). The short half-lives of ^{26}Al and ^{107}Pd require a nucleosynthetic event

much closer in time to condensation than the 2×10^8 yr. previously calculated from the ^{244}Pu and ^{129}I data (Schramm and Wasserburg, 1970). If the factor of 10^4 to 10^5 dilution for Pd or I, as discussed by Kelly and Wasserburg (1978), applies to Pu and U, this excludes reconciliation of the $^{244}Pu/^{238}U$ abundance ratio with this shortened (3×10^6 yr.) free decay time scale because this would require that the $^{244}Pu/^{238}U$ r-process production ratio be more than an order of magnitude greater than the production ratio calculated by Seeger and Schramm (1970) who demonstrated the constancy of the actinide production ratios over a wide range of nucleosynthesis conditions. The ^{129}I can be correlated with either, or both, periods as discussed by Kelly and Wasserburg (1978).

The question of heterogeneities in the initial isotopic compositions must also be considered. Large U heterogeneities were reported by Arden (1977) (>300% enrichments in $^{235}U/^{238}U$ for acid treated residues). Effects of this magnitude were not substantiated by Chen and Tilton (1979) or Unruh et al. (1979), although $^{235}U/^{238}U$ enrichments of up to 1% cannot be excluded. These enrichments could invalidate the assumption of an overall uniform set of $^{244}Pu/^{238}U/^{235}U/^{232}Th$ abundances for the solar system. The observed 'unknown nuclear' isotopic anomalies in Sm, Nd, Ba, Sr, and Ca (McCulloch and Wasserburg, 1978a,b; Lee et al., 1977; Lee et al., 1978; Papanastassiou and Wasserburg, 1978) and, probably, in $^{26}Al/^{27}Al$ (Esat et al., 1979) for a special Allende white inclusion, may suggest that the distribution of nucleosynthetic products from the most recent event is quite 'granular'. This 'granularity' may seriously complicate the interpretations of these short lived, low

abundance radionuclides. However, the large body of data indicating uniform isotopic compositions for most solar system materials suggests that any granularity from any older period of nucleosynthesis has been mixed away, and to the extent that the great bulk of the solar system actinides refer to that older period also, it is still reasonable to assume uniform solar system actinide abundances.

The work done in this study has no bearing on the second, more recent, nucleosynthetic event; only on the time scale of the first, earlier period. Unlike the chronological application of ^{244}Pu discussed in the previous section, the choice of the nuclide used to normalize ^{244}Pu abundances for cosmochronological applications is limited to the actinides. This is a result of the necessity of calculating theoretical nucleosynthetic production ratios. The actinide production ratios follow directly from the decay scheme in the actinide region and are very insensitive to variations in nucleosynthesis conditions (Seeger and Schramm, 1970). Normalization of ^{244}Pu to one of the lanthanides is very imprecise because the actinide-lanthanide production ratios are not correlated as are the actinide-actinide production ratios.

Although ^{232}Th is the most favorable nuclide for normalization of ^{244}Pu abundances because of the long ^{232}Th half-life (as pointed out in Schramm and Wasserburg, 1970), ^{238}U will be used for this discussion as virtually all published measurements are of the form $^{244}Pu/^{238}U$.

Calculations on the time scale of galactic nucleosynthesis (Hohenberg, 1969; Wasserburg et al., 1969b; Fowler, 1971) require a late stage injection of r-process elements immediately prior to the formation of the solar-system if the solar-system $^{244}Pu/^{238}U$ value is

as high as 0.03, the value measured for a St. Severin whitlockite (Wasserburg et al., 1969a). Certainly the value $^{244}Pu/^{238}U=0.087$ (Podosek and Lewis, 1972) for a mixture of Allende Ca-rich inclusions would require an r-process spike. The whole rock St. Severin ratio of 0.015 (Podosek, 1972) leaves the question unresolved (Fowler, 1977). Based on the hypothesis of no Pu/Nd fractionation, Marti et al. (1977) propose that a solar system $^{244}Pu/^{238}U$ value of 0.004 be adopted where this ratio is calculated as the product of the measured Angra dos Reis Pu/Nd value and a chondritic Nd/U value. The relationship between this result and the $^{244}Pu/^{238}U$ value (0.015) of Podosek (1972) for St. Severin is unclear. Assuming analytical uncertainties are negligible (see Jones and Burnett, 1979 for a discussion of possible complications in the interpretation of the Podosek data), this difference must be due to either Pu/Nd fractionation or time differences making the Angra dos Reis Pu/Nd lower than St. Severin. The data in this thesis are relevant to this question and whether or not the magnitudes of chemical fractionation are large enough to obviate the late stage r-process injection.

C. Petrogenesis

Although there is an impressive constancy of Th/U=3.8 for meteorites, lunar, and terrestrial materials (Morgan and Lovering, 1968; Toksoz and Johnston, 1977), many samples show deviations from this ratio (Mattinson et al., 1977; Laul and Fruchter, 1976; Tatsumoto, 1978). It may be that Th/U fractionation is a signature of only a few specific types of differentiation processes, making Th/U ratios different from 3.8 uniquely interpretable.

Experimental determination of actinide fractionations under various, controlled, conditions of temperature, pressure, fO_2, and composition are essential in defining and constraining the petrogenetic models of melting and crystallization in exactly the manner of the well known and studied lanthanides.

An example of the application of this type of data and the significance of the phases, phosphates and clinopyroxene, chosen for this experimental study is given by Beswick and Carmichael (1978). As discussed by these authors, the magnitudes of the partition coefficients are critical in producing models that quantitatively explain both the major and minor element abundances in natural rocks and in quantitatively predicting the range of variation in a rock suite. The variables of pressure, temperature, and composition (especially P_2O_5 content) are referred to, although the effect of fO_2 and valence states of the multivalent ions are not considered. One limitation of the Beswick-Carmichael approach is the use of crystal-liquid partition coefficients, from natural samples. These may be too high due to assuming bulk equilibrium when a Rayleigh type equilibrium may be closer to the truth. The experimental determinations in this study demonstrate the significant effect these variables can have on petrogenetic models.

D. Radioactive Waste Disposal

The problems with disposal of radioactive wastes produced from research and commercial reactors are real and demand urgent attention until progress on energy alternatives relegates nuclear power to specific scientific applications. The problems with current disposal programs have been clearly presented by Ringwood (1978) along with his

proposal for a safer waste material storage, Synroc. The use of natural analogues for synthetically concentrating and permanently trapping radioactive wastes can be enhanced with knowledge of the chemical fractionation of radioisotopes, of which the actinides are the longest-lived subset and therefore determine the required time scale for stable storage conditions. Not only can the most efficient conditions of incorporation (P, T, fO_2, cooling rate) of radioisotopes in minerals be experimentally determined, but the mechanisms and most suitable concentration ranges can also be explored. This may be the most important application of experimental work on the partitioning of radioisotopes in minerals.

Research Scope

Because ^{244}Pu no longer exists in nature and, because ^{244}Pu abundances in meteorites and lunar rocks depend on time as well as chemistry, an understanding of the geochemistry of Pu must depend on laboratory studies more than the other actinides and lanthanides of interest. This research initiates experimental investigation of actinide-actinide fractionations via
determination of crystal-liuqid equilibrium partition coefficients. The overall experimental objectives are: 1) to determine the conditions under which the actinides fractionate and the magnitude of the fractionation; 2) to understand the significance of the constancy of Th/U=3.8 to Pu/U fractionation; and 3) to estimate the magnitude of actinide/lanthanide fractionation.

The techniques of trace element radiography (Fleischer et al., 1975), conventional electron microprobe minor and major element

analysis, and experimental petrology have been combined to yield *in situ* equilibrium partition coefficients for the elements Pu-U-Th between the phases whitlockite, chloro-oxy apatites, and diopsidic clinopyroxene and silicate melts with variable phosphorous content. Pressure, cooling rate, and fO_2 have been varied from 1 atmosphere to 20 kilobars, 1.7 to 71 degrees C/hour, and $10^{-8.6}$ to $10^{-0.7}$ atmospheres, respectively.

Trace element radiography is ideally suited, or nearly so, to determining partition coefficients, experimentally, because a crystal can be examined *in situ*, the radioisotopic concentrations can be held at natural (ppm) levels, higher concentrations can be investigated with the addition of non-radioactive ('cold') isotopes of the trace element with microprobe and track analyses as an internal check, the trace element is not depleted nor is the sample destroyed during analysis, and several different elements may be incorporated into a single experiment yet analyzed separately (provided isotopes with differing decay characteristics are used). The sole drawbacks are the problems of safe handling of radioisotopes, the lower limit to crystal size that can be analyzed due to the finite range of the particles detected by this technique (10-15 microns in silicates) the relatively long time (5 days) to produce and analyze a sample, and the limited number of useful isotopes.

The choice of elements has been discussed in the preceeding sections and the choice of phases being constrained, for this initial study, to the phases observed to be the primary reservoirs or sources of concentration of the actinides and lanthanides in meteorites and lunar rocks, with Pu as the focus. These phases all have Ca as a

major element in their stoichiometric structures. A priori, the actinides are assumed to substitute for Ca as do the lanthanides in phosphates. Thus there are Ca sites in each phase which differ in size and coordination that should result in a systematic correspondence of the partition coefficients for each phase (Matsui et al., 1977).

The variations in pressure, cooling rate, fO_2, and composition yield data that permit discussion of some of the possible parameters that could affect the absolute and relative magnitudes of the experimentally determined partition coefficients and therefore constrain the application of these data to real world environments and processes.

II. EXPERIMENTAL DESCRIPTION

Synthesis

A. Starting Materials

The compositions used, for the most part, are historically related to the compositions initially used by Seitz *et al.* (1974); in fact, three of the Pu-spiked starting materials used were acquired from M. G. Seitz. Due to the exploratory nature of that early study, a simple base composition was chosen. This 'haplobasalt', composed of diopside-albite-anorthite (Figure 1), was combined with $Ca_3(PO_4)_2$ to form two starting materials, one with whitlockite (10) on the liquidus (at 20 kilobars pressure) and the second with clinopyroxene (12) on the liquidus. The remaining starting materials were prepared as described in Appendix I. (See Appendix III-4 for actual compositions).

Although clinopyroxene is the liquidus phase from the phosphorous free 'haplobasaltic' composition, Seitz wished to synthesize clinopyroxenes from a liquid close to the composition from which the whitlockite was grown to minimize the effects of differing bulk composition; consequently 15 wt. % $Ca_3(PO_4)_2$ was added to make the 12 composition. A 3rd composition with apatite on the liquidus (11) was also prepared.

Under the actual 20 kilobar run conditions the whitlockite composition had clinopyroxene present as a nearly co-liquidus phase (as did the apatite composition) and chloroapatite was frequently present in small quantities due to Cl contamination; a problem specifically discussed in Appendix I. The chloroapatite appears to crystallize until nearly all the contaminant Cl is removed from the melt whereupon whitlockite begins to crystallize.

FIGURE 1

Pseudoternary liquidus surface phase diagram, with isotherms, determined by Bowen (1915). This diagram shows the 'haplobasalt' used in this study. The plotted point (X) marks the actual composition used prior to the addition of the phosphates, and thus is also the projection, from $Ca_3(PO_4)_2$ of the pseudoquaternary system enclosing the starting material bulk compositions.

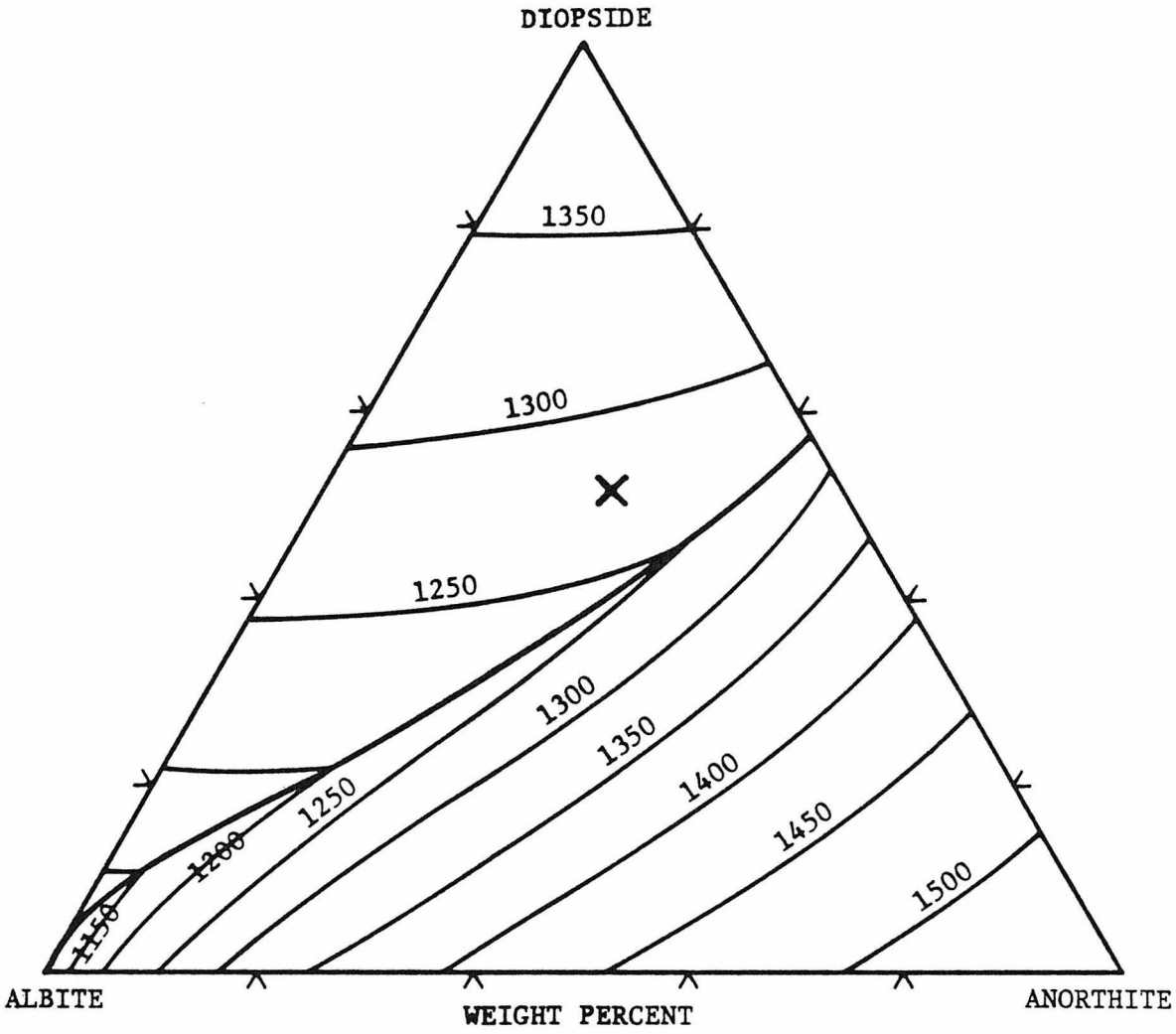

COMPOSITION AT ×

	Atomic %	Weight %
Di	53.7	48.1
Ab	21.6	23.4
An	24.7	28.5

At 1 bar, whitlockite is the liquidus phase for both the 25 and 15 weight percent $Ca_3(PO_4)_2$ starting materials; clinopyroxene does not appear. At this pressure, a trial composition with 10 weight percent $Ca_3(PO_4)_2$ crystallized equal amounts of whitlockite and clinopyroxene as well as abundant plagioclase.

B. Radioisotope Spiking

All ^{239}Pu spiked starting materials (Appendix I) were prepared with a feldspar glass that contained 20 ppm ^{239}Pu so that the final ^{239}Pu concentrations are 7.4 ppm for the 25 weight percent phosphate compositions (10, 11, 15) and 8.4 ppm for the 15 weight percent phosphate composition (12, 14). All 3 original (10,11,12) preparations were also spiked with approximately 200 ppm of 'cold' ^{232}Th so that, if necessary, both Pu and Th could be analyzed on the same sample. To date, no ^{232}Th data have been acquired from these samples.

Chloride solutions of ^{235}U and ^{230}Th were used for spiking the other starting materials used in this study (Appendix I). Final concentrations of approximately 20 ppm ^{235}U and 50 ppm ^{230}Th were used in these materials.

A third isotope, ^{151}Sm, was also added to the later U+Th spiked materials at a concentration of 2 ppm. This turned out to be too little, resulting in imprecise Sm partition coefficients due to large background corrections. More recent preparations (14, 15) containing 10 ppm ^{151}Sm, in addition to ^{239}Pu, produced the runs yielding the Sm data discussed in later sections.

Because of Cl contamination problems in some of the starting materials, Cl removal steps have been added to the preparation proce-

dures. Several methods have been attempted, but as given in Appendix I, the best method appears to be simple melting in an open crucible to outgas the Cl. A drawback to this is the possibility of Na and, more importantly, P loss. Switching to nitrate solutions of the radioisotopes seems to be an alternative worth pursuing in the future.

All spiking, crushing, fusion, and capsule loading steps require strict isolation of Pu from U+Th. ^{235}U and ^{230}Th can be detected separately by alpha particle tracks (^{230}Th) and by thermal neutron induced fission tracks (^{235}U). Cross contamination with Pu has a much greater effect on U+Th analyses than the converse, as Pu partition coefficients are much larger than analogous U or Th partition coefficients. This contamination with Pu would be difficult to detect via track counting techniques as ^{239}Pu is both an alpha emitter (as is ^{230}Th) and is thermal neutron fissionable (as is ^{235}U). The prerequisite separation of Pu from U+Th (and all radioisotopes separated from the experimenter) was achieved by using separate glove boxes, tools, crucibles etc. for the spiked materials. The beta emitting isotope, ^{151}Sm is less of a problem in terms of contaminating the actinide results.

C. 1 Bar Synthesis

The annealed sample capsule (Appendix I) is loaded in a glove box with about 10 mg of crushed glass starting material. The capsule is then squeezed near the middle making a wasp waist (Figure 2A) forming a ledge on which the prepackaged and dried buffer materials are placed. To insure dryness the capsule is crimped nearly shut and placed in a drying oven (T=130+ °C) for at least 12 hours. Just prior to placing the Pt capsule onto the thin wire suspension assembly, the

FIGURE 2

Schematic diagram of the experimental charge configuration in Pt capsules. The solid fO_2 buffer mixtures of Co-CoO, Ni-NiO, Fe-FeO, or Fe_2O_3-Fe_3O_4 are wrapped in a separate Pt foil packet and placed above the sample (A). A double Pt capsule arrangement which could be used with graphite buffers to contain the overpressure produced by oxidation of solid graphite is also shown (B). A third type uses the double capsule technique to minimize the possibility of contamination of the sample charge with the solid buffer (C). Essentially all results reported were obtained with configuration A. Recent runs (UTh 20A-5Co and 6Co) have successfully used configuration C.

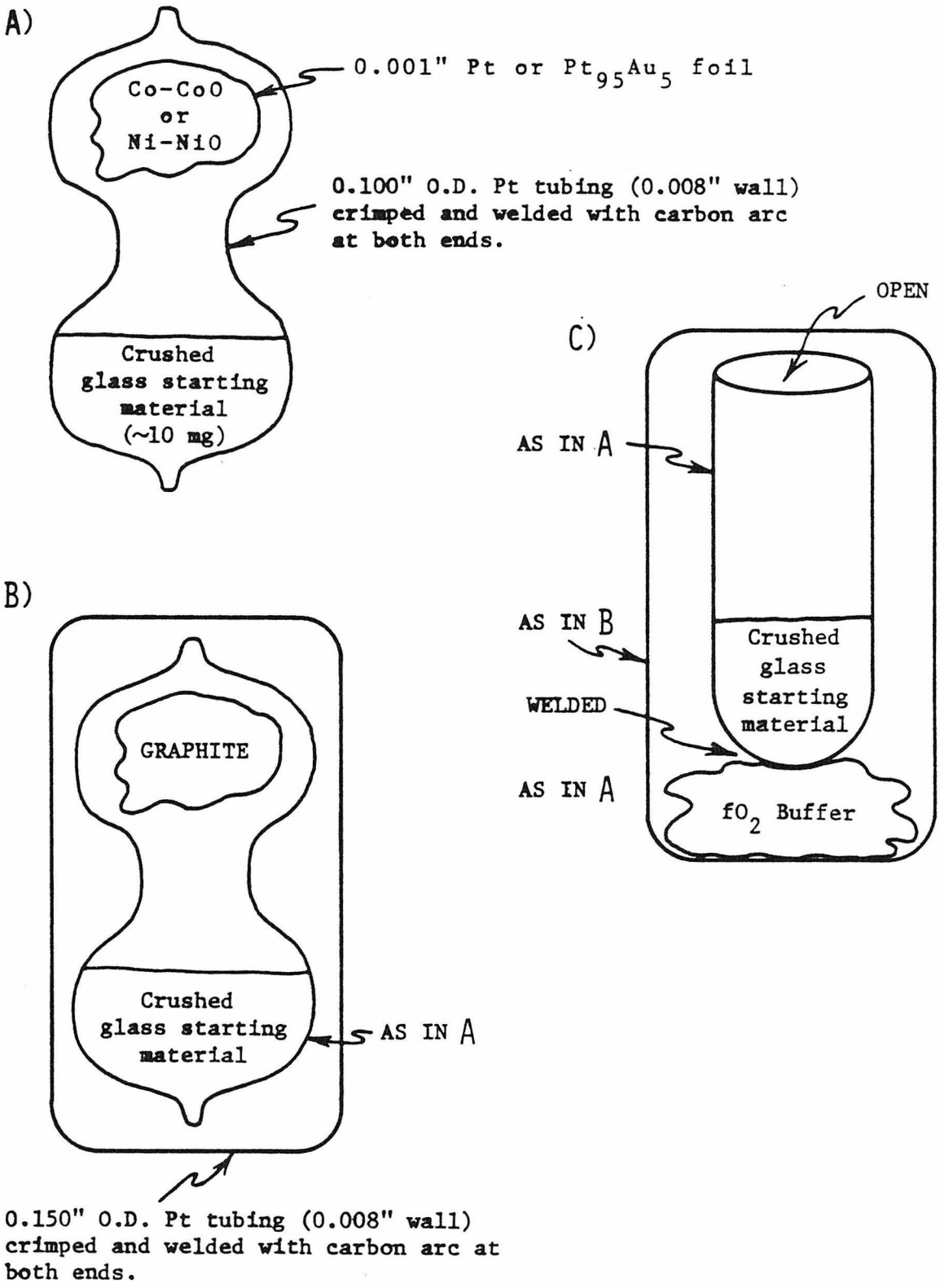
A)
Co-CoO
or
Ni-NiO
0.001" Pt or $Pt_{95}Au_5$ foil
0.100" O.D. Pt tubing (0.008" wall) crimped and welded with carbon arc at both ends.
Crushed glass starting material (~10 mg)
B)
GRAPHITE
Crushed glass starting material
AS IN A
0.150" O.D. Pt tubing (0.008" wall) crimped and welded with carbon arc at both ends.
C)
OPEN
AS IN A
AS IN B
WELDED
AS IN A
Crushed glass starting material
fO_2 Buffer

capsule is welded shut (except for air runs where a pinhole may be left).

The 1 bar pressure synthesis runs were conducted at Caltech with an Astro 1000A ultra-high temperature furnace equipped with a Eurotherm linear programmer and Leeds-Northrup controller. This furnace is a water cooled, graphite insulated, graphite resistance heater type that is used vertically with a 1-3/4 inch I.D. Al_2O_3 muffle tube. A continuous flow of N_2 is maintained over the interior to prevent oxidation of the graphite components. The muffle tube is isolated from the rest of the furnace on O-rings and is open to air. At either end baffles placed in the muffle tube minimize O-ring heating and heat loss. Argon, or better yet, He, must be used in place of N_2 at temperatures above 1650°C, which is also the maximum useful temperature that the muffle tube can be retained. Above this temperature, the furnace must be run without the muffle tube and must have O-ring sealed graphite baffles put in its place. The hot zone is constant to 1°C over a one inch interval, dropping 10°C at one inch from either end of the constant T interval (Astro claims a six inch hot zone). The Pt capsules (Figure 2) were suspended from thin (0.004') Pt wire adjacent to the S-type (Pt vs. $Pt_{90}Rh_{10}$) temperature monitoring thermocouple and then slid down an alignment collar into the hot zone. Alignments were always checked visually for centering. Quenching was achieved by electrically fusing the thin suspension wire thereby dropping the charge into a beaker of water (Donaldson et al., 1975). Quench crystal formation does not occur with our bulk compositions even when quenched in air.

All runs were heated to superliquidus temperatures for 0.2 to 41.0 hours followed by linear cooling (1.6 to 16.8°C/hour) in regular increments of less than 0.5°C. The final temperature was held from 0

to 62.1 hours prior to quenching. The temperature control thermocouple was a boron boron-graphite type produced by Astro Industries. The temperature derivative of the emf output of this thermocouple is roughly four times that of the S-type monitoring thermocouple giving very good control sensitivity. A continuous chart recording (Leeds-Northrup Speedomax W chart recorder) of the S-type thermocouple, for periods of days, records routine stability of 0.5°C. The Speedomax W chart recorder was calibrated against a Leeds-Northrup 8686 potentiometer. The S-type thermocouple was not calibrated with melting point standards; however, the thermocouple used for the 1 bar runs (unlike the 20 kilobar runs, a new thermocouple is not made for each experimental run) agreed with a thermocouple that was checked against a calibrated thermocouple at the Geophysical Lab. The experimental conditions for the samples analyzed are tabulated in Table 1.

D. 20 Kilobar Synthesis

The crystal synthesis experiments were made in a ½ inch single-stage piston-cylinder appartus (designed by D. Lindsley). All runs were pressurized to ~25 Kbar at $\lesssim$800°C, heated to superliquidus temperatures followed immediately by pressure reduction to ~20 Kbar (piston-out runs). Pressure determinations were based on area ratioing of the 4 inch hydraulic ram pressure (as measured on a Heise gauge) to the ½ inch piston. Manual pressure adjustments were made as required. No friction correction has been applied. Temperatures were measured with W3%Re vs. W25%Re thermocouples.

A graphite capsule containing ~10 mg powdered starting material (dried >24 hr. at 120°C) was sealed in a Pt capsule (Figure 3). The

TABLE 1. Experimental Synthesis Conditions (1 Bar)

Experiment Number P=8.4%[##]	T_i[#] (°C)	t_i (hr)	dT/dt (°C/hr)	T_f °C	t_f (hr)	whit	cpx	plag	Σ
Pu10A-1A	1338	1.3	4.7	1275	3.7				
Pu15B-6A	1323	10.5	3.9	1237	2.3				
Pu15B-2Co	1332	10.6	3.8	1245	0.6	9.3±0.5			9.3±0.5
Pu15B-4Co	1333	41.0	3.8	1246	1.4				
Pu15B-6Co	1323	39.5	3.9	1235	1.2	9.8±0.8			9.8±0.8
UTh20A-5A	1313	0.2	4.7	1272	6.6	5.3±0.7			5.3±0.7
UTh20A-9A¢	1336	2.8	4.1	1228	2.3	9.4±1.1			9.4±1.1
UTh20A-11A¢	1336	2.6	5.5	1228	0.6	8.8±0.9			8.8±0.9
UTh20A-1Co	1317	0.2	16.8	1273	1.3	4.9±0.8			4.9±0.8
UTh20A-2Co+	1315	1.3	5.7	1262	5.4	4.5±0.9			4.5±0.9
UTh20A-5Co	1336	24.5	5.1	1227	1.2	11.2±0.2			11.2±0.2
UTh20A-6Co	1335	3.4	5.4	1228	0.5	10.2±0.2			10.2±0.2
UTh40A-1Co	1335	0.7	14.2	1264	2.8				
UTh40A-4Co*	1325	0.4	8.0	1276	10.4	3.3±0.5			3.3±0.5
U23A-3A	1359	1.0	5.0	1268	0	8.9±0.6	(0.3±0.1)**	(2.8±0.4)¢¢	12.1±1.0
U23A-3Co	1357	3.0	4.0	1268	0.5	11.5±0.5			11.5±0.5
U23A-4Co	1332	17.3	--	1332	--	1.8±0.6			1.8±0.6
U23'A-5A+++ -5Co	1332	2.1	2.0	1245	2.6	10.8±0.5 10.5±0.5		(2.1±1.4)	12.9±1.5 10.5±0.5
U23'A-6A+++ -7Co	1336	1.0	9.4	1239	5.5	10.8±0.5 11.7±0.4			10.8±0.5 11.7±0.4

TABLE 1. (Cont.)

Experiment Number	T_i (°C)	t_i (hr)	dT/dt (°C/hr)	T_f °C	t_f (hr)	whit	cpx	plag	Σ
P=5.3%									
UTh30A-6Co	1257	1.1	5.2	1189	9.3				
UTh30A-8Co	1257	1.5	4.7	1188	0.9				
P=2.9%									
UTh-31A-1A	1229	1.4	2.4	1189	2.3	(1.1±0.9)++		5.3±3.8	6.3± 4.1
UTh-31A-10Co	1224	4.0	1.6	1183	62.1	1.5±1.3	17.4±4.3	19.9±5.6	38.8±10.1
P=0%									
Pu14A-2HM	1274	12.4	2.9	1206	1.0				
Pu14A-5A¢	1274	12.2	2.9	1207	1.7		19.3±0.8	(0.9±0.3)**	20.2±0.8
Pu14A-1Co	1276	2.2	3.8	1209	1.6				
Pu14A-7Co	1280	14.9	2.9	1213	0.7		13.3±1.5		13.3±1.5

T_i= Initial temperature; t_i= Time held at initial temperature; dT/dt= Linear cooling rate
T_f= Final temperature; t_f= Time held at final temperature prior to quenching
Phosphorus is in atomic proportions, percent of all cations
+ Slight blue color due to small amount of Co contamination
++ Calculated but not observed apatite
+++ Run in a tandem capsule arrangement
* Pinhole leak in capsule completely oxidized buffer; $fO_2 \leq$ air
** Calculated but not observed forsterite
¢ Capsule open to air; all other runs either with Co-CoO buffer (Co) or welded shut in air with no buffer (A). The welded shut (A) runs appear to be at an indeterminant fO_2 due to a (carbonaceous) contaminant
¢¢ Calculated but not observed plagioclase (of composition observed in UTh31A-1A)

Pt capsule was placed inside a graphite heater cylinder with a plug of crushable alumina below and a tube of crushable alumina above the Pt capsule. This assembly was placed inside a Pyrex sleeve which in turn was placed inside a tube of talc. This furnace assembly was wrapped in Pb foil and lubricated with a commercial molybendum sulfide lubricant just prior to placing in the piston cylinder apparatus. A graphite plug was placed beneath the furnace assembly, above the piston and a bored, pyrophllite insulated, 'base' plug was placed on top. A four-bore (997) Al_2O_3 ceramic tube containing the thermocouple was fed through the base plug, down the crushable alumina tube with the thermocouple junction touching the Pt of the sample assembly. Upon pressurization the thermocouple becomes embedded in the Pt.

An initial study by Seitz et al., (1974) used boron nitride sleeves instead of Pyrex and did not seal the sample in Pt; however this assembly permitted the entrance of H_2O into the experimental charge (from dehydration of talc). The sealed Pt/graphite assembly not only prevents H_2O contamination but also permits the solid graphite to act as a fO_2 buffer. The Pyrex also serves as an H_2O getter (as well as being cheaper than boron nitride); however, the Pyrex must be softened (heated) prior to pressurization. The temperature of ~800°C was chosen so as to soften the Pyrex but not to promote sub-solidus recrystallization or partial melting of the experimental charge on the time-scale required for final pressurization and heating (~10 min.).

Temperature settings were regulated by a power controller which senses the output of a Hewlett-Packard null meter (set at 100μV full scale) monitoring the emf difference between the W3%Re vs. W25%Re (ice cold-junction compensated) and a Leeds-Northrup 8691-2 potentiometer.

FIGURE 3

Cross-section of the furnace assembly used for the 20 kilobar experimental synthesis runs; modified after Figure 1 of Bell and England (1967).

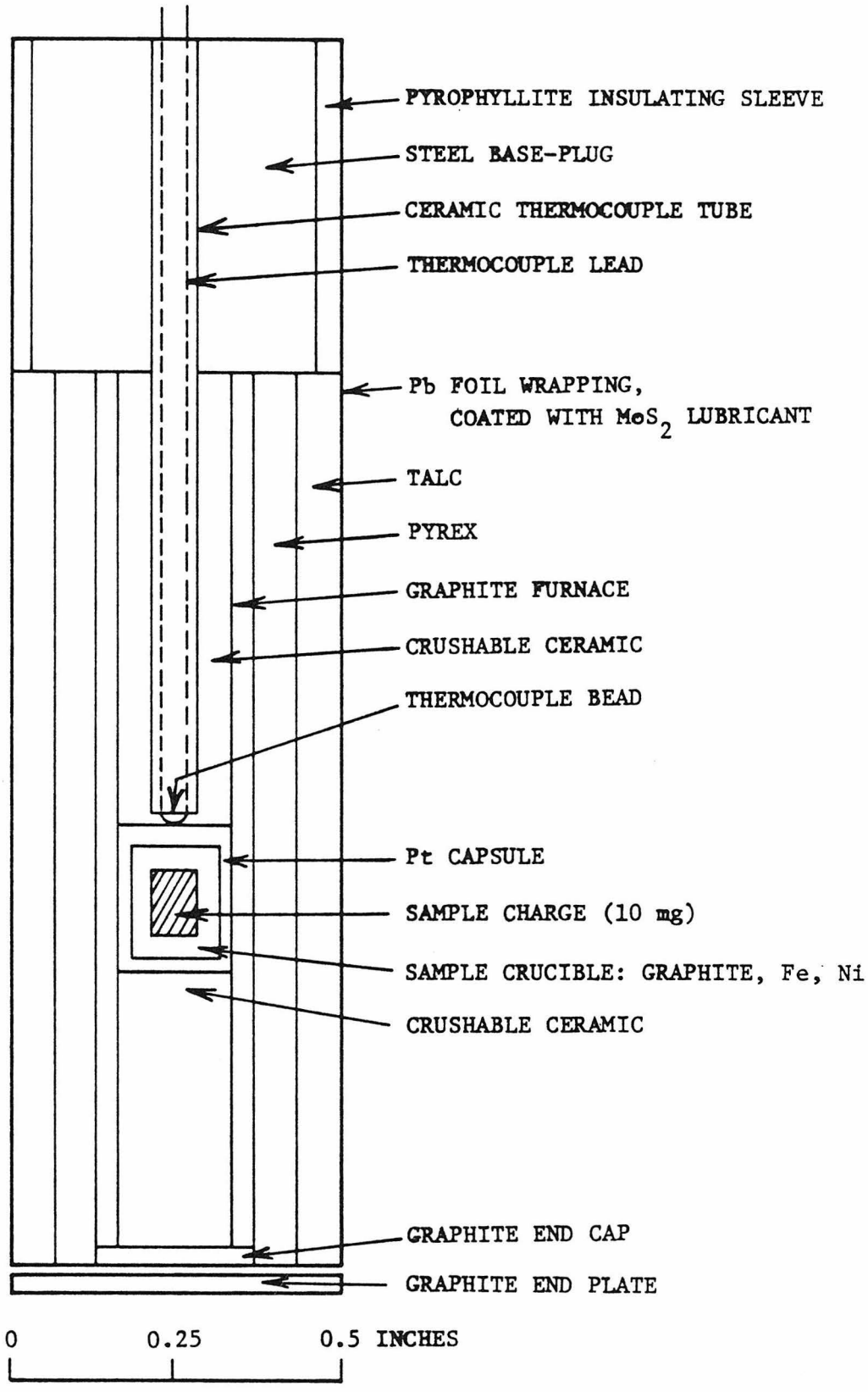
PYROPHYLLITE INSULATING SLEEVE
STEEL BASE-PLUG
CERAMIC THERMOCOUPLE TUBE
THERMOCOUPLE LEAD
Pb FOIL WRAPPING,
COATED WITH MoS2 LUBRICANT
TALC
PYREX
GRAPHITE FURNACE
CRUSHABLE CERAMIC
THERMOCOUPLE BEAD
Pt CAPSULE
SAMPLE CHARGE (10 mg)
SAMPLE CRUCIBLE: GRAPHITE, Fe, Ni
CRUSHABLE CERAMIC
GRAPHITE END CAP
GRAPHITE END PLATE
0
0.25
0.5 INCHES

Control stability routinely fell within ±5μV≈0.3°C. Linear cooling was achieved by mechanical attachment of a Slo-Syn DC driving motor to the thumb wheel of the LN potentiometer. The motor was activated by pulses from a variable frequency pulse generator. Each pulse results in a 0.08°C decrease so the cooling is effectively continuous. (See Figure 4 for schematic layout).

Quenching was achieved by cutting power to the internal graphite heater resulting in ~1000°C of cooling in ~5 sec. Quench crystal formation was not a problem with the 'haplobasaltic' compositions used in these experiments.

The experimental conditions for the samples analyzed are tabulated in Table 2. The thermal history of each run consisted of heating to an initial superliquidus temperature T_i for a time t_i, followed by linear cooling (dT/dt, °C/hr) to a final temperature T_f which was held from 0-21 hr. (t_f) prior to quenching.

E. Solid fO_2 Buffers

Maintenance and control of the oxygen fugacity is essential when conducting experiments on multivalent cations such as U and Pu in this study or Eu, Ce, Fe, Mn, and Cr in other studies (Morris and Haskin, 1974; Johnston, 1965; Schreiber, 1977; Schreiber et al., 1978). The choice of solid fO_2 buffers is limited in piston-cylinder experimentation (the 20 kilobar experiments in this study). The buffer must be either the sample capsule (graphite, Ni, Fe, etc.) or contained in an inert sample capsule (PtO_2 or oxalates in Pt capsules). The buffer is ideally non-reactive with the charge, but this is not always possible. Experiments at 1 bar are not so restrictive in that gas mixing

TABLE 2. Experimental Synthesis Conditions (20 Kbar)

Experiment Number	T_i (°C)	t_i (hr)	dT/dt (°C/hr)	T_f °C	t_f (hr)	% crystallized (a) whit	cpx	apatite	Σ
P=8.4% (b)									
UTh-20-288	1430	1	2.8	1390	0	3.9±0.2	11.9±0.4	0.9±0.1	16.7±0.5
UTH20-211	1400	1	68	1375	21	13.7±0.8	20.9±2.0	0.2±0.3	34.8±2.5
UTH20-326	1450	0.2	2.8	1390	0	13.4±0.7	24.2±1.6	1.1±0.4	38.7±1.8
UTh20-266	1420	4	1.9	1375	1.2	14.5±0.1	28.3±0.2	1.5±0.1	44.3±0.2
Pu10-293 (e)	1440	1.7	3.1	1388	0	A-13.7±0.6	23.4±1.1		37.1±1.3
						B-(9.8±0.8)(e)*	17.7±1.3		27.5±1.5
Pu10-234	1450	2.5	36	1375	1	15.4±0.6	28.9±1.7	0	44.3±1.7
P=5.3% (b)									
Pu12-267 (c)	1415	-	-	-	-	0	6.9±3.8	0	6.9±3.8
Pu12-261	1415	4	2.4	1380	1	0	14.0±0.9	0	14.0±0.9
Pu12-320	1420	0.5	2.4	1380	0				
Pu12-236	1450	1	36	1375	1				
UTh30-231	1450	2.5	71	1375	12	0	18.4±0.6	0	18.4±0.6
UTh30-269	1425	22	1.8	1390(d)	0	0	18.9±2.2	0	18.9±2.2

(a) Modes calculated by least squares (Reid et al., 1973) from microprobe data
(b) Atomic proportion in starting composition
(c) Thermal history complicated by several unintentional quenches due to power interruptions
(d) Temperature control and measurement not reliable due to spurious emf produced by water leaking into cold junction assembly
(e) Pu-293 A and B modes suggest that the charge was positioned in a thermal gradient and equilibrium was not continuously maintained in the melt on the scale of the entire charge
* Pu10-293B has calculated but not observed whitlockite

FIGURE 4

Schematic layout of temperature control, monitoring, and linear cooling assembly used for the 20 kilobar experiments at the Carnegie Geophysical Laboratory.

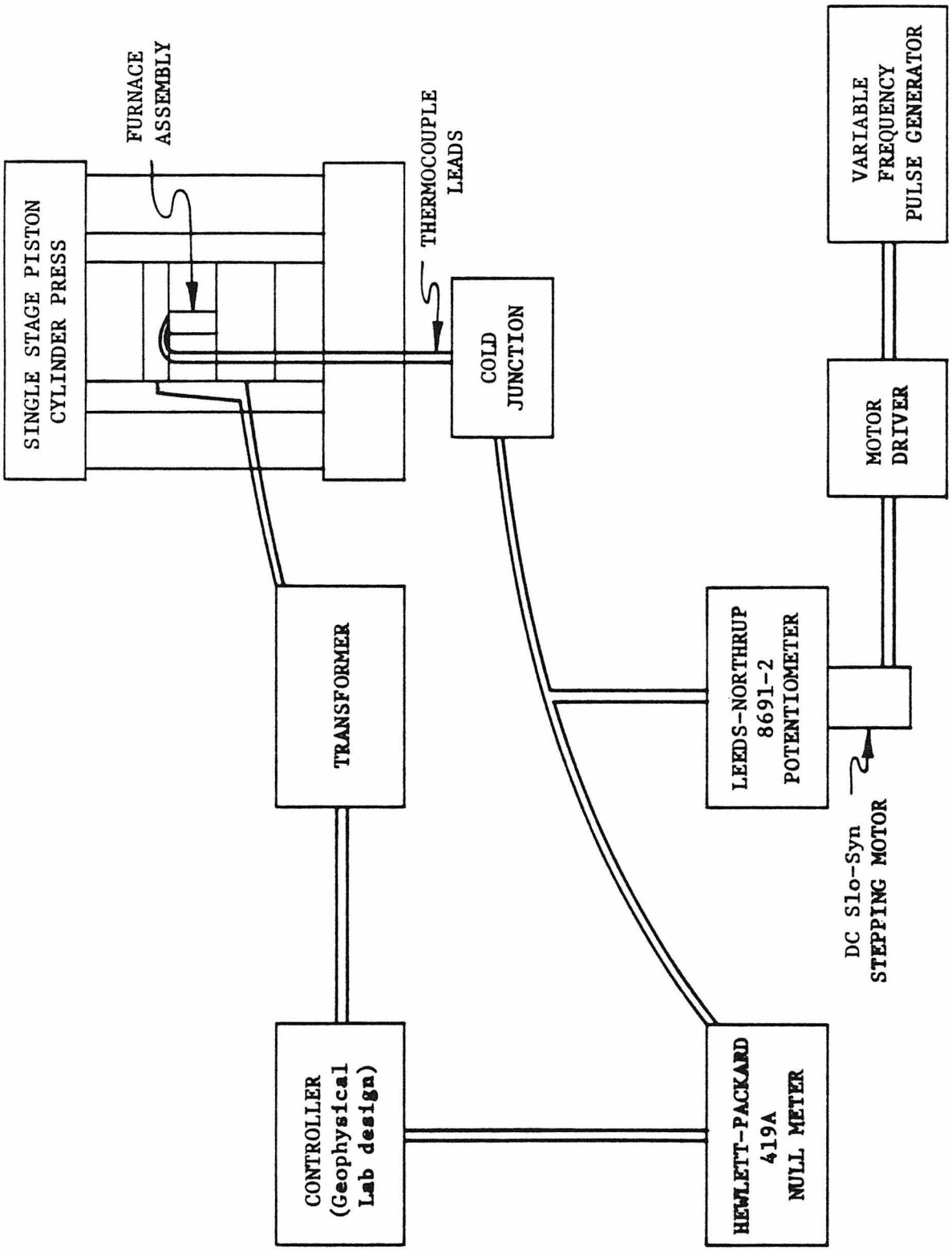
SINGLE STAGE PISTON CYLINDER PRESS
FURNACE ASSEMBLY
THERMOCOUPLE LEADS
COLD JUNCTION
VARIABLE FREQUENCY PULSE GENERATOR
MOTOR DRIVER
TRANSFORMER
LEEDS-NORTHRUP 8691-2 POTENTIOMETER
DC Slo-Syn STEPPING MOTOR
CONTROLLER (Geophysical Lab design)
HEWLETT-PACKARD 419A NULL METER

techniques (Huebner, 1975; Sato, 1970; Williams and Mullins, 1976) as well as solid buffers can be used.

The majority of 20 kilobar runs used the graphite buffer, producing a reducing environment without detectable interaction with the silicate charge. A few runs were made with Fe or Ni metal capsules. The buffer curves given in Appendix II are taken from Huebner (1971) and Myers and Gunter (1979).

Solid fO_2 buffers were also used for the 1bar runs. The sealed capsules minimized loss of Na and P. A mixture of Co and CoO was the principal buffer although Ni-NiO, Fe-FeO, and Fe_2O_3-Fe_3O_4 were also used. The Co-CoO buffer maintains an fO_2 at the 1 bar conditions near the fO_2 maintained by graphite buffers at 20 kilobars (Appendix II). Capsule and buffer configurations for the 1 bar runs are shown in Figure 2. Pt capsules with pinholes or sealed in air were used in 1bar experiments to attain high fO_2 conditions. As discussed in Section III-I, the runs sealed in air seem to have been partially reduced by a contaminant, probably carbonaceous material.

Buffer equilibration requires serious consideration. Not only must the buffer equilibrate with the vapor phase but the multivalent cations in the silicate melt must also equilibrate. Schreiber et al. (1978) state that times on the order of 8-12 hours are needed to equilibrate the multivalent ions in their experiments. Morris et al. (1974) demonstrate Eu^{+2}/Eu^{+3} equilibration after only one hour. Myers and Gunter (1979) report that the Co-CoO buffers equilibrate with the vapor phase in minutes at the temperature used in experimental studies. The only buffer commonly used which takes significant time, hours, to equilibrate is Fe-FeO. This is because wustite is non-stoichiometric

and must change Fe-O ratio, in bulk, to change the fO_2, unlike the Co-CoO buffer which merely oxidizes or reduces the number of atoms required (Myers and Gunter, 1979).

Buffer equilibration should be attained in this study in that the runs are generally much longer than eight hours; however, except possibly for some experiments sealed in air (in contrast to unsealed air runs), the results are consistent at each of the different desired fugacities. This would not be the case if a well-defined and constant fO_2 did not maintain a fixed valence state (ratio) of the multivalent cation (Section III-G).

Trace Element Detection

A. Sample Mounting and Irradiation Assembly

Polished thick sections were made of a portion (usually about ½) of the synthesis products by placing the fragment in a 'cup', made by epoxying a one inch nylon ring (3/16" deep) to glassine weighing paper, and filling with Techkit 's type E-7 epoxy. Curing took about 15 minutes in the drying oven. After cooling, the paper is easily scraped off and any excess epoxy on the outer edge of the now solid ring is removed with 'side-cutter' pliers. Brief application of the sample side of the disc to 600 grit grinding paper suffices to expose the sample. A Buehler Mini-met polisher is used for the final series of 1 micron and 0.3 Al_2O_3 micron polishings. An ultrasonic cleaner is used between polishing steps and separate bowls (a feature of the inexpensive Mini-met) are used for each polishing compound grit size as well as each isotope.

Only runs which produced sufficiently large (>50 microns) crystals

were subjected to detailed study. (As discussed in a later section, crystal sizes are required which are larger than the range of the fission fragments or alpha particles being detected).

Three holes are drilled around the rim of the sample disc for assembly with the appropriate detector: muscovite mica (fission fragments) for ^{235}U or ^{239}Pu and Kodak-Pathé CA80-15 cellulose nitrate (alpha particles) for ^{230}Th.

Obtaining flush contact between sample surface and the mica or plastic (cellulose nitrate) detector is extremely important in measuring low ($\lesssim 0.1$) crystal/liquid partition coefficients because any gap between sample and detector can lead to interfering tracks from the high actinide glass regions into the area of the detector corresponding to the crystals. In order to get satisfactory results it is necessary to use nylon plugs to provide strong axial compression (Figure 5) on the region of the epoxy mount containing the sample. This was necessitated by a tendency of the epoxy to deform slightly during thermal neutron irradiation. A layer of DuPont RTV rubber can also be placed in the center of the assembly to give gentle pressure on the detectors (Figure 5). This RTV can be safely used as it is thermally stable enough to be used for making molds for lead castings (Johnson, 1969).

B. Irradiation Conditions

For ^{235}U and ^{239}Pu, the irradiation assembly was exposed to thermal neutrons in the UCLA Nuclear Energy Laboratory reactor (fluences, cm^{-2}, $=7\times10^{15}$ for U and 2×10^{15} for Pu at a flux of 2×10^{12} n/cm^2-sec.). These fluences resulted in fission track densities of 0.5 to $2\times10^8/cm^2$ over

FIGURE 5

The sample irradiation assembly consists of a pair of discs containing polished experimental charges, the appropriate detector (mica or cellulose nitrate), and (optionally) RTV rubber compressed together with nylon screws and end plates with a small nylon plug for strong axial compression. An additional layer to this 'sandwich' is added when a double polished standard glass is desired.

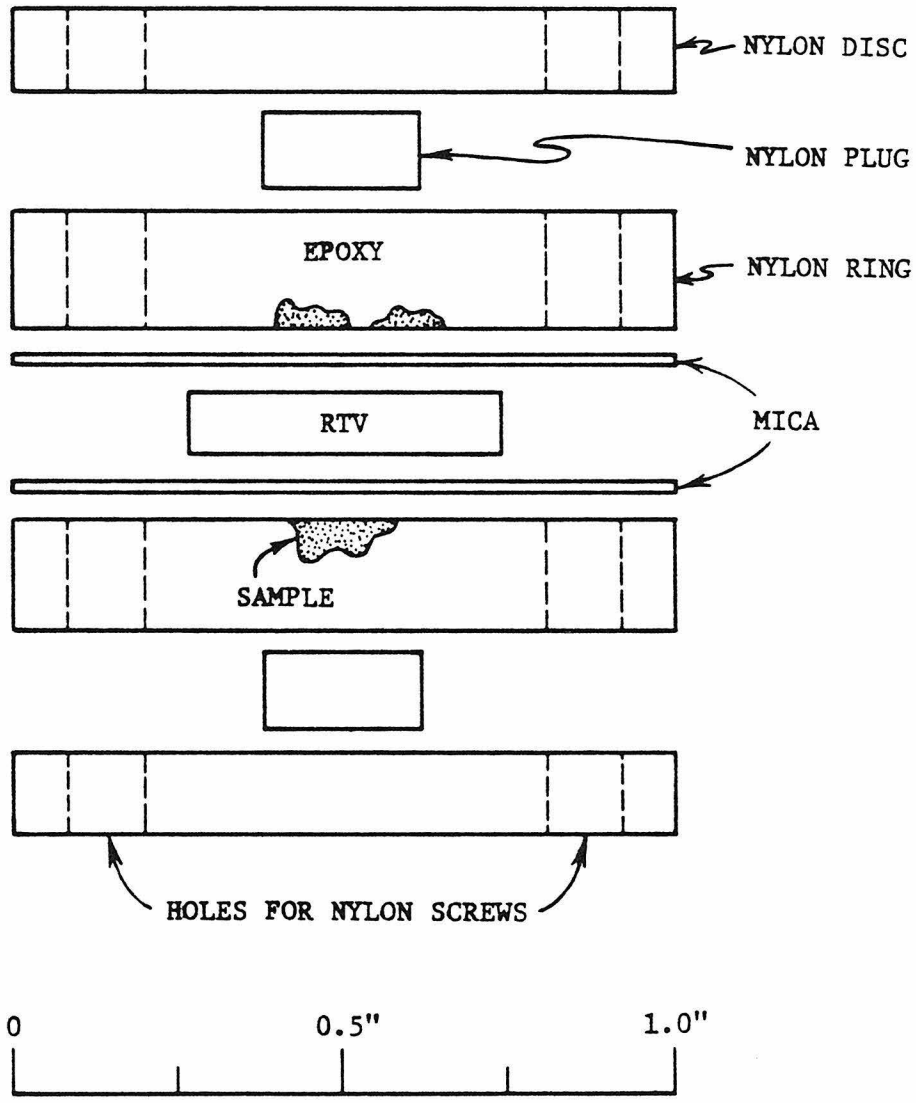
NYLON DISC
NYLON PLUG
EPOXY
NYLON RING
RTV
MICA
SAMPLE
HOLES FOR NYLON SCREWS
0
0.5"
1.0"

the detector area corresponding to glass, permitting good counting statistics to be obtained over small areas for most crystal/liquid partition coefficients (≥ 0.05).

The ^{230}Th exposures use the same assembly as does the above; however, no reactor irradiation is required because the alpha particles are from spontaneous decay of the ^{230}Th. To measure low partition coefficients, two exposures are made: a short (2 to 4 days) exposure to measure track densities for the glass (typical densities of $2 \times 10^7/cm^2$) and a long (30 days for the case of clinopyroxenes) exposure to increase the counting statistics for the crystals. Both detectors must be etched simultaneously (see next section). Only a single, short, exposure is required for partition coefficients near or greater than unity.

C. Detector Etching

After irradiation, the muscovite detectors were etched in 48% HF at room temperature. As discussed in the next section, scanning electron microscope (SEM) photomosaics were made for track counting of the crystalline phases. To avoid excessively large numbers of photographs, two stages of etching were employed when partition coefficients much less than 1 were measured. Because of the highly anisotropic etching rate of muscovite, the width of the fission tracks can be varied without affecting the other geometrical properties (Fleischer et al., 1975); that is, the tracks become wider without changing the track density. Of course over-etching will result in a lowered track density as the tracks become overlapping; so careful etching is required. For clinopyroxenes, track densities corresponding to the coexisting

glass were measured after six to eight minutes of etching at 10 K magnification, then the mica detectors were re-etched (20 to 60 minutes total) and photomosaics of the crystals were taken at 1 to 3 K magnification thereby reducing the number of photographs by one or two orders of magnitude. Using track densities of $5 \times 10^5/cm^2$ to avoid overlapping tracks, test measurements at 3% counting statistics showed that, over the range of etching times used, the fission track etching and counting efficiencies were independent of etching time.

The cellulose nitrate plastic (Kodak-Pathé) dececters used for the ^{230}Th alpha particle analyses are more sensitive to etching conditions than the muscovite fission track detectors. The ^{230}Th alpha particle energy is 4.6 MeV, but because the samples are infinitely thick compared to the alpha particle range, a continuous spectrum of energies (0 to 4.6 MeV) enter the plastic detectors. Careful registration experiments by Mascettelli and Woolum (private communication) using monoenergetic alpha particles from an accelerator have shown that, for the etching conditions used in this study, tracks for alpha particles of energies greater than 4 MeV would not be etched sufficiently to be reliably counted. Consequently, for a given set of observation techniques, the track density will depend on etching time (see Figures 2 and 3 in Woolum et al., 1979 for registration characteristics of a cellulose nitrate plastic similar to the plastic used in this study). Because of this, two different exposure times (as mentioned previously) were used instead of two different etching times (as for the mica) to improve counting statistics over crystals with low partition coefficients. Plastic detectors from both exposures were etched together (6.25 N NaOH, 60 to 120 minutes at 40°C)

to avoid any variations in etching efficiency.

D. Track Counting

All track counting was done on SEM photographs of the gold-coated mica and plastic detectors using an ISI Super II instrument. This permitted the optimization of track counting statistics by increasing resolution, relative to counting with an optical microscope, so that high track densities ($10^8/cm^2$) could be utilized. The fission track counting on the mica detector was straightforward, the diamond shapes are distinctive even when several tracks partially overlap, and the track sizes are all nearly equal.

Alpha track counting in plastic is not nearly as easy. To avoid counting biases introduced by the highly variable width and shape of the alpha tracks, track counting for the glass and the crystals was done at constant SEM magnifications. Reproducible track densities for a given sample can be obtained over at least a factor of two in magnification (Table 3).

Track counting was done from the SEM photographs by the same person for both crystals and glass to minimize differences due to personal biases (Table 4). Unless there is a high proportion of overlapping tracks, recounts of the same photographs by an individual are reproduced within expected statistical limits; however, for two different individuals, even with experience, systematic differences of 5% can occur in the derived partition coefficients. Alpha particle track counting is more difficult, requiring experience (Table 5). In general, the track counting errors set a minimum error of about 5% (standard deviation) on a measured partition coefficient. This

TABLE 3

Reproducibility of alpha track counting at two differeng nominal magnifications**

	3K A*	2K A
	129	276
	116	293
	131	282
	134	
	122	
	139	
	128	
Average	128±8	284±9

2K/3K	Expected
2.21	2.25

* Designates the individual doing the track counting in this and following tables.

** Each entry represents the number of tracks on separate SEM photographs of a plastic detecter exposed to a homogeneous, infinitely thick source of ^{230}Th alphas. The 2K and 3K pictures are of the same area; consequently essentially the same tracks are contained in both sets of photographs.

TABLE 4

Reproducibility of fission track counting on the same Polaroid photographs by different individuals

Sample 1

Photograph	A	B	C
a	178	180	180
b	177	185	182
c	179	181	187
d	166	186	182
Average	175±6	183±3	183±3

Sample 2

Photograph	A	B	C
e	64	67	65
f	66	67	71
g	70	70	71
h	49	50	48
Average	62±9	64±9	64±11

Sample 1/2

	2.81	2.88	2.87

TABLE 5

Reproducibility of alpha track counting on the same Polaroid photographs by different individuals, experienced and inexperienced

Sample 1*

Photograph	A	B	C
a	319	339	296
b	328	337	287
c	322	324	298
average	323±5	333±8	294±6

Sample 2#

	A	B	C
d	173	185	188
e	205	209	216
f	182	195	189
average	187±17	196±12	198±16

Sample 3+

	A	B	C
g	432	484	533
h	410	435	511
i	428	433	523
average	423±12	451±29	522±11

Sample 1/2

1.73 1.70 1.49

Sample 3/2

2.27 2.30 2.64

* Sample 1 has a very high background of what appears to be small alpha tracks which require visual discrimination during counting. Individual C has had no previous alpha counting experience.

Sample 2 has both a low background as well as a moderate track density which is easily counted with little experience. Note that the two (A and B) experienced alpha counters remain relatively consistent throughout.

+ Sample 3 has a high track density that produces many overlaps of the somewhat irregular alpha tracks although the background of small tracks is low.

precision could probably be improved but is adequate for applications at present. Periodic measurements with two SEM calibration grids and by comparing measured spacings between pairs of fission tracks showed that the relative SEM magnifications corresponded to those given by the manufacturer and were constant with time to better than 2%. The absolute magnifications, at the working distance utilized throughout the SEM work, were determined to be 53.8% of the nominal, indicated, magnifications.

Occasionally the Au coat must be removed so that the detectors can be re-etched. A simple method to do this and one that does not immediately destroy the cellulose nitrate plastic (the mica is untouched by most reagents) is to swirl, for a minute or two, the Au coated detector in a bromine water solution. The solution is easily made by adding household liquid bleach to an aqueous solution of NaBr, followed by mild acidification with dilute HCl (this must be done in a fume hood).

Microprobe Analysis

A. Major and Minor Elements

Nearly all samples used for track density measurements were analyzed for major and minor elements by a computer controlled MAC-5 SA3 electron microprobe x-ray analyzer at 0.05 microamps (on brass) and 15 KeV using a 30 micron spot where possible. On line corrections were performed by the method of Bence and Albee (1968). Slight variations in both software and hardware occurred over the years in which the data were taken. The changes primarily had the effect of increasing precision of the minor elements by automated beam current regulation and increas-

ing counting times (achieved by lowering the peak to background discriminator cutoff).

B. Uranium

U-rich whitlockites were synthesized from the basic 25 weight percent $Ca_3(PO_4)_2$ starting material to which 3.4 and 3.9 weight percent of isotopically depleted UO_2 were added using the standard preparation procedures (Appendix I). At these concentrations, U partition coefficients can be determined using the electron microprobe, but the initial U microprobe analyses were very poor due to the low count rate and peak to background ratio using the standard LiF crystal spectrometer (M_β). Precision was markedly improved by switching to the PET crystal spectrometer (M_α) because of the greater efficiency of PET relative to LiF and the ability to monitor a more intense x-ray line ($M_\beta=0.7M_\alpha$). The U peak occurs near the end of the useful range of the PET crystal. Background at shorter wavelengths rapidly increases; thus the conventional taking of background on either side of the peak and the interpolating was ruled out. Fortunately the U peak lies on the linear portion of the long wavelength background range of PET, as determined by stepping through this region on a U-free sample with the same composition. The rapid background increase begins just to the short wavelength side of the peak. This permitted calculation of the background beneath the U peak from background taken only on the long wavelength side of the peak. The microprobe program was modified so that the measured, long wavelength, background was multiplied by 1.098 (obtained from the U-free sample) prior to subtraction from the U peak. The total background correction amounts to roughly ten percent for the

U analyses of the glass and thirty percent for the whitlockite crystals; therefore the error in the 1.098 value should have negligible effect on the final results. These results are presented and discussed in Section III-I.

III. RESULTS

A. Data Reduction

Three techniques of acquiring data from tracks corresponding to the actinide concentrations in the synthetic crystals can be used. In order of complexity of acquisition and increasing precision, they are: 1) counting only over the center of the crystal, 2) counting across the crystal from edge to center to edge forming a 'profile', and 3) counting the entire interior area of the crystal. These techniques are applied based on the size of the crystal, the magnitude of the partition coefficient (D), and the extent of crystallization. For the track densities utilized, large crystals require excessive numbers of SEM photographs unless the D values are low which may permit longer etching times and thus lower SEM magnifications. Low D values require large areas to be counted for accumulation of counting statistics, whereas high D values give adequate counting statistics over small areas. Small amounts of crystallization require the least correction due to zoning (Section III-C). Proper utilization (Appendix V, eqn. 2) of method 1 requires very large crystals (hundreds of microns in all dimensions); consequently all data reported, even for partition coefficients $\gtrsim 0.1$, are based on methods 2 and 3.

i. Contouring Track Densities

As an example, the treatment of a typical sample detector is presented. Figure 6 is a transmitted light photomicrograph of a mica detector containing a fission track image of a medium-sized clinopyroxene crystal synthesized from Pu-spiked starting materials. The

figure shows the mica after a long etch which makes measurement of the crystal track density easier. The contrasting track densities between the clinopyroxene and surrounding glass dramatically illustrate the strong partitioning of the actinides into the melt relative to the clinopyroxene. The rim of the crystal cannot be analyzed (counted) because tracks from the glass extend into the mica region corresponding to the crystal rim, forming a steep track gradient. The distance over which interference is important is set by the fission fragment (~10 micron) or alpha particle (15 micron for ^{230}Th) ranges and by the subsurface boundary geometry. In order to assess objectively when the measured crystal track density is free from interference from the glass while maximizing statistical precision (by counting as many tracks as possible), a 'contouring' technique as illustrated in Figure 7 is used. A high magnification SEM mosaic of the track distribution (corresponding to the low magnification image shown in Figure 5) is subdivided into squares, usually chosen to contain no more than ~10 tracks (for optimum resolution), forming a 'digitized' track map. An initial (outer) contour is drawn corresponding to the actual crystal/glass boundary. This is easy for the high track density contrast samples such as shown in Figure 6, but for D values close to unity the location of the boundary is less easily placed by simple visual inspection. In the latter cases the initial contour is drawn on the track image based on the size, shape, orientation and location of the crystal. The latter two quantities are determined by reference to clearly identified (high contrast) features in the track image (pyroxene grains, glass/epoxy boundary, etc.). After the initial contour is placed, a second contour is drawn by uniformly incrementing inward, either ~10 micron (average

FIGURE 6

Optical transmitted light photomicrograph of a ^{239}Pu fission track image of a 100 by 150 micron sized clinopyroxene grain surrounded by quenched liquid (glass). The individual tracks are clearly resolved in the interior. Pu contents are proportional to track density. The track density is much higher in regions corresponding to the glass, reflecting a much higher Pu content. Quantitative track density measurements for the glass are done by track counting of SEM photographs at much higher magnification and with less etching of the mica detector than is shown in this figure. A 15 micron wide bit of graphite is present on the left edge of the crystal. The upper and lower right corners correspond to epoxy.

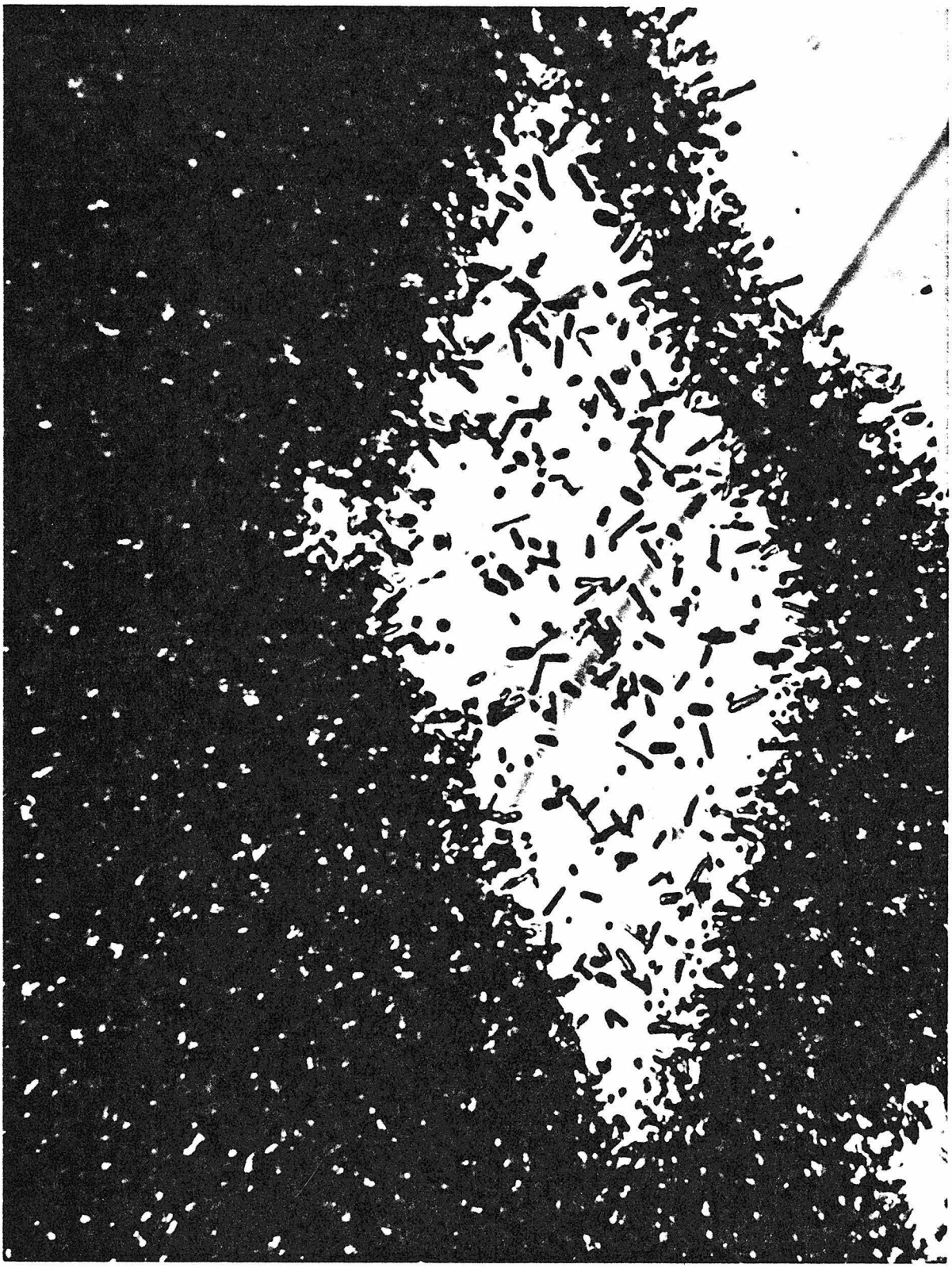

FIGURE 7

This figure illustrates how the crystal shown in Figure 6 was subdivided ('contoured') in order to obtain an objective assignment of tracks to the crystal and glass. This is necessary because there is a gradient of tracks into the crystal from the surrounding glass due to the finite range of the fission fragments. An initial contour is drawn corresponding to the apparent glass-crystal boundary. Successive inner contours are drawn by incrementing the initial contour inward by ~10 microns. The successive contour lines define intervals (Roman numerals) in which track counts are made. A 'good' track profile is indicated by constant track densities in adjacent interior intervals.

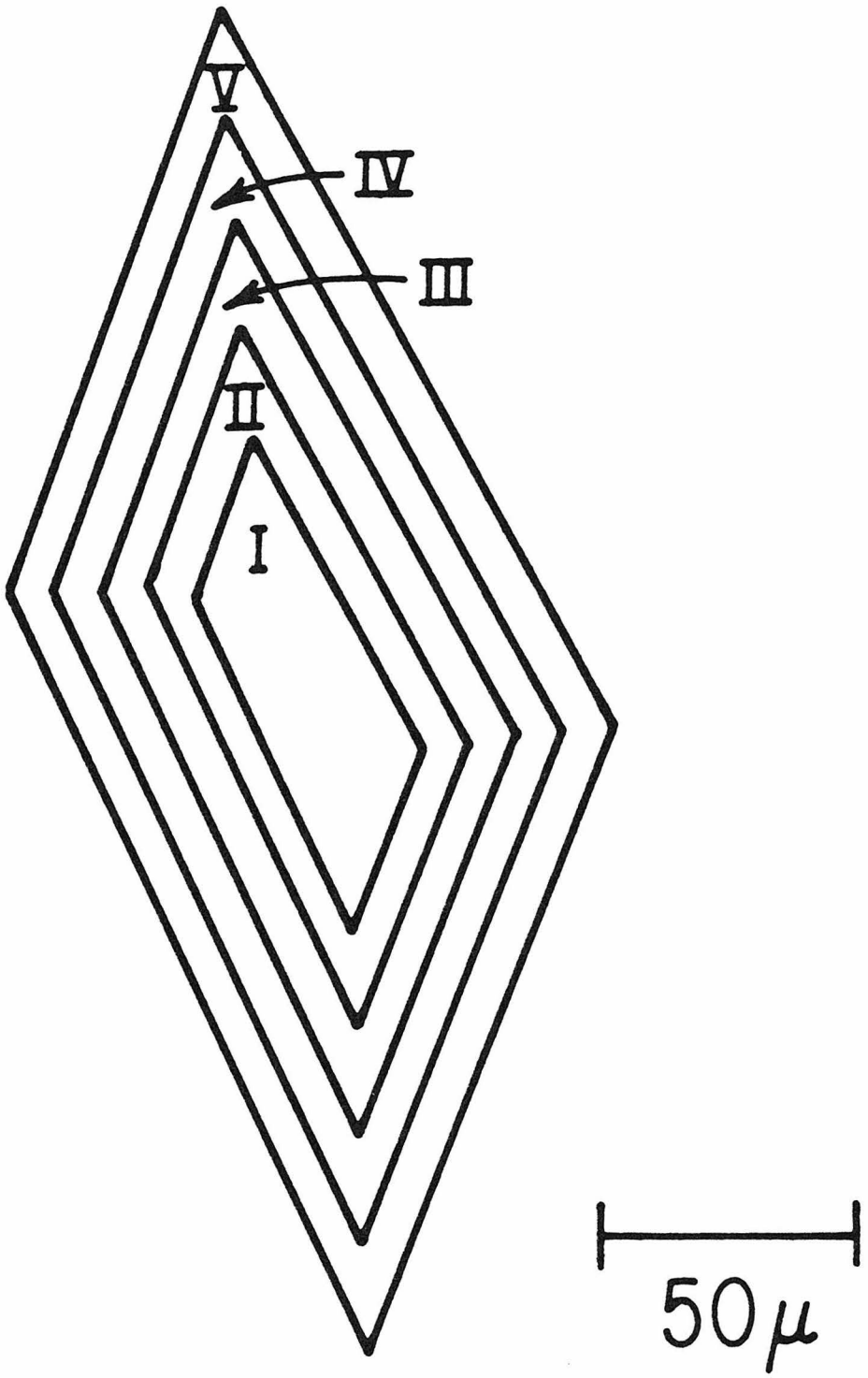

Schematic Contour Intervals for Clinopyroxene

fission fragment range) or by an amount designed to leave at least 50-100 tracks in the interval between two contour lines. (Each interval is designated by a Roman numeral in Figure 7). This process is repeated until a statistically insignificant number of tracks is left in the crystal interior. As illustrated in Figure 8, a plot of track density against contour interval can be used to assess when a relatively constant interior track density has been obtained. (The effect of actinide zoning must be allowed for, as discussed below). A 'well-behaved' track density profile (like Figure 8) is a criterion for an acceptable actinide concentration determination for a given crystal. Figure 9 shows the actinide track density as observed in a thin pyroxene crystal and provides an example of a non-converging 'soft' profile. Even the most central point in the profile through the crystal (Figure 9) is 40 times the track density corresponding to the actinide concentration. 'Soft' profiles can also be produced by inward-sloping (i.e., towards crystal center) subsurface crystal/glass contacts or by grains that are not thicker than the range of the particle detected. However, with track densities per contour interval determined to only a ten percent standard deviation, interpretation of profile slopes is sometimes ambiguous and we have therefore tried to analyze at least 2-3 grains per synthesis experiment if possible. In the case of large whitlockite crystals for which the number of tracks is large, contouring is not necessary; measurement of track densities versus distance from the crystal/glass interface (profiles) are sufficient to determine the crystal interior track density. Measured D values, D_m, are calculated as the ratio of the crystal interior track density to that of the glass.

FIGURE 8

This figure shows the Pu fission track density for the clinopyroxene contour intervals from Figure 7. The higher track densities for the outer contour interval, V, result from tracks that originated in the glass surrounding the crystal. The glass track density would plot at 48 on the ordinate scale. The track densities of the inner four contours are equal within statistical errors and zoning, as seen in comparison with the calculated zoning profile (constrained to pass through the contour I data point). The ratio of the average track density for intervals I-IV to that of the surrounding glass is the measured crystal/liquid partition coefficient, D_m. Slight zoning is difficult to observe in this crystal, given the relatively large statistical errors on the inner contour intervals.

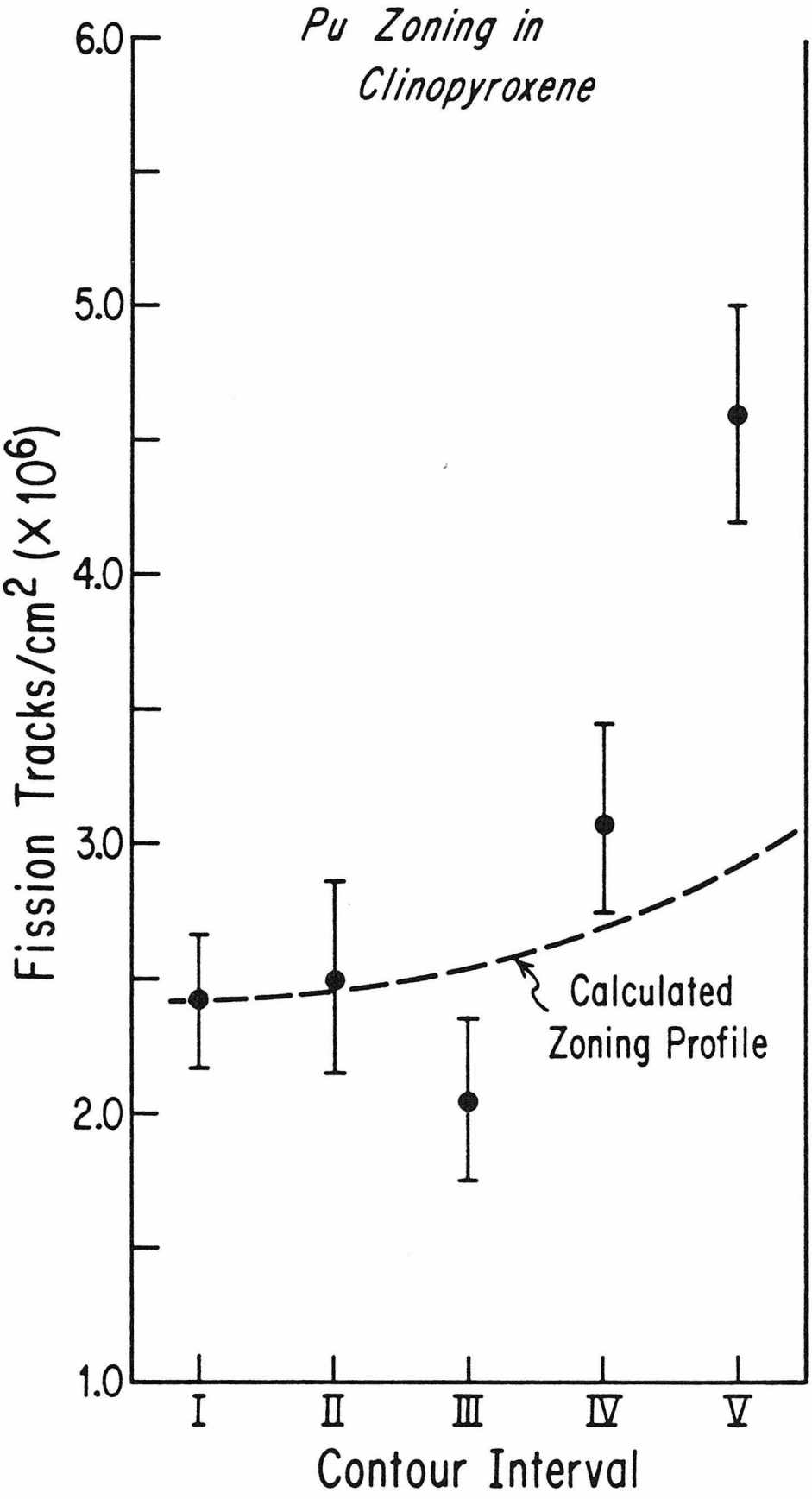
Pu Zoning in
Clinopyroxene
6.0
5.0
4.0
3.0
2.0
1.0
Fission Tracks/cm² (X 10⁶)
Calculated
Zoning Profile
I
II
III
IV
V
Contour Interval

FIGURE 9

^{235}U fission track density as a function of distance from a small (16x100 micron) clinopyroxene grain synthesized at 20 kilobars. The data points are the number of tracks in a strip 6 microns wide (3 microns divisions in the crystal) and parallel to the 100 long micron edge of the crystal. This sample was quenched immediately upon reaching the final temperature at the end of the linear cooling stage in the thermal history (Table 2). There is no gradient in the glass track density in the direction away from the crystal/glass interface except that due to the finite fission fragment range, supporting the assumption that actinide diffusion in the liquid is fast compared to crystal growth. This is typical of many such profiles
The track density in the crystal drops sharply from the glass interface, however. This type of profile is described as 'soft' in that a constant interior track density is never reached (because the grain width is not large compared to the fission fragment range). The lowest track density measured in the crystal (~.08 of the glass) is still much higher (factor of 40) than that obtained in larger crystals (0.002 of the glass track density).

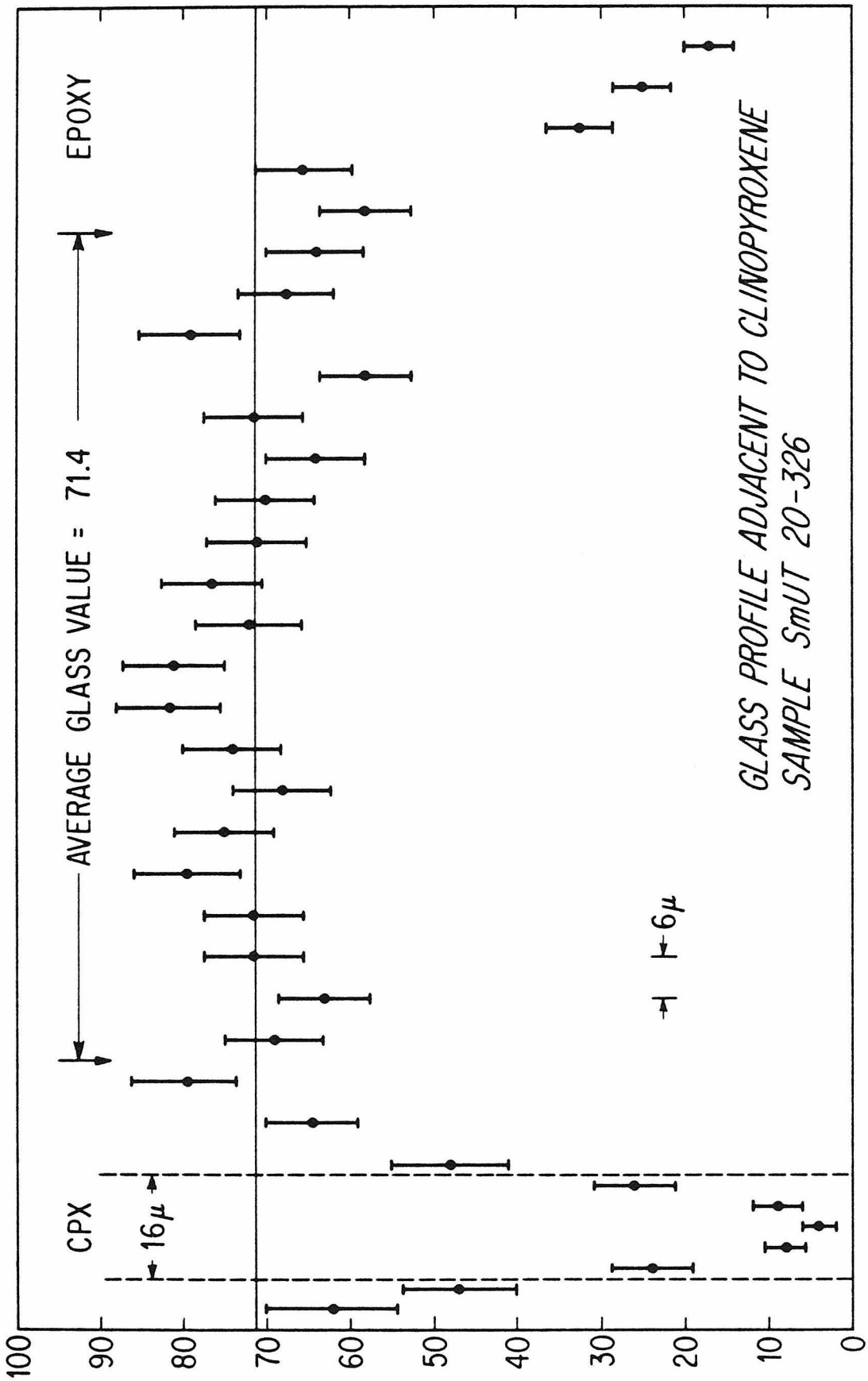
GLASS PROFILE ADJACENT TO CLINOPYROXENE
SAMPLE SmUT 20-326
AVERAGE GLASS VALUE = 71.4
EPOXY
CPX
16μ
6μ
100
90
80
70
60
50
40
30
20
10
0

ii. Track Range Corrections

The mean mass/unit area (i.e., mg/cm^2) traversed by an alpha particle or fission fragment is by definition the 'range' of that particle. The measured track densities are proportional to the detected particles range as well as the actinide concentration. For materials of different compositions, such as the clinopyroxene, whitlockite, apatite, and coexisting glass produced in this study, the various ranges of a given particle in each phase will result in slightly differing volumes (and thus, differing numbers of atoms) contributing to the tracks observed in the detectors.

For the fission fragments, a small correction (maximum 6%, Appendix IV) has been applied to the partition coefficients based on the empirical (Mory et al., 1970) proportionality between range in pure elements and $Z^{\frac{1}{2}}$, where Z is the atomic number. This relationship is consistent with the heavy ion ranges calculated by Northcliffe and Schilling (1970). Little difference results if the exponent is varied, based on Northcliffe and Schilling, from 0.4 to 0.6. An error corresponding to this variation in exponent is propagated into the tabulated, final errors (Tables 8, 9, 10, 11, and 12).

The alpha particle ranges and corresponding partition coefficient corrections were calculated from the alpha particle ranges in pure elements (Northcliffe and Schilling, 1970; Friedlander et al., 1964; Appendix IV).

iii. Microprobe Data

As an example, phase compositions for a 20 kilobar experiment with a relatively high degree of crystallization (44%) are given in Table 6. (Starting material compositions are given in Appendix III and are discussed in Section III-E). The observed minor constituents are typical for these minerals, except that a small amount of P is consistently seen in the diopsidic clinopyroxene. (The tabulated compositions are an average of two sets of microprobe data taken six months apart, which slightly increases the observed standard deviations relative to a single data set). P-bearing clinopyroxenes have also been reported by McSween (1976) for a lunar soil fragment. In this study, the P in the clinopyroxene may have been incorporated into the crystal structure as a consequence of growth in a very P-rich melt. Alternatively, some trapped liquid could be present within the pyroxene crystals; this is discussed further below. A reasonable pyroxene structural formula, $NaMgPSiO_6$, can be postulated as an end member component.

The presence of chloroapatite reflects a small amount of Cl contamination in one of the starting materials, probably from incomplete volatilization of the chloride spiking solution. The apatite is of a very unusual composition, being halogen deficient and silica rich. Because of the anhydrous conditions from which the apatite was synthesized, it is unlikely that the remainder of the halogen sites unfilled by Cl are instead OH groups. The possibility of natural oxyapatites as well as oxyapatite synthesis (Ito, 1968) has been discussed in the literature (Portnov et al., 1970; Young and Munson, 1966; McConnell and Hey, 1969) and the synthetic apatites may actually be chloro-oxy-apatites. Since the apatites are a minor part of this

TABLE 6

Microprobe Phase Analyses for a Single 20 Kilobar Synthesis Run (UTh20-266). Relative Atomic Proportions (x 100)(e)

	Whitlockite (14)(b)	Diopside (17)	Apatite (5)	Glass (11)
Na	1.37±0.10	1.90±0.16	0.91±0.14	6.03±0.32
Mg	4.84±0.23	20.62±0.87	1.27±0.05	5.41±0.14
Al	0.15±0.08	7.49±0.81	0.54±0.06	17.11±0.46
Si	0.35±0.07	46.87±0.58	4.77±0.29	45.40±0.40
Ca	54.02±0.94	22.92±0.80	58.52±0.76	21.74±0.89
Fe	BDL(a)	BDL	BDL	0.07±0.05
P	39.19±0.63	0.12±0.07	33.91±0.43	4.23±0.10
F	BDL	BDL	BDL	BDL
Cl	BDL	BDL	3.37±0.39(e)	0.03±0.02
Wt. % Total(c)	99.18±1.61	100.72±0.91	98.61±0.56	98.91±1.76

(a) Below Detection Limit: standard deviation ≥100%
(b) Number of points analyzed
(c) <0.03 atomic percent: Y, Ce, La, Nd
(d) Errors are 1 standard deviation estimated from the spread in the individual analyses and reflect the extent of variations due to zoning
(e) Cations total to 100%, halogens are in relative atomic proportions

study, further characterization has not been attempted (see Section III-J).

The synthetic whitlockites are enriched in Na and Si relative to natural whitlockites, but fit within the compositional range of phosphate end members defined by Dowty (1977). From the $Ca_3(PO_4)_2$-$Mg_3(PO_4)_2$ phase diagram of Ando (1957a,b) and powder x-ray analysis, the synthetic whitlockite is the β-polymorph, which is also the natural polymorph found in meteorites and lunar samples (Dowty, 1977). Dowty proposes that lunar and meteoritic, H-free, β-$Ca_3(PO_4)_2$ be called merrillite as distinct from terrestrial, H-bearing, whitlockite. The distinction in H content is not proven although there is a distinct, small, structural difference. The more common name, whitlockite, will be used throughout this study.

The synthetic phases grown at 1 bar (Table 7) contain less Na, Al, and Si substitution as is expected from the well-known behavior of natural and synthetic phases crystallized under differing pressure conditions.

B. Mode Calculations

The last four columns of Tables 1 and 2 give the modes and their standard deviations (percent) for each run as calculated from microprobe data via the least squares routine of Reid et al. (1973) using the average atomic proportions of each phase. These calculated modes are required for the zoning corrections discussed in the next section because crystal settling problems prevent conventional point counts from being used. The presence of apatite in the (20 composition) 8.4 P cation percent (25 weight percent $Ca_3(PO_4)_2$) U+Th 20 kilobar runs probably reflects Cl contamination from spike solutions. For each run,

TABLE 7

Microprobe Phase Analyses for Two 1 Bar Synthesis Run
Relative Atomic Proportions (x 100)(e)

	14A-4A (28% crystals)		15A-1Co (8% crystals)	
	Diopside (4)(b)	Glass (4)	Whitlockite (4)	Glass (6)
Na	0.31±0.04(d)	6.66±0.20	0.50±0.07	3.99±0.08
Mg	23.92±0.17	7.54±0.12	5.32±0.09	10.00±0.12
Al	3.50±0.25	19.12±0.20	BDL	12.94±0.14
Si	49.09±0.17	51.74±0.33	0.28±0.04	42.71±0.27
Ca	23.14±0.21	14.93±0.12	55.11±0.14	24.74±0.13
P	BDL	BDL	38.75±0.32	5.59±0.16
F	BDL(a)	BDL	BDL	BDL
Cl	BDL	0.89±0.01	BDL	0.06±0.01
Wt. % Total(c)	101.84±0.32	102.33±0.55	97.76±0.94	97.39±0.46

(a) Below Detection Limit: standard deviation ≥100%
(b) Number of points analyzed
(c) <0.03 atomic percent: Fe, Ni, U, Co
(d) Errors are 1 standard deviation estimated from the spread in the individual analyses and reflect the extent of variations due to zoning
(e) Cations total to 100%, halogens are in relative atomic proportions

all combinations of five crystalline phases (whitlockite, apatite, clinopyroxene, olivine, and plagioclase) were tried in the mode calculation. Only the best fit result is given in Tables 1 and 2.

Runs 12-267 and 30-269 are special cases in that, for 12-267, a series of power failures resulted in several unintentional quenches and restarts, and therefore 12-267 has a complicated thermal history. Run 30-269 temperature determinations are uncertain due to spurious emf produced by leakage of H_2O into the cold junction assembly.

There is variability in the amounts of crystallization shown in Table 2 which does not simply reflect variations in T_f. There are two reasons for this: (a) a new batch of thermocouple wire was used for runs after number 20-306. According to Mao et al. (1971) calibration errors in W3%Re vs. W25%Re thermocouples could amount to 1.5%, equivalent to 20°C at 1375°C. This can account for the much larger amount of crystallization for sample 20-326 compared to 20-288 although both have T_f = 1390°C. (b) The thermocouple was sheared off in disassembling the press; consequently a new portion of the thermocouple wire was used for each run. For the same batch of wire, Mao et al. estimate that variability could be as high as 1%. This can account for smaller differences in crystallization, e.g., between 20-211 and 20-266.

The problems of precise reproduction of temperature in experimental synthesis runs at high pressure are not confined to W3%Re/W25%Re type thermocouples. According to Mao et al. (1971), at 20 kilobars, the standard S-type(Pt/Pt10%Rh) thermocouple precision errors can be twice that of the W3%Re/W25%Re type as well as exhibiting substantial emf drift at high, sustained, temperatures. However, at 1 bar the S-type thermocouple is a factor of two better and is

much easier to use than is the W3%Re/W25%Re type used for the 20 kilobar experiments.

Sample 10-293 has two distinct modes (Table 2) for the two sample mounts, whereas all other samples with two or more mounts yield only a single mode. The two modes for 10-293 indicate that different parts crystallized the same phases but to a different extent. This is most easily explained as a result of a thermal gradient (10-15°C) over the sample during the piston-cylinder run due to a small displacement of the sample from the center of the furnace assembly. This sample was quenched immediately after reaching the final temperature so the final liquids could not homogenize.

The experimental run conditions and modes at 1 bar are tabulated in Table 1. At 1 bar, the modes should be in better agreement with the final temperatures than is the case of the 20 kilobar data (Table 2) discussed above. The S-type thermocouple is also used repeatedly without replacement at 1 bar whereas the 20 kilobar experiments require a new junction for each run. Reproducibility of the furnace temperature at initial furnace power settings indicates that S-type thermocouple drift is negligible. However, additional complications come into play at 1 bar which affect the extent of crystallization: 1) Occasionally a run will be contaminated by the buffer as is the case for UTh20A-2Co, the blue color is from the cobalt buffer which has the effect of lowering the liquidus (analogous to Fe). Otherwise, the modes for samples 20A-1Co and 20A-2Co, which have the same T_f, agree well. 2) Olivine crystalliza-

tion may be indicated by the mode calculation (but not observed in any run nor indicated for any 20 kilobar run). This is not unexpected in that olivine frequently forms metastably in these types of experiments (Walker et al., 1978). 3) Plagioclase, which is present in two (31 composition) runs and is calculated to be present in several more, is well known to resist nucleation even at large (200°C) undercoolings (opposite the behavior of olivine)(Kirkpatrick, 1974; Kirkpatrick et al., 1976). This may have an effect on the appearance and abundance of other phases (see 31-1A vs. 31-10Co, Table 1). 4) The higher viscosity at 1 bar (Kushiro, 1976; Kushiro et al., 1978) may result in more liquid heterogeneity (see Section III-E). Fortunately the presence (or absence) of a few percent of olivine or plagioclase does not induce inordinate errors in the corrections nor in the modes of the principle phases, whitlockite and clinopyroxene. More importantly, zoning corrections are small for the 1 bar runs because the amounts of crystallization are small, therefore the necessity for knowing precise modes is removed.

C. Zoning Corrections

Experiments reported by Seitz (1973) indicate that, for any practical laboratory time scale, actinide diffusion in the crystalline phases is negligible. Thus, the bulk actinide concentrations in the crystals and glass are not equilibrated in the traditional sense; nevertheless, if crystal growth is not too rapid, and diffusion in the melt is sufficiently rapid to maintain a homogeneous melt during crystal growth, it is reasonable to expect equilibrium partitioning at the crystal/melt interface with a well-defined partition coefficient

(D). For D significantly different from 1, the melt actinide concentration will systematically change with the amount of crystallization which will in turn lead to actinide zoning in the crystalline phases. The observed zoning may also, in part, be due to the linear cooling utilized in our synthesis experiments as partition coefficients are generally temperature and composition dependent. Additionally, the zoning profiles may be altered by the appearance of subsequent, subliquidus, phases as temperature is decreased although, in this study, it is assumed that all phases crystallize simultaneously in constant, modal, proportions. The assumption of modal co-crystallization (Appendix V) can be checked using the calculated modes from the 20 composition, 20 kilobar, experiments. Figure 10 supports this assumption in that clinopyroxene is about 1.67 times as abundant as the sum of whitlockite and apatite. This assumption is made to simplify the zoning correction calculations (Appendix V). In many cases for small amounts of crystallization, which is the case for the example shown in Figure 8, the zoning is expected to be small and, for small values of D, it is difficult to detect with the statistical errors applicable to the different contour intervals. However, distinct zoning is observed for the minor elements, as illustrated in Figure 11. This figure shows the results of averaging microprobe analyses at different points (~200 points total) within the contour intervals shown in Figure 7. As pyroxene crystallization proceeds, the concentrations of Na, Al, and P in the melt increase (only 0.5% whitlockite crystallized in this experiment). The concept of a well-defined partition coefficient implies that the concentrations of these elements at any point in the crystal are proportional to the concentrations in the liquid at the time when

FIGURE 10

The assumption of modal co-crystallization is checked by plotting the calculated modal abundances of the phases present in the 20 composition, 20 kilobar experiments. The plot of whitlockite plus apatite versus clinopyroxene results in a roughly linear array that appears to be constrained to pass near the origin, in essential agreement with the zoning correction model assumption of modal co-crystallization.

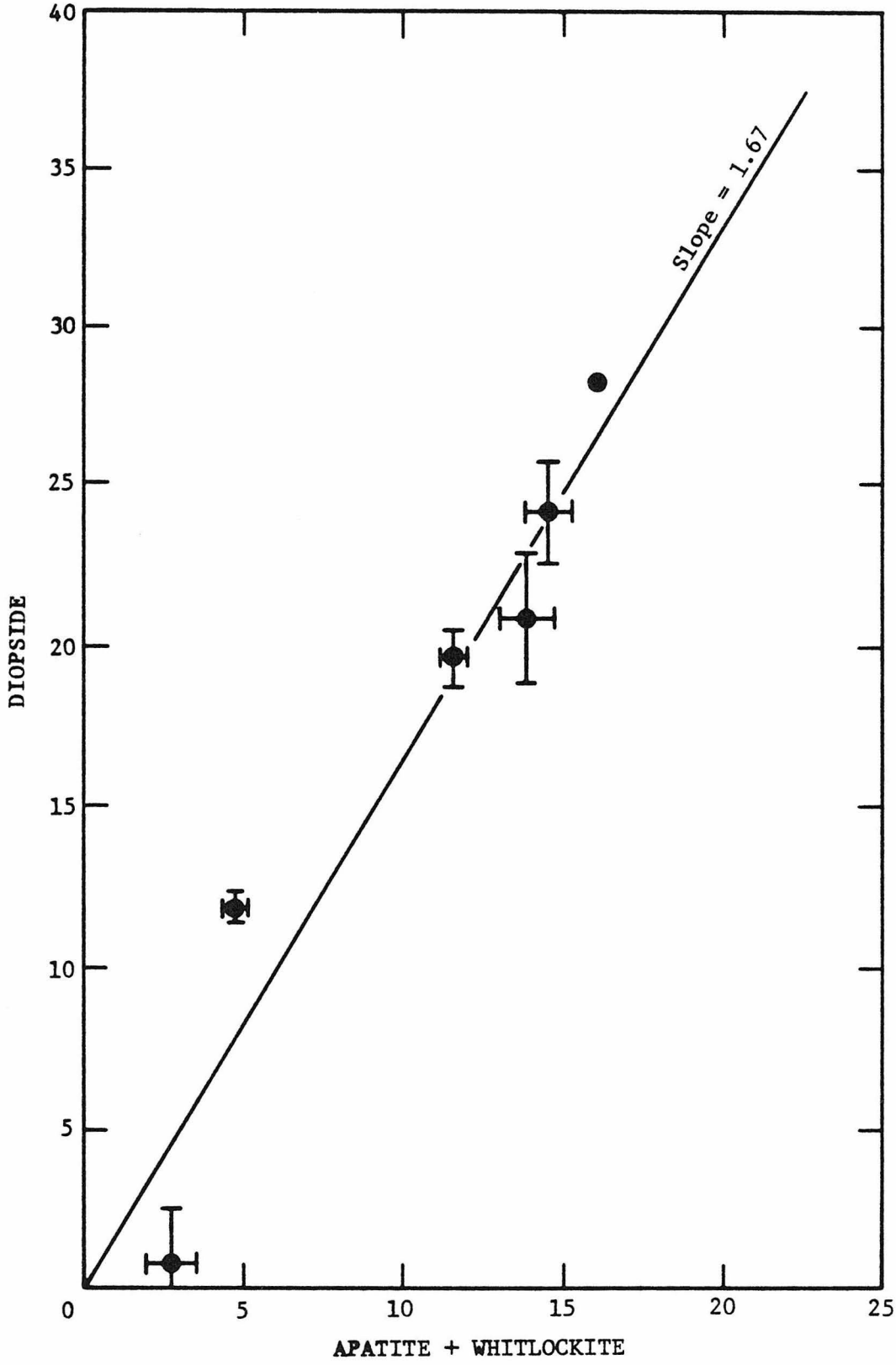
40
35
30
25
20
15
10
5
0
5
10
15
20
25
DIOPSIDE
APATITE + WHITLOCKITE
Slope = 1.67

FIGURE 11

Average minor element contents for the contour intervals illustrated in Figure 7. The data were obtained from about 200 total points within the grain imaged in Figure 6 and have good statistical precision even for the P_2O_5, which is present in very low levels. The bulk partition coefficients for all three elements are less than one, so concentrations increasing from core (I) to rim (V) are expected, if diffusion in the crystal (which would flatten the profiles) and if the effects of changing temperature, and melt compositions are negligible. The Na_2O zoning profile agrees well from what would be expected (Hollister, 1966) for the amount of crystallization of this sample. The amount of Al_2O_3 zoning is larger than expected, reflecting either a strong dependence of D_{Al}(cpx) with temperature, or melt composition. The P_2O_5 zoning is anomalous, it probably reflects a marked temperature dependence of D_P(cpx) or the effect of changing melt composition.

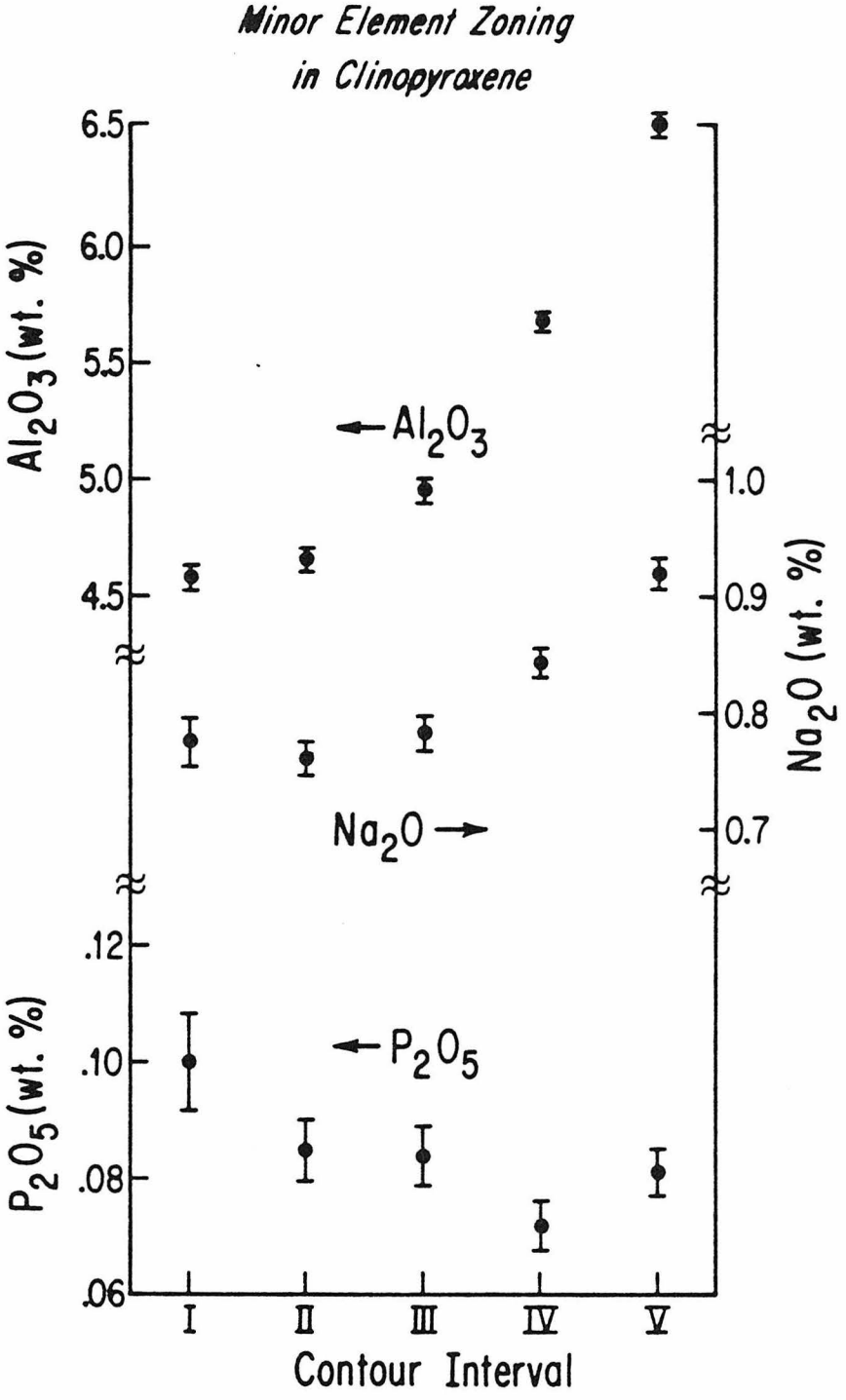
Minor Element Zoning
in Clinopyroxene
6.5
6.0
5.5
5.0
4.5
Al_2O_3 (wt. %)
Al_2O_3
Na_2O
1.0
0.9
0.8
0.7
Na_2O (wt. %)
.12
.10
.08
.06
P_2O_5 (wt. %)
P_2O_5
I
II
III
IV
V
Contour Interval

that point was on the crystal-liquid boundary, thus concentrations of these elements are expected to increase from core to rim. However, the P_2O_5 concentrations, if anything, decrease from core to rim. This may be due to a decreasing D value for P with decreasing temperature during crystal growth. The effect of ~1% submicroscopically-dispersed glass in the grain core could also cause the relatively high P content of the crystal core although no glass is observed. This amount of dispersed glass would cause an ~20% increase in the core Pu content and, although this is not inconsistent with the Pu track profile (Figure 8), the increase is not statistically significant. The low P_2O_5 concentration for interval V shows that glass contributions to the measured Na_2O and Al_2O_3 concentrations in this interval are negligible. The Na_2O zoning profile is close to that calculated (compare Hollister, 1966) for a uniformly growing single crystal which nucleated on the liquidus; however, the Al_2O_3 profile is steeper, suggesting that D_{Al}(cpx) increases with decreasing temperature. Secondary x-ray fluorescence from Al in the glass adjacent to the crystal cannot account for the magnitude of the observed increase (Wittry, 1959; Reed and Long, 1963).

The distinct minor element zoning strongly argues that actinide zoning is also present. Thus, a correction is required to the measured actinide partition coefficient, D_m. D_m is defined as the average track density of the fraction of the crystal interior which was analyzed divided by the glass track density. D_m differs from the interface (true) D because of the zoning. An exact correction is not possible because it is not known at what point the grain nucleated during the slow cooling and because the location and orientation of the section

plane through the crystal is not known. In Benjamin et al., (1978) an approximate correction was made assuming that the interior track density represented the average of the crystal (using Equation 14 in Albarede and Bottinga, 1972); however, as discussed in Benjamin et al. (1978), this approximation will tend to undercorrect for zoning. An alternative approach is used here in which the approximations made in deriving the correction factor lead to an over correction (Appendix V), thus bracketing the true D between the measured D_m and the over corrected or limiting value, D_1. One simple approach is to assume that the measured crystal track density corresponds to the core and correct according to a calculated (^{rim}/core) zoning ratio, since the true D = ^{rim}/glass. However, for some runs this is a large correction (up to 60%); consequently, in order to put tighter constraints in D, a more complicated calculation of D_1 has been adopted. This calculation assumes: (1) the analyzed crystal nucleated on the liquidus and grew uniformly (i.e., same shape at all stages of growth) until the final temperature (T_f). (2) The section analyzed is a central section which includes the initial crystal nucleus. (3) The area analyzed has the same shape as the crystal outline in the section. (This latter assumption will not be exactly true for the "incremented contour" method of analysis described above (Figure 7); consider a long thin rectangular crystal to see this easily). Although none of these simplifying assumptions is valid, the errors all make the derived correction factor too large. For these assumptions the relationship between the analyzed area A, and the associated amount of crystallization, X is: $A/A_f = (X/X_f)^{2/3}$ where A_f is the total crystal area and X_f is the total amount of crystallization. The measured D_m and over

corrected D_l are related in Equation (1) (see Appendix V for derivations):

$$(1) \quad D_{lj} = \frac{q' \, D_{mj} \, [1-X_f]^{(D_b-1)}}{\int_o^{q'} [1-q^{3/2}X_f]^{(D_b-1)} dq}$$

where D_b is the bulk partition coefficient:

$$D_b = \sum_i^i X_i \, D_i / X_f$$

where the sum is over all crystalline phases and X_i is the mode of phase i. The subscript j is added to Equation (1) to emphasize that D_m and D_l apply to a specific phase. q is the fractional crystal area integrated from 0 to q', where q' is the fraction of the total area included in the track analysis (i.e., q' = 1 if analysis could be carried out right up to the crystal-glass boundary). Equation (1) applies to the case of a contour analysis as illustrated in Figure 7. For those cases where D_m was calculated from a "one-dimensional" profile through a large crystal, a modified (one-dimensional instead of two) version of Equation (1) applies in which the factor $q^{3/2}$ in the integral becomes q^3, and q' = the fraction of the strip used to calculate a crystal interior track density. In practice Equation (1) is solved by first approximating $D_i = D_{mi}$, calculating $D_b K$, solving Equation (1) for D_l and then iterating. The values of X_f and X_i are calculated from microprobe analyses of all phases in a given experiment (Tables 1 and 2). Values of D_m and D_l for the experiments listed in Tables 1 and 2 are shown on Tables 8, 9, 10, 11, and 12. The direction of the correction depends on D_b: if $D_b \leq 1$, D_l is an upper limit and D_m

is a lower limit; if $D_b \geq 1$, D_1 is a lower limit and D_m is an upper limit. In Tables 8, 9, 10, 11 and 12, D_m and D_1 are averages over all crystals giving usable track profiles for a given experiment, although D_1 was calculated for each crystal. Ideally, at least two crystals for each experiment are analyzed, but this was not possible in all cases.

D. Data

From the above discussion D_m and D_1 bracket the true D; consequently, the best estimate of D is the mean of D_m and D_1, as shown in Tables 8, 9, 10, 11, and 12. The quoted error on D is $1/2[D_m - D_1]$ or the error in D_m, whichever is larger. In general D values from different 20 kilobar experiments agree well except for D(cpx) for U and Th. These are discussed systematically below. The 1 bar D values are not only in good internal agreement, but also agree well with the 20 kilobar data (at the same fO_2 conditions).

One complication that tends to get lost in the assigned errors in D is that there is better agreement between the uncorrected D_m values for U and Th in the 20 kilobar whitlockite than for the D values after correction (Figure 12). In other words, the D_m values should decrease with increasing amounts of crystallization, whereas they appear to remain constant. Since the factor D_1/D_m is the maximum correction, it is possible that in all cases the crystals analyzed require much less correction than was applied, (i.e., coincidental violations of the model assumptions) but this seems statistically unreasonable. However, the minor element data discussed in a later section indicate that the correction techniques are valid; consequently, at present, the agreement and error bars in D_{Th} and D_U(whit) are accepted at face value,

TABLE 8

Whitlockite Crystal/Liquid Partition Coefficients
(20 kilobar) (a)

Experiment Number	Percent Cryst.	Thorium			Uranium		
		D_m	D_1	D	D_m	D_1	D
20-288	17	1.08±4	1.19	1.13±6	0.50±2	0.57	0.58±4
20-211	35	1.18±7	1.42	1.30±12	0.58±3	0.74	0.66±8
20-326	39	1.19±6	1.50	1.34±15	0.53±2	0.67	0.60±7
20-266	44	1.08±6	1.39	1.23±15	0.54±2	0.79	0.67±12
		Plutonium					
10-293 A	37	3.55±11	3.3	3.4±2			
12-320	45 (b)	4.6±6	3.9	4.2±6			
10-234	44	4.49±16	3.8	4.1±3			

(a) Values tabulated are averages of all crystals yielding acceptable track profiles (see text). Quoted errors apply to last significant figure. Errors in D_m and 1 standard deviation from track counting statistics; errors in D are $1/2[D_1-D_m]$ or error in D_m, whichever is larger.

(b) Estimated.

TABLE 9

Clinopyroxene Crystal/Liquid Partition Coefficients
(20 kilobar) (a)

Experiment Number	Percent Cryst.	Thorium (10^{-3})			Uranium (10^{-3})		
		D_m	D_1	D	D_m	D_1	D
20-326 (c)	39	2.8±6	3.6	3.2±6	1.6±9	2.2	1.9±9
20-266 (c)	44	2.6±6	3.3	3.0±6	2.7±8	3.7	3.2±8
30-231	18	5.1±5	6.1	5.6±5	4.2±4	5.1	4.7±5
30-269	19	1.7±1	2.0	1.9±2	1.7±1	2.1	1.9±2
20-288 (c)	17	3.0±7	3.6	3.3±7	2.3±7	2.8	2.5±7
		Plutonium (10^{-3})					
12-267	7	61±5	63	62±5			
10-293 A (c)	37	66±9	61	64±9			
12-261	14	49±2	52	50±2			
12-320	45 (b)	59±6	50	55±6			

(a) Errors refer to last significant figures (see note a, Table 4)

(b) Estimated

(c) Initial P_o = 8.4 cation percent; all other results are for P_o = 5.3%

TABLE 10

Apatite Crystal/Liquid Partition Coefficients
(20 kilobar)

Experiment Number	Percent Cryst.	Thorium			Uranium		
		D_m	D_1	D	D_m	D_1	D
20-326	39	1.19±18	1.44	1.29±15	1.70±7	2.14	1.92±22
20-266	44				1.40±8	1.80	1.60±20
20-288	17				1.72±7	1.90	1.81±9

TABLE 11

Whitlockite Crystal/Liquid Partition Coefficients
(1 Bar)

Experiment Number†	Percent Cryst.	Thorium			Uranium		
		D_m	D_1	D	D_m	D_1	D
20A-5A	5	1.41±5	1.33	1.37±5	0.43±2	0.44	0.44±2
20A-9A	9	-	-	-	0.0024±4	0.0026	0.0025±4
20A-11A	9	-	-	-	<0.0056±7	0.0061	<0.0059±7
20A-1Co	5	-	-	-	0.48±3	0.49	0.49±3
20A-2Co	5	1.42±6	1.34	1.38±6	0.48±3	0.50	0.49±3
20A-5Co	11	-	-	-	0.52±4	0.55	0.54±4
20A-6Co	10	-	-	-	0.48±3	0.51	0.49±3
40A-1Co	10**	1.39±9	1.29	1.34±9	-	-	-
40A-4Co†	3*	1.31±9	1.25	1.28±9	0.053±7	0.053	0.054±7
30A-6Co	10**	-	-	-	<0.68±3	0.70	<0.69±3
30A-8Co	10**	-	-	-	<0.72±3	0.74	<0.73±3

		Plutonium		
		D_m	D_1	D
10A-1A	10**	0.58±4	0.61	0.59±4
15B-6A	10**	0.73±13	0.75	0.74±13
15B-2Co	9	4.57±26	3.23	3.9±7
15B-4Co	10**	4.29±20	3.23	3.8±5
15B-6Co	10	4.89±36	3.27	4.1±8

TABLE 11 (continued)

† See footnotes on Table 1 for explanation of buffer conditions.

* Pinhole leak in Pt capsule resulted in complete oxidation of the Co-CoO buffer so the fO_2 is between air and $10^{-8.5}$.

** Assume 10% crystallization.

TABLE 12

Clinopyroxene Crystal/Liquid Partition Coefficients
(1 Bar)

Experiment Number	Percent Cryst.	Plutonium		
		D_m	D_l	D
14A-2HM**	20[xx]	0.016±3	0.020	0.018±3
14A-5A[†]	20	<0.043±9	0.053	<0.048±9
14A-1Co[x]	20[xx]	0.162±8	0.195	0.179±16
14A-7Co[x]	13	0.142±20	0.160	0.151±20

[x] Co-CoO oxygen buffer

[xx] Assume 20% crystallization

[†] Capsule open to air

** Hematite-magnetite oxygen buffer

FIGURE 12

The uncorrected (D_m) partition coefficients for U and Th in whitlockite at 20 kilobars are in better agreement than the corrected (D_l) values although the converse is expected to be true for the model of modal co-crystallization and Rayleigh (trace element) partitioning. An example of the expected trend is given by the line passing through the D_{Th} and D_U(whit) values with the least amount of crystallization. The Th data are offset horizontally to aid visibility. Note the difference in scale. At present this difference is unresolved and awaits future experiments for elucidation.

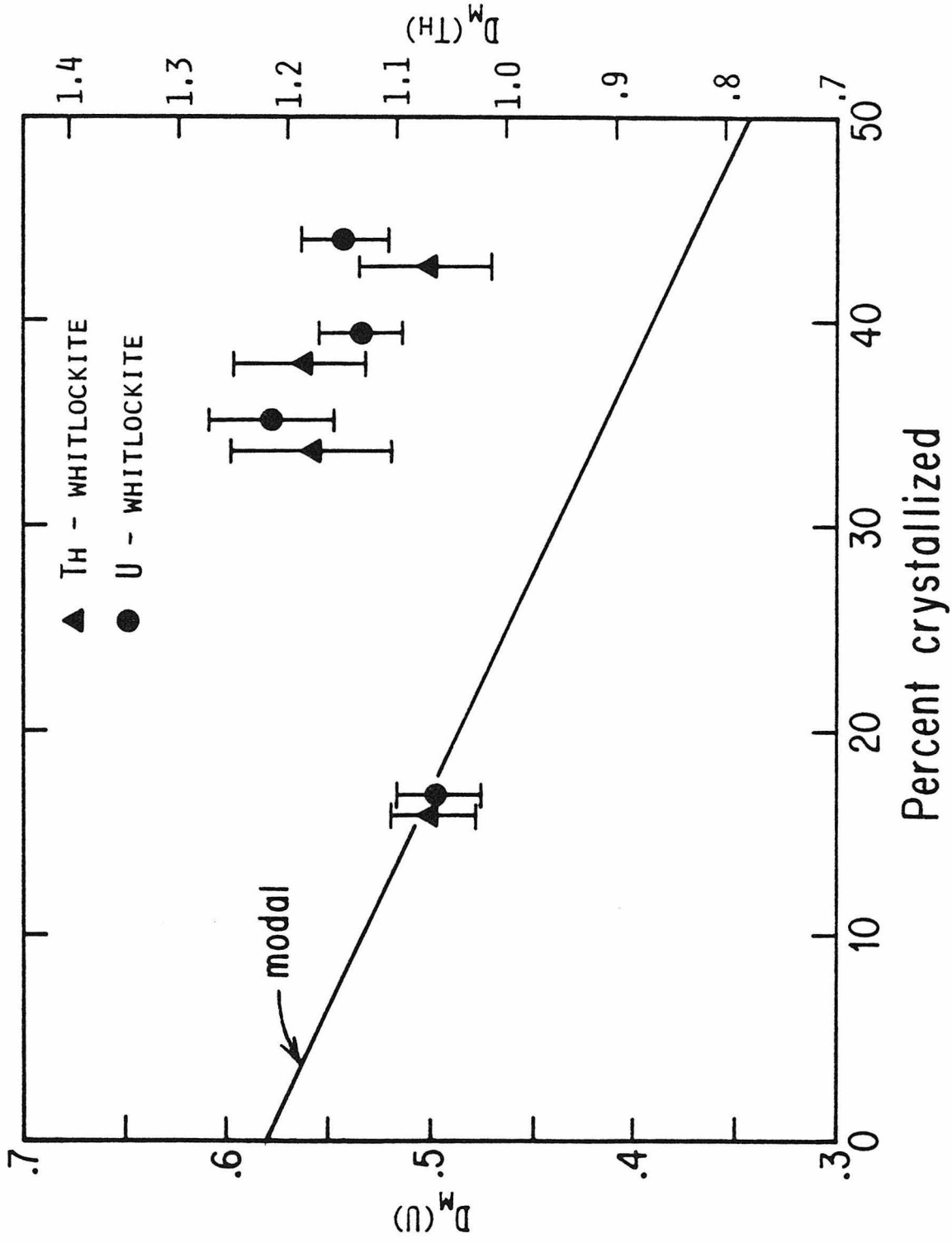
$D_M(U)$
$D_M(T_H)$
Percent crystallized
modal
▲ T_H - WHITLOCKITE
● U - WHITLOCKITE
.7
.6
.5
.4
.3
1.4
1.3
1.2
1.1
1.0
.9
.8
.7
0
10
20
30
40
50

although future work must re-examine the effect of crystallization on these partition coefficients. Conceivably, variations of D with changes in temperature and melt composition are roughly cancelling the effects of zoning.

E. Equilibrium

The partition coefficients discussed above are valid if equilibrium partitioning at the crystal/melt interface has been maintained, but this is an assumption which should be tested. The problems of possible metastable olivine crystallization and supercooling with respect to plagioclase crystallization in the 1 bar runs indicate a lack of total phase equilibrium; however, the question of interface equilibrium partitioning is not constrained by nucleation problems with these phases, and may be treated as a separate equilibrium problem.

Four tests, necessary but not sufficient to prove equilibrium partitioning, have been used in evaluating the experimental runs and the partitioning data acquired from them. These tests are based on the hypothesis that most disequilibrium effects would not be reproducible from crystal to crystal, from experiment to experiment, or upon variation of experimental conditions. The degree to which the data represent equilibrium are evaluated on: 1) absence of actinide zoning in the coexisting glass; 2) independence of the results on experimental conditions, especially cooling rate; 3) reproducible actinide partition coefficients; and 4) reproducible partition coefficients for the minor elements, allowing for zoning.

i. Glass Homogeneity

The mode calculation required for the zoning corrections to be made on the minor and trace elements in a particular phase from any given run assumes that the glass starting material is homogeneous and that the coexisting silicate liquid remains homogeneous during the synthesis run. This latter assumption is also important to the general question of interface equilibrium. As previously mentioned, the initial Pu spiked starting materials (compositions 10, 11, and 12) contained relict crystals, so in a comparison of different runs, homogeneity may not be obtained. However, the superliquidus times and temperatures were chosen to melt these relict crystals, and the compositions given in Appendix III show little variation outside that expected from typical microprobe errors (Champion et al., 1974). Al and P show the largest magnitudes of inhomogeneity in the quench glasses although Ca inhomogeneity, relative to the very low expected (0.1 to 0.4%, counting statistics) standard deviations, is common. These starting material heterogeneities are acceptable, though far from ideal, and, excluding the previously mentioned 10, 11, and 12 compositions, are probably the result of insufficient numbers of grinding and fusing cycles (Hofmann and Margaritz, 1977).

Microprobe analyses of glass taken both near (20–30 microns) and far (up to mm) from crystals show that no significant heterogeneities exist at 20 kilobars, but small heterogeneities, especially in Al and P (standard deviations=4 to 6 times counting statistics), do occur over a mm scale in the 1 bar runs. This may be the result of incomplete diffusive/convective re-equilibration of these elements in the liquid during crystal growth or it may be inherited from the starting materials. The inhomogeneity seen in sample 293 (Table 2)

is unusual and, as discussed earlier (Section III-B), does not yield a unique mode.

The difference in homogeneity between synthesis runs at the two pressures is probably the result of the factor of ten lower viscosity at the higher pressure and correspondingly higher temperature (Kushiro, 1976; Kushiro et al., 1976). Diffusion coefficients are (approximately) inversely proportional to viscosity (Donaldson, 1975) as are convection rates. Any initial heterogeneities in the starting materials appear to be well homogenized during the 20 kilobar synthesis runs, whereas the higher viscosity of the 1 bar runs hinders the homogenization of both the inherited and crystallization induced inhomogeneities, although the data in Appendix III suggest that the 1 bar heterogeneities are mainly due to crystallization. The diffusion coefficients of Hofmann and Margaritz (1977) are 10^{-6} to 10^{-7} cm^2-sec^{-1} for divalent cations in an olivine tholeiite melt at 1 bar pressure and 1450°C (the initial temperature of the 20 kilobar runs). Taking the higher diffusion coefficient for the 20 kilobar runs and the factor of ten lower value for the 1 bar runs; then in 24 hours (roughly the duration of a synthesis experiment) divalent cations at 20 kilobars will diffuse a characteristic distance of 3 mm = $(Dt)^{\frac{1}{2}}$, the scale of the experimental charge, whereas the characteristic distance at 1 bar is only 1 mm. Of course convection affects this problem in aiding mixing of the liquid thereby reducing heterogeneities.

An important distinction to be made is that the divalent cations in the experimental charges are generally homogeneous; it is the Al and P that are most often heterogeneous. The divalent cations are considered 'network modifiers' in contrast to 'network formers', Al, Si, and

P (Bottinga and Weill, 1972). It is likely that the diffusion coefficients are significantly lower for the ions involved in the extended 'network' relative to the ions that terminate or exist independently from 'network' chains. This appears to be the case for the samples in this study. Si appears more homogeneous than Al and P, probably because the greater abundance of Si minimizes the percentage change during crystallization. The clinopyroxenes do not markedly disturb the local Si concentrations (D_{Si}(cpx) = 1), and the Si is involved in several components of the starting materials (Appendix I) and is therefore more homogeneous initially.

In the liquid phase the actinides must be nearly homogeneous at all times in order for accurate measurement and correction of the trace element partition coefficients to be made. The large, highly charged, actinides are likely to be 'network modifiers' rather than 'network formers', so the above discussion of divalent cation behavior should apply. Seitz (1974) showed that for cooling rates of about 600°/hour, thorium diffusion in the liquid is slow compared to crystal growth rates and "halos" of high Th concentration were observed in the glass surrounding the crystals. This result has dictated the type of thermal history and the choice of cooling rates used in the synthesis experiments. In general, the glass actinide contents are homogeneous for a given experiment with one standard deviation counting statistic per point analyzed (typically 10-20 microns in dimension) of 5-15%. Careful checks for gradients in the glass track density around crystals were made, examples of which are shown in Figure 9 (20 kilobars) and Figure 13 (1 bar). These samples were chosen because they were quenched at the end of the slow cooling cycle ($t_f \approx 0$) before any

FIGURE 13

^{239}Pu fission track density as a function of distance from a large (150 micron wide) clinopyroxene grain synthesized at 1 bar. The data points are the number of tracks in a strip 4.6 microns wide and parallel to the long edge of the crystal. This sample was quenched 0.7 hours after reaching the final temperature at the end of the linear cooling stage in the thermal history (Table 1). There is no gradient in the glass track density in the direction away from the crystal/glass interface except that due to the finite fission fragment range, supporting the assumption that actinide diffusion in the liquid is fast compared to crystal growth. The average glass track density given in this figure agrees with the glass track density obtained from several random areas of the glass in this run. The track density in the crystal drops sharply from the glass interface and, although the data in this figure are not extended into the interior of the crystal, forms a good, sharp, profile.

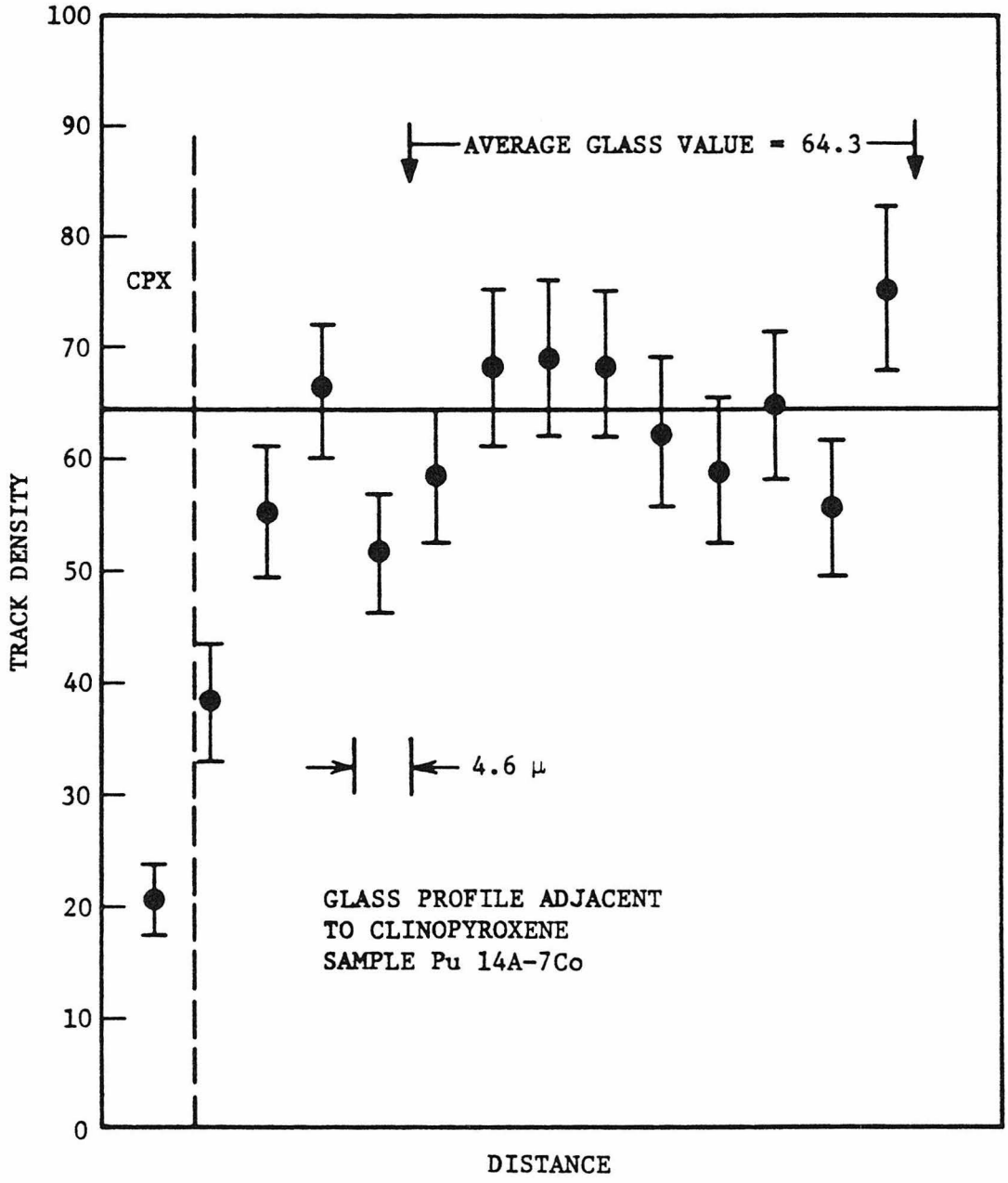
100
90
80
70
60
50
40
30
20
10
0
TRACK DENSITY
AVERAGE GLASS VALUE = 64.3
CPX
4.6 μ
GLASS PROFILE ADJACENT
TO CLINOPYROXENE
SAMPLE Pu 14A-7Co
DISTANCE

gradients in the glass could diffuse away. As can be seen in Figures 9 and 13, the glass track densities do not increase, within counting statistics, right up to the crystal-glass boundaries, demonstrating actinide melt homogenization.

It is concluded that, overall, the actinides are well homogenized and that the assumptions made in measuring and correcting the actinide partition coefficients are justified, and that the heterogeneities in major elements in the starting materials and the 1 bar runs are unimportant although not ideal.

ii. Reproducibility of Actinide Partition Coefficients at Variable Cooling Rates

Figures 14, 15, and 16 are crystal by crystal displays of the uncorrected D_m values plotted versus cooling rate for the 20 kilobar (Figure 14) and 1 bar experiments (Figures 15 and 16). The error bars, one standard deviation track counting statistics, vary considerably depending on the value of D and on crystal size; the standards for reproducibility vary accordingly.

The 20 kilobar crystal by crystal data are shown on Figure 14. The whitlockite D values agree reasonably well for all cooling rates except possibly for Pu. It is conceivable that some intrasample variations can be explained by zoning effects (e.g., the plane of the crystal analyzed corresponds to the surface of the crystal rather than a cross-section through the interior of the crystal) and some intersample variations result from differing degrees of crystallization. The averages of the whitlockite data from each of these runs are given in Table 8 for comparison.

FIGURE 14

This is a crystal-by-crystal display of uncorrect 20 kilobar D_m values plotted versus cooling rate. Grains from the same sample have been displaced horizontally to aid visibility. The errors shown are standard deviations from counting statistics which range from the size of the plotted point to about 80 percent of the D_m value depending on the magnitude of the partition coefficients and on crystal size. At low cooling rates, the D values obtained in duplicate experiments usually agree but at higher cooling rates there is more scatter and, in clinopyroxene, the D values appear systematically higher, which probably means that equilibrium at the crystal melt interface was not obtained in the high cooling rate experiments.

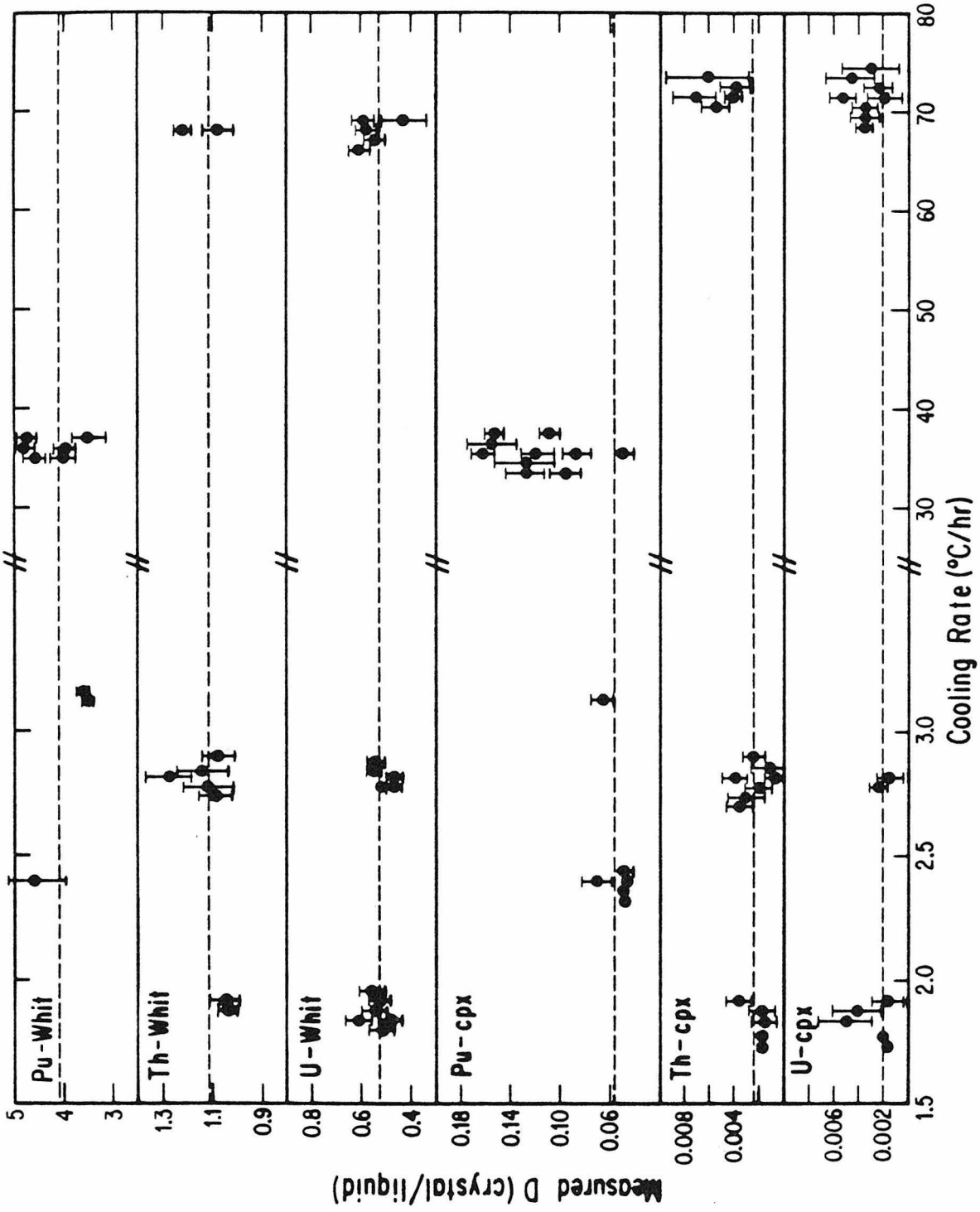
Pu-Whit
Th-Whit
U-Whit
Pu-cpx
Th-cpx
U-cpx
Measured D (crystal/liquid)
Cooling Rate (°C/hr)

FIGURE 15

This is a crystal-by-crystal display of uncorrected 1 bar whitlockite D_m values plotted versus cooling rate. Grains from the same sample have been displaced horizontally to aid visibility. Points plotted as upper limits are discussed in the text.

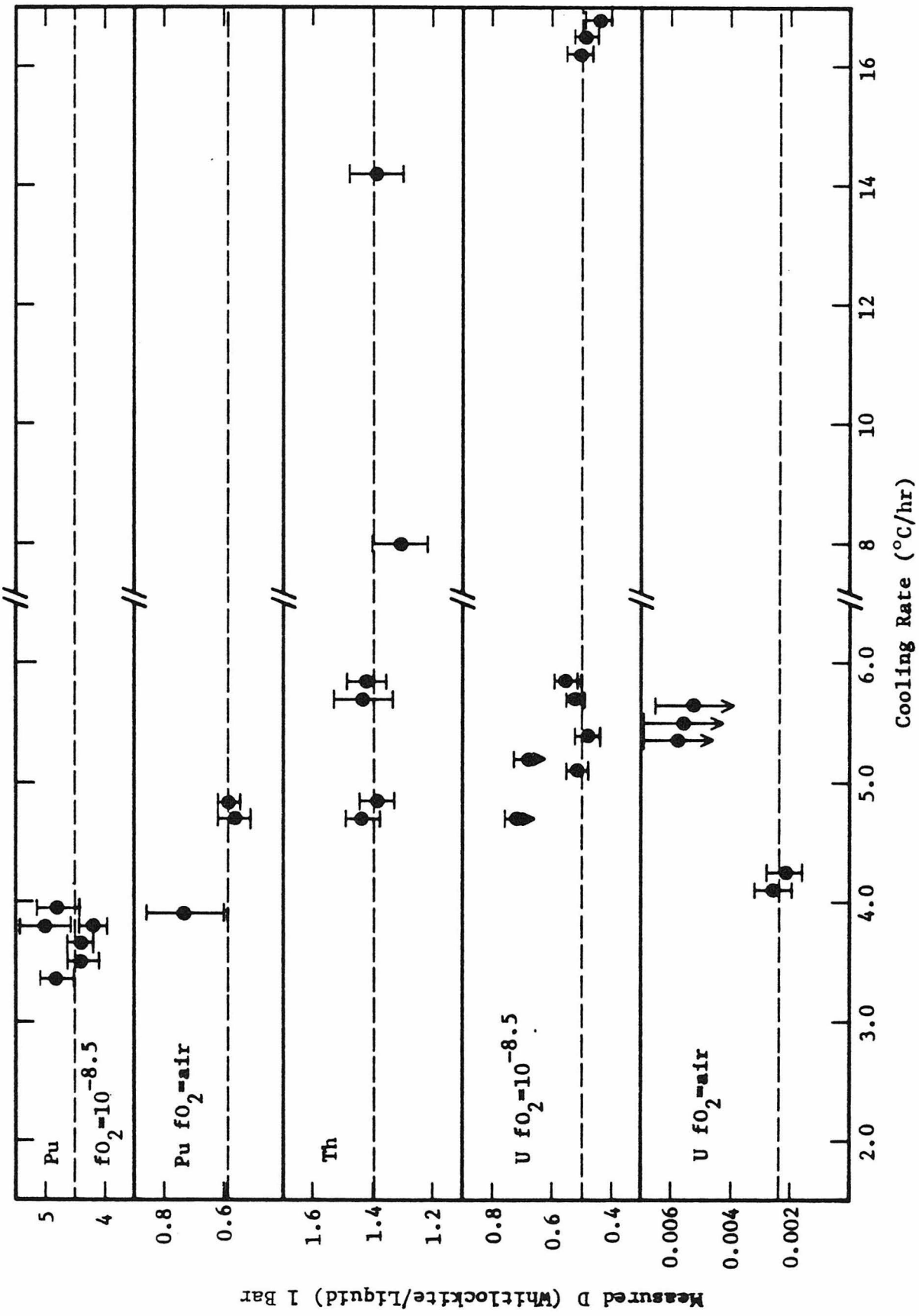
Pu
$fO_2=10^{-8.5}$
Pu fO_2=air
Th
U $fO_2=10^{-8.5}$
U fO_2=air
Measured D (Whitlockite/Liquid) 1 Bar
Cooling Rate (°C/hr)
5
4
0.8
0.6
1.6
1.4
1.2
0.8
0.6
0.4
0.006
0.004
0.002
2.0
3.0
4.0
5.0
6.0
8
10
12
14
16

FIGURE 16

This is a crystal-by-crystal display of uncorrected 1 bar clinopyroxene D_m values plotted versus cooling rate. Grains from the same sample have been displaced horizontally to aid visibility. Points plotted as upper limits are discussed in the text.

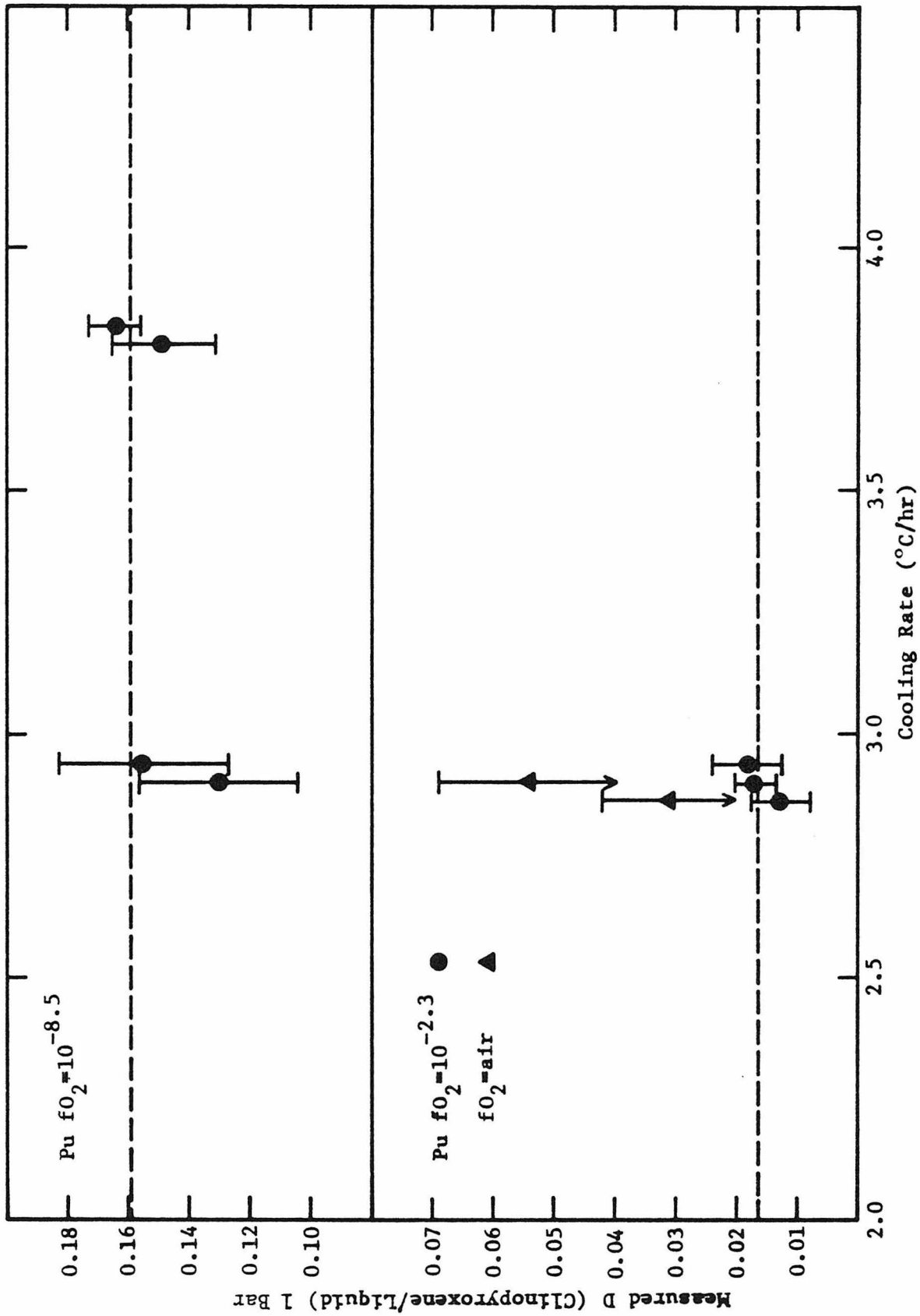
Measured D (Clinopyroxene/Liquid) 1 Bar
0.18
0.16
0.14
0.12
0.10
0.07
0.06
0.05
0.04
0.03
0.02
0.01
Pu fO_2=$10^{-8.5}$
Pu fO_2=$10^{-2.3}$
fO_2=air
2.0
2.5
3.0
3.5
4.0
Cooling Rate (°C/hr)

The D_m(cpx) in Figure 14 show more scatter, in part reflecting the larger errors for smaller D_m values. The high D_{Pu}(cpx) values at high cooling rates are for small grains and should be regarded as upper limits due to 'soft' profiles. These data are not tabulated in Table 9. However, as discussed below, disequilibrium at high cooling rates is also likely. The measured D_{Pu}(cpx) value of 0.066 for sample 293 (Table 9) is from an experiment using the 25% $Ca_3(PO_4)_2$ starting material which had co-crystallizing whitlockite and a bulk partition coefficient greater than one, resulting in a zoning correction opposite that of the other runs. Table 9 shows that zoning can account for the differences in D_m between 293 and the other samples that the D_m(cpx) results for Pu are consistent with this equilibrium criterion.

The very low D_m(cpx) for U and Th result in relatively few tracks/grain; nevertheless the high cooling rate crystals appear to have systematically higher D_m, particularly for Th. Also compare 30-231 (71°C/hour) and 30-269 (1.8°C/hour) U and Th partition coefficients in Table 9. Thus our D(cpx) result for U and Th may not represent equilibrium partitioning. Since most types of disequilibrium (glass cores, defect substitution) and analytical error (imperfect detector contact) will deviate D_m toward unity, our measured D(cpx) for U and Th should be regarded as upper limits; however the values (~0.002) are already so low that they can be considered to be zero for the purposes of petrogenetic analyses.

The apatite U partition coefficients (Table 10) are reproducible within errors although the general applicability of the data is questionable given their unusual composition. The synthetic apatite composition will be discussed separately in Section III-J.

The 1 bar crystal-by-crystal versus cooling rate data shown in Figures 15 and 16 are less extensive in terms of both the number of analyses and the range of cooling rates than the corresponding 20 kilobar data (Figure 14). It is also necessary to plot the data at different fO_2 conditions separately, except for Th. No significant variations in the partition coefficients are seen with respect to cooling rate; however, note that some extreme D values are plotted as upper limits. Two upper limit D_U(whit, $fO_2=10^{-8.5}$) data points are from runs 30A-6Co and 30A-8Co that were irradiated in an early sample arrangement that resulted in poor detector contact in many cases. Since the two values agree, it is unclear as to whether their relatively high D_U(whit) values are a product of a compositional difference (30 versus 20) or a coincidental agreement resulting from poor detector contact. Re-irradiation of these two runs as well as new 30 composition runs is needed.

As discussed in Section III-I, there is a problem of maintaining a well-defined fO_2 for runs nominally done in air (capsules welded shut in air). Some of the data in Tables 11 and 12 probably reflect this variability in oxidizing conditions. (See Tables 1 and 2 for oxidizing run conditions, welded or open to air). However, the upper limits for D_U(whit, fO_2=air) and D_{Pu}(cpx, $fO_2=10^{-2.3}$)(Figs. 15 and 16) are due to the small number of tracks present for such low D values combined with small crystals. The lowest values are probably more nearly correct than the assigned upper limit values although the consistency of the D_U(whit, fO_2 =air) upper limit values suggest the need for additional experiments. For most practical purposes, even the upper limit D values are effectively 0.

Overall, reproducible results are obtained at low cooling rates (<30°C/hour) but, at least for D_U(cpx) and D_{Th}(cpx) at 20 kilobars, variations are seen at cooling rates far below the 600 °C/hour rate at which Seitz (1974) observed large deviations from interface equilibrium. The 600°C/hour upper limit was based on a large disequilibrium effect in the melt that could be seen visually in the track image. Seitz (1974) reported no observable disequilibrium effects at the order of magnitude lower cooling rates used in part of this study. The cause of observed deviations at cooling rates ≥30°/hr is not known. Possibilities include: 1) equilibrium partitioning at the crystal-liquid interface, but small gradients existing in the liquid that are obscured by the track ranges or too close to the crystal for reliable microprobe analyses, 2) disequilibrium uptake of elements that may be a result of rapid growth of the crystal surface, even though diffusion in the liquid may be sufficiently rapid to maintain liquid homogeneity, 3) uptake of submicroscopic bits of liquid (skeletal crystals are common in anhydrous experiments) a very serious effect when low D values are being measured , or 4) analytical problems with aquiring data on small crystals that frequently are the product of the greater nucleation rate at higher cooling rates (and undercoolings). (Large crystals were grown in 30-231, but these are an exception.)

iii. Reproducibility of Minor Elements

In addition to the following discussion of minor element partitioning as an equilibrium argument for the trace element partitioning, minor elements are important for characterizing the specific phases

under study and can also be used as partition coefficients in interpreting minor element abundances in rocks (e.g., P contents of lunar pyroxenes).

As illustrated by Figure 11, these elements are zoned, and this must be allowed for in a quantitative interpretation. With the better spatial resolution of the microprobe analyses with respect to track analyses, an attempt to measure the minor element concentrations on either side of the crystal/glass boundary can be made. However, this has not been done because: (1)given the low D values in some cases, analyses must be sufficiently within the crystal to avoid thin crystal edges that may exist at the boundary and to avoid interference by x-ray fluorescence from the adjacent glass, (2) the concentration gradient is steepest near the crystal rim and (3), most importantly, to test the effect of zoning correction procedures similar to those used for the actinides. Consequently, measurements are usually made at a point approximately half-way between core and rim on small crystals. Larger crystals are analyzed at several points, core to rim, with the average obtained being corrected by the same method as the smaller crystals. The average D_m values obtained in this way, for all crystals in a given run, are tabulated in Tables 13 and 14. Analyzing a spot several times on the same day, and the Durango apatite microprobe standard over a period of months, demonstrated reproduction of the analyses to approximately the precision given by counting statistics (Appendix III). Similarly, analyses of the (20 kilobar) coexisting glass at several different locations for a given sample generally are also reproducible (293 is the exception), but intercrystal variations with the same sample show standard deviations that are typically 2-3 times those due

TABLE 13

Uncorrected Microprobe Minor Element Partition Coefficients (D_m); 20 Kilobars

Sample Number													(dT/dt)	
	WHITLOCKITE													
P=8.4 cation%	Na	%sd*	%cts**	Mg	%sd	%cts	Al	%sd	%cts	Si	%sd	%cts	°C/hr	%Xls
UTh20-288	0.294	4.3	5.0	0.573	3.7	1.4	0.008	17.3	39.8	0.0086	4.5	3.0	2.8	17
UTh20-211	0.271	7.6	8.6	0.748	3.0	1.4	0.008	53.9	41.1	0.0128	42.5	5.5	68	35
UTh20-326	0.255	5.1	7.4	0.748	4.7	1.4	0.006	22.6	53.9	0.0070	5.0	4.7	2.8	39
UTh20-266	0.227	8.5	7.4	0.895	5.3	1.3	0.009	54.5	30.5	0.0078	19.4	9.7	1.9	44
Pu 10-234	0.235	1.7	4.1	0.721	3.8	1.4	0.005	49.9	45.6	0.0066	2.9	3.2	3.1	37
Pu 10-234	0.234	15.5	5.7	0.942	12.3	1.4	0.010	18.4	23.9	0.0075	17.3	5.6	36	44
	CLINOPYROXENE													
	Na			P			Al							
UTh20-288	0.420	4.2	1.9	0.030	25.3	6.3	0.576	7.0	1.4				2.8	17
UTh20-211	0.357	8.5	2.6	0.061	58.2	12.1	0.513	8.6	1.3				68	35
UTh20-326	0.352	4.9	2.5	0.018	34.3	28.8	0.505	8.5	1.3				2.8	39
UTh20-266	0.315	10.0	2.6	0.029	58.6	21.7	0.438	11.2	1.3				1.9	44
Pu 10-293A	0.346	2.4	2.0	0.038	9.8	5.0	0.494	2.3	1.2				3.1	37
Pu 10-293B	0.339	2.4	2.1	0.022	59.7	11.8	0.457	6.5	1.3				3.1	28
Pu 10-234	0.349	15.3	2.2	0.205	23.8	2.5	0.457	5.6	1.3				36	44
P=5.3 cation%														
Pu 12-267	0.380	5.3	2.8	0.023	17.7	24.2	0.484	12.6	1.4				--	7
Pu 12-261	0.321	7.6	2.5	0.015	20.1	23.3	0.409	9.4	1.3				2.4	14
UTh30-231	0.342	2.8	2.6	0.040	7.6	14.2	0.463	1.2	1.3				71	18
UTh30-269	0.333	10.2	2.8	0.008	67.7	45.6	0.418	5.2	1.4				1.8	19

* %sd=percent standard deviation from actual analyses using $\sigma=\sqrt{\frac{1}{n-1}\left[\Sigma x^2-\frac{(\Sigma x)^2}{n}\right]}$

**%cts=percent counting statistics standard deviation using $\sigma=\sqrt{cts_{peak}+cts_{bkgd}}/(cts_{peak}-cts_{bkgd})$; all counts for equal times

TABLE 14

Uncorrected Microprobe Minor Element Partition Coefficients (D_m); 1 Bar

Sample Number				WHITLOCKITE						(dT/dt)	
P=8.4 cation%	Na	%sd†	%cts†	Mg	%sd	%cts	Si	%sd	%cts	°C/hr	%X1s
Pu.15B-2Co	0.123	17.6	13.6	0.560	3.1	1.3	0.0050	8.5	3.9	3.8	9
Pu 15B-6Co	0.187	-**	9.6	0.553	-	1.3	0.0057	-	3.6	3.9	10
UTh20A-5A	0.193	18.9	11.3	0.478	5.3	1.4	0.0056	2.5	10.7	4.7	5
UTh20A-1Co	0.168	23.1	12.8	0.484	0.3	1.4	0.0065	2.4	12.9	16.8	5
UTh20A-2Co	0.176	16.7	11.4	0.504	5.7	1.4	0.0067	12.4	9.8	5.7	5
UTh40A-4Co*	0.143	7.0	16.2	0.510	4.9	1.4	0.0064	7.6	9.9	8.0	3
UTh20A-9A	0.165	11.0	9.6	0.497	2.2	1.4	0.0065	3.4	3.3	4.1	9
UTh20A-11A	0.172	4.5	9.4	0.507	6.2	1.3	0.0077	21.5	3.1	5.5	9
UTh20A-5Co	0.160	2.4	10.3	0.525	2.7	1.4	0.0057	4.9	3.7	5.1	11
UTh20A-6Co	0.158	3.6	10.4	0.511	0.8	1.4	0.0071	15.9	3.2	5.4	10
U 23-3A	0.178	4.5	4.3	0.529	1.5	1.4	0.0134	11.0	2.3	5.0	12
U 23-3Co	0.149	2.7	4.9	0.511	1.8	1.4	0.0111	6.0	2.5	4.0	12
U 23-4Co	0.168	-**	4.9	0.575	-	1.3	0.0109	-	2.6	-	2
U 23'-5A	0.176	6.5	7.2	0.521	1.4	1.4	0.0107	13.4	2.5	2.0	13
U 23'-5Co	0.175	2.8	4.0	0.530	1.4	1.4	0.0093	6.2	2.7	2.0	11
U 23'-6A	0.172	5.9	4.1	0.526	2.2	1.4	0.0113	4.0	2.5	9.4	11
U 23'-7Co	0.177	2.5	4.0	0.546	1.5	1.4	0.0126	31.6	2.4	9.4	12
				CLINOPYROXENE							
P-O cation%	Na			Al							
Pu 14A-5A	0.064	12.3	10.9	0.221	18.9	1.3				2.9	20
Pu 14A-7Co	0.075	19.7	9.0	0.191	13.6	1.4				2.9	13

* Pinhole leak in capsule completely oxidized buffer; $fO_2 \leq$ air

** Only one good crystal analysis; presence of detectable Al and high and variable Si indicative of glass in analyzed areas of all other crystals

† See definitions, Table 13

to counting statistics (Tables 13 and 14) as a result of zoning in the crystals and thus the 'half-way' point analyzed, or the several averaged points, will not necessarily correspond to the same degree of crystallization for different crystals. Figures 17 and 18 contain both uncorrected and zoning-corrected 20 kilobar D_1 values for minor elements in whitlockite and clinopyroxene, respectively, plotted as a function of the total amount of crystallization in the experiments. The data points are the average of all crystals analyzed and the error bars reflect the larger of the tabulated errors in Table 13. The 20 kilobar data are chosen because of the greater range in crystallization which requires much more correcting than the corresponding 1 bar data and are therefore a better test of the correction procedure.

For the analysis of a single point midway between crystal core and rim the equation relating the measured D_m and the over-corrected D_1, equivalent to equation 1 (Section III-C) for a contour, is (see Appendix V for deviations):

$$(2) \qquad D_1 = D_m \frac{(1-X_f)^{D_b-1}}{(1-X_{\frac{1}{2}})^{D_b-1}}$$

Where D_b is the bulk partition coefficient as defined for equation 1, X_f is the total amount of crystallization and $X_{\frac{1}{2}}$ is the amount of crystallization corresponding to the core-rim midpoint. Assume: 1) nucleation on the liquidus (i.e., at X=0), 2) uniform crystal growth, and 3) the plane of the section analyzed is a central section passing through the initial nuclei. Then for $r=1/2r_o$, in a direction where the center-rim dimension is r_o, it follows that

FIGURE 17

Plot of 20 Kbar minor element D in whitlockite as a function of the total (phosphate + clinopyroxene) amount of crystallization. The different symbols illustrate the effect of approximately correcting for crystal zoning according to methods given in the text. If equilibrium at the crystal/melt interface is maintained, a well-defined corrected D value, independent of percent crystallization, would result. The Na and Mg data provide a good test of the correction method (and underlying assumptions), giving consistent results. One (high cooling rate) sample has anomalously high and variable D_{Si}. The dotted lines are constructed to pass through the corrected D value of the sample with the least amount of crystallization.

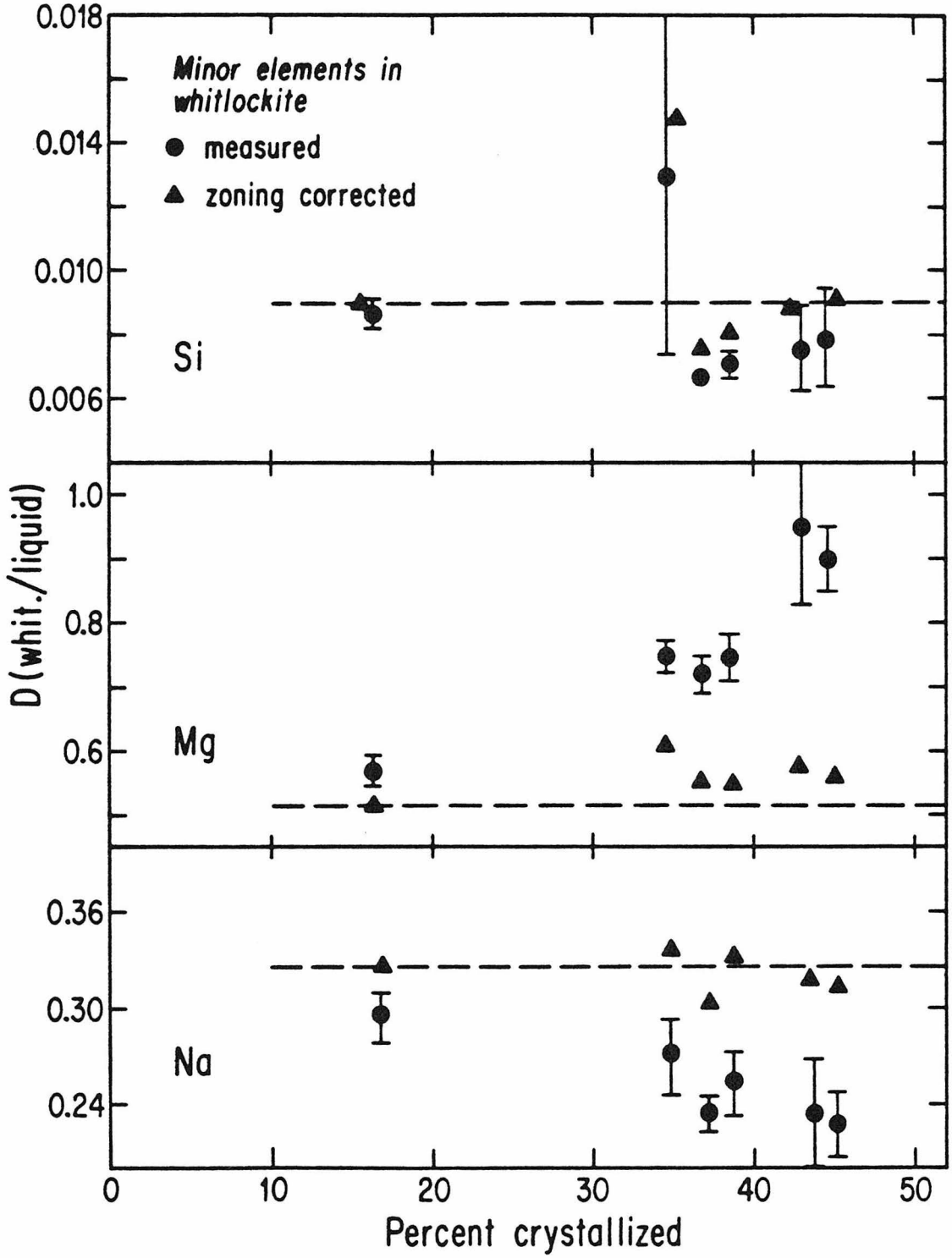
Minor elements in whitlockite
measured
zoning corrected
Si
Mg
Na
D(whit./liquid)
0.018
0.014
0.010
0.006
1.0
0.8
0.6
0.36
0.30
0.24
0
10
20
30
40
50
Percent crystallized

FIGURE 18

Minor element, 20 Kbar, D values in clinopyroxene plotted against fraction crystallized for a given run, analogous to Figure 17. As in Figure 17, if crystal/liquid interface equilibrium is maintained, the zoning-corrected D values should be independent of percent crystallized. The data are consistent with this expectation as well as demonstrating that D_{Al} and D_{Na} depend on the initial P_2O_5 content. The dotted lines are constructed to pass through the corrected D value of the sample with the least amount of crystallization. Note the relatively anomalous 10-293B data. The P values given are the bulk concentrations in cation percent.

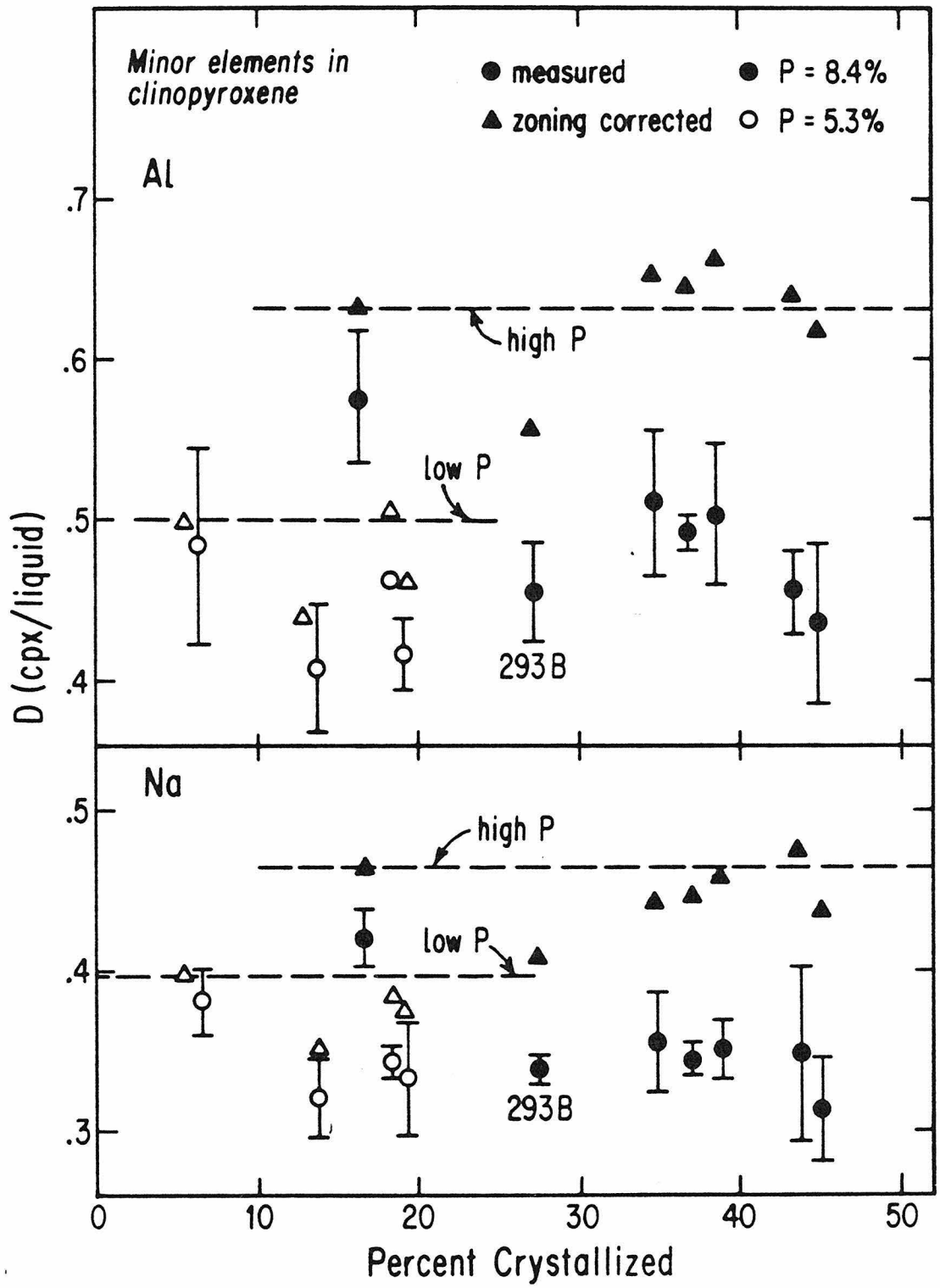
Minor elements in clinopyroxene
measured
zoning corrected
P = 8.4%
P = 5.3%
Al
high P
low P
293B
Na
high P
low P
293B
D (cpx/liquid)
Percent Crystallized
.7
.6
.5
.4
.5
.4
.3
0
10
20
30
40
50

$$(r/r_o)^3 = (X_{1/2}/X_f) = (1/2)^3$$

which can be used to calculate $X_{1/2}$. As for equation (1), none of the above assumptions are exactly correct; however, the effect of the errors is an over-corrected D_l (Appendix V). The whitlockite Mg and Si were treated somewhat differently because the measured variation in these elements with crystallization is mainly due to the change in melt composition reflecting pyroxene crystallization, for which Mg and Si are stoichiometric constituents. Therefore, for these elements we used equation 10 (Appendix V) which is derived assuming that Mg and Si were stoichiometric constituents in pyroxene and that whitlockite incorporated these elements by Rayleigh-type (trace element) partitioning.

The trends in Figure 17 for the measured D_m values for Na and Mg in whitlockite agree well with those expected with increasing amounts of crystallization and the zoning-corrected values (D_l) show good agreement, supporting the assumption of equilibrium interface partitioning. The measured D_{Si}(whit) in Figure 17 show little variation since D_b(Si) $\cong$ 1 (0.7); however, the whitlockites from the experiment (211) with 35% crystallization show high and variable Si contents. This sample was grown with a high cooling rate (Table 2). Because of these results and because of the systematically higher D(cpx) for U and Th (Section III-Eii, Table 9, and Figure 14), we have not used any of the data from the high cooling rate experiments in our final evaluation of actinide D values although, as Figure 14, 15, and 16 show, many results at high and low cooling rates are similar.

Figure 18 is more complex in that there appears to be a systematic difference for Na and Al in clinopyroxene, depending on the initial P

concentration in the melt, with lower D values for the lower P contents. In particular, the high P point at ~17% crystallization, relative to all low P points, requires this interpretation. Phosphorus content has been found to be very important in partitioning between immiscible silicate liquids (Ryerson and Hess, 1978; Watson, 1978) and also affects actinide partitioning into clinopyroxene, as discussed below. Consequently, the interpretation that Na and Al partitioning also depends on the P concentration of the melt is reasonable. However, it is also possible to interpret Figure 18 as showing that there is a large scatter in the measured clinopyroxene Na and Al contents with no consistent trend with percent crystallization, e.g., suggestive of diffusive re-equilibration of Na and Al. However, Figure 11 shows that Na and Al are distinctly zoned in the clinopyroxenes making this alternative unlikely. The apparently undercorrected data (Figure 18) for the anomalous (Table 2) 10-293-B sample has no ready explanation but the overall distinction between the high P and low P clinopyroxene data persists. With the interpretation that different D values apply to the low and high P systems, Figure 18 shows that the zoning corrected D values are reasonably consistent, supporting the validity of the trace element corrections (as does Figure 17). Note that the compositional dependence of the Al minor element data is approximately twice that of Na; the relative partition coefficients of Na and Al are not independent of composition (Table 15).

Table 15 summarizes our best estimates of the 20 kilobar minor element D values. In addition to the elements presented in detail on Figures 17 and 18, rough D values for Al in whitlockite and P in clinopyroxene are given (see Table 13). Although definitely present, these

TABLE 15

Zoning Corrected Minor Element Partition Coefficients

(20 kilobar; 1375-1390°C)

	Si	Mg	Na	Al	P
Whitlockite	$8.3\pm0.7\times10^{-3}$*	0.562±.031	0.321±.012	0.010±.003	-
Clinopyroxene					
Initial P = 8.4%**	-	-	0.453±.014	0.641±.016	0.023±.010†
Initial P = 5.3%	-	-	0.375±.019	0.477±.031	0.025±.016

*Excludes 20-211

**Excludes 10-293B

†Also excludes 10-234

elements have poor counting statistics during routine microprobe analysis. The apparently distinct P partitioning of the uncorrected clinopyroxene data for the two compositions are brought into agreement by the correction procedure; a further indication that the proper approach to correct for zoning has been taken.

In contrast to the 20 kilobar data, the 1 bar data require little correction due to the smaller amounts of crystallization. The 1 bar whitlockite data given in Table 14 are corrected and tabulated in Table 16. The corrections are the rim/core (Equation 2, Appendix V) and the Albarede-Bottinga correction (Equation 4, Appendix V). The rim/core correction is an overcorrection (Appendix V) that, for these small amounts of crystallization (10%), is negligibly different (higher) than the correction used for the 20 kilobar minor element data (Equation 2, Section IIIE)and Equation 10, Appendix V). The Albarede-Bottinga correction assumes knowledge of the average compositions of the crystalline phases, resulting in a correction of roughly one-half that of the core/rim correction. Because of the small amounts of crystallization, the difference between these correction procedures is insignificant.

Table 16 includes data from the 15, 20, and 40 compositions, which are nominally the same; however, there are differences in detail (Appendix III). The average values for the 20 and combined 23-23' compositions are also given in Table 16. Although there may be somewhat more intersample variability than expected from the estimated errors in some cases (e.g. Si in the 23 samples), the overall agreement is good. Table 17 summarizes the best estimates of the 1 bar minor element D values.

TABLE 16

Corrected Whitlockite Minor Element Partition Coefficients, 1 Bar

Sample No.	Na	1σ+	rim/ core	Albarede-Bottinga	Mg	1σ+	rim/ core	Albarede-Bottinga	Si	1σ+	rim/ core	Albarede-Bottinga
Pu 15B-2Co	0.123	±.022	0.134	0.128	0.560	±0.17	0.583	0.572	0.0050	.0004	0.0055	0.0053
Pu 15B-6Co†	0.187	±.018	0.203	0.195	0.553	±.007	0.578	0.566	0.0057	.0002	0.0063	0.0060
UTh40A-4Co	0.143	±.023	0.147	0.145	0.510	±.025	0.518	0.514	0.0064	.0006	0.0066	0.0065
UTh20A-5A	0.193	±.036	0.202	0.197	0.478	±.025	0.491	0.485	0.0056	.0006	0.0059	0.0058
UTh20A-9A	0.165	±.018	0.179	0.172	0.497	±.011	0.521	0.509	0.0065	.0002	0.0072	0.0068
UTh20A-11A	0.172	±.016	0.185	0.179	0.507	±.031	0.529	0.519	0.0077	.0017	0.0084	0.8081
UTh20A-1Co	0.168	±.039	0.175	0.172	0.484	±.007	0.496	0.490	0.0065	.0008	0.0068	0.0067
UTh20A-2Co	0.176	±.029	0.183	0.179	0.504	±.029	0.515	0.510	0.0067	.0008	0.0070	0.0069
UTh20A-5Co	0.160	±.016	0.176	0.168	0.525	±.014	0.554	0.540	0.0057	.0003	0.0064	0.0061
UTh20A-6Co	0.158	±.016	0.173	0.165	0.511	±.007	0.537	0.524	0.0071	.0011	0.0079	0.0075
U23-3A*	0.178	±.008	0.191	0.185	0.529	±.008	0.564	0.547	0.0134	.0015	0.0147	0.0140
U23-3Co	0.149	±.007	0.165	0.157	0.551	±.009	0.580	0.566	0.0111	.0007	0.0125	0.0118
U23-4Co†	0.168	±.008	0.171	0.169	0.575	±.007	0.579	0.577	0.0109	.0003	0.0111	0.0110
U23'-5A*	0.176	±.013	0.191	0.184	0.521	±.007	0.560	0.541	0.0107	.0014	0.0120	0.0113
U23'-6A	0.172	±.010	0.189	0.180	0.526	±.012	0.554	0.540	0.0113	.0005	0.0126	0.0120
U23'-5Co	0.175	±.007	0.191	0.183	0.530	±.007	0.557	0.544	0.0093	.0006	0.0104	0.0098
U23'-7Co	0.177	±.007	0.196	0.186	0.546	±.008	0.576	0.561	0.0126	.0040	0.0142	0.0134
Ave UTh20	0.170 ±0.012		0.182 ±0.010	0.176 ±0.011	0.501 ±0.016		0.520 ±0.022	0.511 ±0.019	0.0065 ±0.0007		0.0071 ±0.0009	0.0068 ±0.0008
Ave U23 &# U23'	0.171 ±0.010		0.185 ±0.012	0.178 ±0.011	0.540 ±0.019		0.567 ±0.011	0.554 ±0.014	0.0113 ±0.0013		0.0125 ±0.0015	0.0119 ±0.0014

† Only one good crystal analyzed, errors are 1σ counting statistics

*

+ Errors are the larger of the 1σ errors tabulated in Table 14

23 and 23' samples have U added at percent concentrations

TABLE 17

Zoning Corrected (Rim/Core) Minor Element Partition Coefficients
(1 Bar; 1190-1330°C)

	Si	Mg	Na	Al
Whitlockite	$7.1\pm0.9\times10^{-3}$	0.520±.022	0.182±.010	-
Clinopyroxene Initial P = 0%	-	-	0.0809±.0050	0.228±.024

In summary, except for three of the systems studied, the data meet the four criteria for equilibrium interface partitioning, and it is reasonable to adopt the low cooling rate values as equilibrium D values. At 20 kilobars, U(cpx), Th(cpx) and perhaps Pu(cpx) appear to have different D values at cooling rates greater than 30 ^{o}C/hr. compared to the results at 1-2 ^{o}C/hr. Future work will check the D values at cooling rates intermediate to those used in this work.

Tables 18 and 19 summarize the best D values for the systems investigated. Range and zoning corrections have been applied and corrected averages of the low cooling rate measurements are tabulated. The differences in D_U(cpx) and D_{Th}(cpx) between the 8.4 and 5.3 cation percent P compositions are probably not significant because smaller clinopyroxene crystals were obtained from high P starting materials.

The P-free clinopyroxene U and Th data were obtained from a single run (32-321) that grew large (hundreds of microns) crystals. This sample has been reanalyzed to check the validity of the relatively large D values. The P-free Pu(cpx) data (Table 19) were obtained from a pair of 1 bar runs.

F. Effects of Pressure and Temperature on Partitioning

The trace element partition coefficients (Tables 18 and 19) do not appear to be particularly sensitive to the differences between the 20 kilobar and 1 bar experiments. The pressure effect of the trace element substitution into the crystalline phases is expected to be small because the proportion of the trace element component (i.e., $Pu^{+3}MgAlSiO_6$) is so small that, thermodynamically, the ΔV part of the $P\Delta V$ term is negligible. Similarily, the effect of the

TABLE 18

Summary of Adopted Partition Coefficients [a) b)]

(20 kilobar; 1375-1390°C; $fO_2 = 10^{-8.6}$)

(Range and Zoning Corrected)

	Initial P (Cation%)	D_{Th}	D_U	D_{Pu}
Whitlockite	8.4	1.15±6	0.58±3	3.5±2
Clinopyroxene	8.4	0.0032±4	0.0028±5	0.064±9
	5.3	0.0019±2	0.0019±2	0.053±3
	0	0.029±2	0.018±1	-
Apatite	8.4	1.22±14	1.69±8	-

a) Errors refer to last significant figure.

b) The measured track densities are proportional to the detected particles range (in mg/cm^2) as well as the actinide concentration. Therefore a small range correction (maximum 6%) has been applied to the partition coefficients to correct for the differences between the crystals and coexisting glass based on the empirical (Mory et al., 1970) proportionality between range in pure elements and $Z^{1/2}$, where Z is the atomic number. This relationship is consistent with the heavy ion ranges calculated by Northcliffe and Schilling (1970). Little difference results if the exponent on Z is varied from 0.4 to 0.6; an error corresponding to this variation in exponent is propagated into the tabulated errors. (Appendix IV).

TABLE 19

Summary of Adopted Partition Coefficients
(1 Bar; 1190-1330°C; $fO_2 = 10^{-8.5}$ and 0.209)
(Range and Zoning Corrected)*

	fO_2		$10^{-8.5}$	0.209	$10^{-8.5}$	0.209
	Initial P (cation%)	D_{Th}	D_U	D_U	D_{Pu}	D_{Pu}
Whitlockite	8.4	1.30±3	0.48±2	0.0024±4	3.7±3	0.58±4
	5.3		≤0.68±2			
Clinopyroxene	0	-	-	-	0.17±1	0.018±3**

* See footnotes on Table 18

** Fe_2O_3-Fe_3O_4 buffer; $fO_2 = 10^{-2.3}$

trace element $T\Delta S$ and ΔH of mixing contributions should be negligible, so a marked temperature sensitivity of the crystalline phases is not expected. In general, thermal expansion of the crystal lattice will not necessarily ease the trace element substitutions (e.g., thermal expansion in diopside is principally along the longest Ca-O bond in the distorted M2 site; the minimum expansion is along the shortest Ca-O bond; Finger and Ohashi, 1976). This asymmetric thermal expansion that increases the distortion of the M2 site in diopside does not ease the substitution of ions that are either larger or smaller than Ca^{+2}; qualitatively, the shortest bond length constrains the maximum acceptable ionic radius whereas the maximum bond length constrains the minimum acceptable ionic radius for the substituting species.

The most likely cause of any variations in the partition coefficients, in response to variations in pressure and temperature, lies with the liquid, not the crystalline phase. The viscosity, and probably the degree of polymerization, decreases markedly with the change from 1 bar to 20 kilobar conditions (Kushiro et al., 1976; Kushiro, 1976; see Section III-F). The more 'basic' (i.e., dissociated) nature of the melts at high pressure favors incompatible elements relative to the more polymerized liquids (Watson, 1976; Ryerson and Hess, 1978). The prediction would be for the partition coefficients to be lower at high pressure (the actinides being retained to a greater degree in the melt) than at 1 bar. Although the effect is small (13%), this appears to be true for D_{Th}(whit) (Tables 18 and 19); however no further simple comparisons can be made due to compositional effects seen for the pyroxenes (Table 18) and a lack of 1 bar Th data for clinopyroxene (Table 19). The effects of temperature and pressure (melt

structure) on the valence state distribution complicate the discussion for the multiple valent actinides (Pu and U) (as is discussed in the next section, III-G).

Of course, it is possible that the 20 kilobar pressure difference is just offset by the 130°C temperature difference. More precise measurements are required to resolve this beyond the apparent 13% difference between the Th-whitlockite data from the two pressures (Tables 18 and 19).

The minor elements show distinct partitioning differences with changes in pressure and temperature (Tables 16 and 17). At some point, the changes to the minor element content of the phases under consideration would probably affect the trace elements although, in this study, the only compositional changes that produced a marked effect were U and P in the melt. These are discussed in the later sections.

G. Effects of Multiple Valence States

As mentioned previously, the measured partition coefficients (Tables 18 and 19) are sensitive to the fO_2 conditions of experiments containing multivalent cations (U and Pu). The large differences between the $fO_2 = 10^{-8.6}$ and $fO_2 = 0.209$ (air) partition coefficients for U and Pu in whitlockite and for Pu in clinopyroxene are certainly due to the stabilization of reduced valence states (Pu^{+3} and U^{+4}) at the lower fO_2 (see Appendix VI and Benjamin et al., 1978 for further discussion of these valence assignments). The actual proportions of Pu^{+3} and U^{+4} as well as the other possible valence states, Pu^{+2} and Pu^{+4}, and U^{+3}, U^{+5}, and U^{+6} are important in quantifying the individual partition coefficients for these ions. The marked differences in D

values for the individual actinide valence species is a result of both ionic radius and charge. The ionic radius controls the site into which the trace element can substitute whether the site is a regular crystal lattice position or a defect in the crystalline structure. The charge of the cation determines the difficulty in charge balance and the resultant complexity of the coupled substitution mechanism. These coupled substitutions are addressed, for the case of U at high concentrations, in a later section (III-I).

The redox calculations presented in Appendix VI can be used to estimate the partition coefficients, D_i, for each valence state of the actinides. The limiting cases, where ideality is assumed or where all the individual valence state partition coefficients but one are sequentially set to zero with the observed D value ascribed solely to the remaining valence state, have been discussed in Benjamin et al. (1978). The following calculated partition coefficients (D_i) are rough estimates in that the calculations incorporate a parameter, k, assumed to be constant for all the actinide valence states, which results in a strong preference for reduced valence states compared with the k=1 (ideal) calculation. Factor of two variations in k will have little effect (5% absolute) for the cases where 1 valence is $\geq$80% of all ions of that element; however larger effects may be seen for the less abundant valence states. The parameter, k, is based on 1 atmosphere optical spectroscopic U valence state distributions (Calas, 1979). In the 20 kilobar experiments this parameter may not have the same value, as the structures of melts change with pressure (Section III-F). As shown in Appendix VI, the value of k_{46}^{U} for equilibria between U^{+4} and U^{+6} ($2x10^5$), which forms the basis of this discussion, appears to be nearly independent of

composition and fO_2 over the range of simple compositions that were investigated by Calas (1979) although, the Eu valence state data of Morris and Haskin (1974) and Morris et al. (1974) indicate that Eu is much more reduced in acidic compositions than in basic compositions and that k_{23}^{Eu} is fO_2 dependent. Consequently k may only be an order of magnitude estimate. Recently these Eu data have been disputed by Mysen et al. (1978) because they were unable to detect any Eu^{+2}, by Mössbauer spectroscopy, in experiments designed to encompass the compositions and fO_2 conditions used by Morris and Haskin (1974) and Morris et al. (1974). This disagreement is yet to be resolved.

The Th partition coefficients are predicted to be independent of fO_2 as Th^{+4} is the only known stable valence state, a prediction borne out by the data in Tables 18 and 19.

The measured Pu partition coefficients are the sum of the concentration (C_i) weighted contributions of Pu^{+2}, Pu^{+3}, and Pu^{+4} partition coefficients. The equation for Pu partitioning at the temperature of the 20 kilobar experiments is given below (the coefficients are the calculated proportions of the individual valence states; Table VI-6, Appendix VI).

1) $D_{Pu} = 0.01\ D_{Pu}^{+2} + 0.81\ D_{Pu}^{+3} + 0.18\ D_{Pu}^{+4}$ $\quad T=1380°C;\ fO_2=10^{-8.6}$

At 1 bar, two fO_2 conditions result in two similar equations:

2) $D_{Pu} = <.01\ D_{Pu}^{+2} + 0.55\ D_{Pu}^{+3} + 0.45\ D_{Pu}^{+4}$ $\quad T-1250°C;\ fO_2=10^{-8.6}$

3) $D_{Pu} = <<.01\ D_{Pu}^{+2} + 0.01\ D_{Pu}^{+3} + 0.99\ D_{Pu}^{+4}$ $\quad T=1250°C;\ fO_2=0.209$

For the 1 bar data the contribution from Pu^{+2} is negligible unless an unrealistically high D_{Pu}^{+2} is chosen. Using D_{Pu} tabulated in Tables 18 and 19, solving Equations 2) and 3) for D_{Pu}^{+4} results in a value

of 0.52 for whitlockite and 0.015 for clinopyroxene; solving for D_{Pu}^{+3} results in a value of 6.30 for whitlockite and 0.30 for clinopyroxene. Assuming $k_{34}^{Pu}=2x10^5$ at 20 kilobars, Equation 1 can be used to test these values of D_{Pu}^{+3} and D_{Pu}^{+4}. The result is a calculated D_{Pu}(whit) value of 5.1 and a D_{Pu}(cpx) value of 0.25. These values are much higher than the measured values. Also, eqns. 1 and 2 imply that Pu^{+4} is still important at $fO_2=10^{-8.6}$, and the effect of assuming $k=2x10^5$ at both pressures is that the temperature difference results in a factor of 4 difference in the calculated C_4/C_3 values (Equations 1 and 2); however, the measured D_{Pu}(whit) values are very similar (3.5±0.2 at 20 kilobars and 3.7±0.3 at 1 bar pressure).

The calculated difference in C_4/C_3 directly reflects the temperature variation of the ΔG^o of the Pu^{+3} oxidation reaction (Equation v, Table VI-1, Appendix VI). Thus, for the measured D_{Pu}(whit) values at the two pressures to agree, there must be some effect that cancels the 130°C temperature difference, if Equations 1 and 2 are accurate. The Eu data (discussed in Appendix VI) show a factor of two decrease in k_{23}^{Eu} over temperature intervals of this magnitude. The U data show no change (Calas, 1979), whereas a decrease of an order of magnitude is required in k. The possibility of a temperature dependence of D_{Pu} cancelling the change in C_4/C_3 is not supported by the D_{Th}(whit) data which decrease from 1.30±0.03 at 1 bar to 1.15±0.06 at 20 kilobars. Alternatively, the k value appropriate to all Pu valence states may be larger than $2x10^5$. This would make C_4/C_3 small and less sensitive to temperature variations. In order to yield equal proportions of Pu^{+3} at both temperatures, k_{34}^{Pu} must be about 10^7. However, assuming $k_{23}^{Pu}\approx k_{34}^{Pu}$, a problem arises in that even at a k^{Pu} of 10^6, the proportion

of Pu^{+2} becomes significant at the higher temperature and, since the D_2 value is probably comparable to, or greater than, the D_3 value, the expectation would be that the observed D values at the two temperatures may not converge. If the concept of k values remaining roughly constant (of the same order of magnitude) for different valence state pairs of the same element is incorrect (e.g., for Pu, $k_{23}=10^4$ and $k_{34}=10^6$), then the concentration of Pu^{+2} is negligible. In this case, a small C_4/C_3 ratio at the lower temperature would remain small, although different, at the higher temperature so that the measured D_{Pu} values would be similar; reflecting the partition coefficient of Pu^{+3} exclusively. This simple explanation requires no accidental cancellation of factors but does require very different solute-solvent interactions among the three Pu valence states and the same silicate liquid.

A third possible explanation for the lack of a temperature variation in D_{Pu}(whit) is the effect of pressure on the structure of melts, as discussed in the previous section. If the 20 kilobar melt is more oxidizing than the corresponding 1 atmosphere melt, then a lower k value would apply to the 20 kilobar data. To reconcile the observed whitlockite partitioning data with the redox calculations (Appendix VI and Equations 1 and 2 in this section), the 20 kilobar k^{Pu} must be 1.5×10^4. That is, with this k value, the C_4/C_3 in Equation 1 would equal that given in Equation 2. This value of k also explains the clinopyroxene data provided the factor of 3 difference between the D_{Pu} (cpx) values for phosphorus free and phosphorus containing compositions (Tables 18 and 19; next section) is taken into account.

Which of the last two alternatives, presented above, is a better description of the Pu valence state distribution in silicate melts can

be determined experimentally. At 1250°C (1 atmosphere), the graphite buffer will maintain an $fO_2=10^{-14}$ (Appendix II). The first of the two possibilities predicts that, because the C_4/C_3 value is low at $fO_2=10^{-8.6}$ and the partitioning is dominated by Pu^{+3}, the observed D_{Pu}(whit) at $fO_2=10^{-14}$ will remain at approximately 3.7. The second alternative predicts that the D_{Pu}(whit) at $fO_2=10^{-14}$ will be approximately 6 because this model has only 55% Pu^{+3} at $fO_2=10^{-8.6}$ (Equation 2).

The corresponding equations for U, under the same T and fO_2 conditions, are:

4) $D_U = 0.01\ D_U^{+3} + 0.96\ D_U^{+4} + 0.03\ D_U^{+5}$ T=1380°C, $fO_2=10^{-8.6}$

5) $D_U = <.01\ D_U^{+3} + 0.97\ D_U^{+4} + 0.02\ D_U^{+5}$ T=1250°C, $fO_2=10^{-8.6}$

6) $D_U = <.01\ D_U^{+3} + 0.06\ D_U^{+4} + 0.14\ D_U^{+5} + 0.80\ D_U^{+6}$ T=1250°C, $fO_2=0.209$

From the data presented in Tables 18 and 19, as well as the high concentration U data (Table 21 , the U^{+6} partition coefficient for both whitlockite and clinopyroxene must be nearly 0. From the magnitudes of the measured partition coefficients and Equations 5 and 6, it is clear the U^{+4} dominates and the partition coefficient of U^{+5} must also be near 0. The difference between the 20 kilobar (0.58±0.03) and 1 bar (0.48± 0.02) whitlockite data could be due to U^{+3}, if $D_U^{+3}\approx 10$, not a totally unreasonable value considering the uncertainty of the U^{+3} abundance (double the amount of U^{+3} halves the required D_U^{+3}). Use of $k=1.5\times10^4$ for Equation 4 (as for Pu, Equation 1) produces a negligible shift toward the more oxidized U species and therefore cannot resolve between the alternative models of Pu valence state distributions presented above.

Many more experiments on the reductive capacity of melts under differing conditions as well as more trace element partitioning data are needed to further understand and quantify the partitioning of multi-valent ions.

H. Effects of Phosphorus on Partitioning

Throughout this study, phosphorus has been observed to have a major effect on the partitioning of the trace and minor elements (Figure 18, Tables 13, 15, 18, and 19) between the synthetic clinopyroxenes and liquids of variable P content (0, 5.3, and 8.4 cation percent). The actinide D values show an order of magnitude decrease for Th and U and a factor of 3 for Pu between a P-free liquid and a P-rich liquid (Tables 18 and 19). In contrast, the Na and Al partition coefficients increase with increasing P content (Figure 18, Table 15). The data of Watson (1976) on immiscible silicate liquids, show that P (and incompatible elements) favor a basic (less polymerized) liquid over an acidic (more polymerized) liquid. This implies that P is not simply a 'network forming' species, but in some respects a 'network modifier' in the terminology of Bottinga and Weill (1972). Thus P will tend to make silicate melts more basic and the P-bearing silicate liquid will retain incompatible elements relative to P-free liquids. This conclusion is consistent with the clinopyroxene data acquired in this study. These results are in essential agreement with the recent work of Mysen et al. (1980) on the structural role of phosphorus in aluminous silicate melts. Both Na and Al increasingly favor the crystalline phases as the P content of the liquid is increased. The Al prefers polymerized structures (Ryerson and Hess, 1978) and appears to override the preference of Na for depolymerized structures in order to maintain charge balance.

I. Henry's Law and Uranium Substitution Mechanisms

Table 20 is a comparison of the minimum and maximum dimensions of the Ca (and Mg) sites for clinopyroxene, whitlockite, and apatite with the ionic radii (Shannon, 1976) of the various actinide ions. The diopside data were acquired at 700°C (Finger and Ohashi, 1976). The fassaite (Al+Ti clinopyroxene) data from the meteorite Angra dos Reis (Hazen and Finger, 1977) are included because the synthetic clinopyroxenes are Al-rich. The whitlockite data were acquired at liquid N_2 temperatures, but Calvo and Gopal (1975) found no significant difference between these low temperature data and comparison data taken at room temperature. There is little difference between these data and the site dimensions for Angra dos Reis whitlockite (Dowty, 1977). The data tabulated were obtained by subtracting 1.40 Å from the published Ca-O and Mg-O bond distances for easier comparison with the ionic radii of Shannon (1976) which are based on this value (1.40 Å) for the ionic radius of O^{-2}. The apatite data (Kreidler and Hummel, 1970) are the minimum and maximum ionic radii of cations that, when totally substituted for Ca, form a synthetic phase with the apatite structure. The ionic radii given are from Ahrens (1952) CN=VI. Since these radii are also based a 1.40 Å O^{-2} radius, they are compatible (not identical) with the Shannon (1976) radii.

The important point to be made from Table 20 is that the +3 and +4 actinide ions are quite close to Ca^{+2} in size and that the Ca sites in all three phases should accommodate the actinides. No obvious prediction as to which actinide will be favored can be made. The relative values of the partition coefficients, Tables 18 and 19, do correspond to the ranges of acceptable ionic radii that the phases will accommo-

date; that is, the magnitudes of the actinide partition coefficients are greater for whitlockite than for diopside.

The +5 and +6 U ions are too small, as well as too highly charged, for easy substitution into the Ca sites (CN = XI and VIII). The Mg sites (CN = VI) in diopside and whitlockite (Dowty, 1977) are probably too small for favorable substitution of these highly charged ions even if the charge could be compensated by a coupled substitution.

Substitution of the actinides for tetrahedrally coordinated (CN = 4) P^{+5} is a priori unreasonable because of the great difference in ionic radii although McConnell (1973) considers U^{+6} substitution a possibility because of the known Si^{+4} and Al^{+3} substitutions and the occurrence of U^{+6} in phosphorites.

In order to assess the validity of the hypothesis that the actinide elements substitute for Ca in the structures of the phases synthesized in this study, an attempt was made to observe a correlation between concentrations of U and the other elements in whitlockite for 1 bar experimental charges spiked with bulk quantities of U (Appendix III, Compositions 23 and 23'). These experiments, buffered at $fO_2=10^{-8.5}$ and sealed in air, can also be used as a check on the track counting and correcting procedures used for the data previously presented, as the U partition coefficients for the 23 and 23' composition samples are obtained by two methods: track counting and microprobe (Table 21). On this count, the two methods agree remarkably well.

Furthermore, these high concentration (microprobe detection levels) experiments are important in addressing the current debate over Henry's Law partitioning and the necessity of using trace element concentrations in laboratory measurements of partition coefficients

TABLE 20

Comparison Between Substituting Cation Radii and Ca-site Radii* for Clinopyroxene, Whitlockite and Apatite

	Ca-site Radii (Å)			Mg-site Radii (Å)	
Diopside	Min.	Max.	Mean	Mean	
(Finger and Ohashi, 1976)					CN=VI
Site M2, CN† = VIII	0.975	1.395	1.144	0.723	
Bassaite (Al+Ti cpx)					
(Hazen and Finger, 1977)					
Site M2, CN† = VIII	0.949	1.287	1.089		
Whitlockite					
(Calvo and Gopal, 1975)					CN=VI
Site Ca(IIB1), CN† = IX	0.913	1.372	1.079	0.683	
Ca(IIB2), CN = VIII	0.971	1.238	1.070		
Ca(IB) , CN = VIII	0.978	1.528	1.136		
Ca(IIA'), CN = VI	1.136	1.322	1.229		
Fluorapatite					
(Kreidler and Hummel, 1970)					
Site Ca, CN† = VII and IX	0.95	1.35**			
Chlorapatite					
(Kreidler and Hummel, 1970)					
Site Ca, CN† = VII and IX	0.80	1.35**			

Ionic Radii (Shannon, 1976)

CN	Ca^{+2}	Sm^{+3}	Th^{+4}	U^{+3}	U^{+4}	U^{+5}	U^{+6}	Pu^{+3}	Pu^{+4}
VI	1.00	0.958	0.94	1.025	0.89	0.76	0.73	1.00	0.86
VII	1.06	1.02	-	-	0.95	0.84	0.81	-	-
VIII	1.12	1.079	1.05	-	1.00	-	0.86	-	0.96
IX	1.18	1.132	1.09	-	1.05	-	-	-	-

	P^{+5}	Si^{+4}	Al^{+3}	U^{+6}
IV	0.17	0.26	0.39	0.52

† CN = Coordination Number

* Tabulated radii calculated by subtracting 1.40 Å (the ionic radius of O^{-2}) from published bond lengths to conform to the convention used by Shannon (1976).

**Data based on ionic radii (Ahrens, 1952) of elements that can be completely substituted for Ca while maintaining the apatite structure. Assumed CN = VI and with the ionic radius of O^{-2} = 1.40 Å.

(Mysen, 1978; Harrison, 1977; Lindstrom and Weill, 1978). In this context Henry's Law is regarded as a relationship in which the concentration of an element in a crystalline phase is proportional to the concentration of that element in the coexisting liquid (D is independent of concentration). This relationship is expected to be valid at relatively low concentrations. The basis of the debate is the word 'relatively'. One extreme viewpoint is that differing mechanisms of incorporation of an element in a crystalline phase dominate partitioning at distinct concentration ranges and that partition coefficients must be measured over these concentrations, typically $\leq$1000 ppm (Mysen, 1978). The other extreme maintains that the partitioning observed at concentrations detectable with a microprobe (10000 ppm, more or less) are validly extrapolated to the low ppm levels that more closely match the concentrations extant in nature (Lindstrom and Weill, 1978). The high concentration analytical techniques are more fully developed and understood (and accessible) than are the trace element techniques. The measurements (via trace level β-radiography techniques) of several partition coefficients, each valid over only a distinct concentration range (Mysen, 1978), have been questioned (Lindstrom and Weill, 1978).

The high U experiments conducted in this study do not support the extrapolation of percent concentration based partition coefficients to trace levels, at least for U in whitlockite at $fO_2=10^{-8.5}$. The trace (20 ppm) level D_U(whit) = 0.48±0.02 (Table 19) under conditions identical (except for the U concentration) to those giving D_U(whit) = 0.31±0.02 at high U concentrations (Table 21). This result may be due to either: 1) the nature of the substitution mechanism being different

TABLE 21

Whitlockite Partition Coefficients at Percent Level

UO_2 Concentrations

$fO_2 = 10^{-8.5}$

	UO_2 (wt.%)		D_m		D
23'	3.38%	7Co	0.303 ± .017	(a)	0.326
		5Co	0.293 ± .011		0.313
		5Co T	0.299 ± .027		0.311
23	3.92%	3Co	0.293 ± .009		0.315
		3Co T	0.302 ± .018		0.316
		4Co	0.300 ± .010		0.303
	Ave				0.314 ± .009
		Sealed in air**			
23'		5A	0.354 ± .022		0.384
		6A	0.379 ± .014		0.403
23		3A	0.343 ± .016		0.373
	Ave				0.387 ± .015

(a) Errors are standard deviations from counting statistics. Each value tabulated is the average of all crystals from a given run. Zoning corrections are small, as all data tabulated are for runs with ~10% crystallization.

T Partition coefficients obtained by fission track counting. Observed (range corrected) and final zoning corrected values are tabulated. All others from microprobe U analyses.

** Appear to be reduced by a contaminant; a follow-up <u>open</u> air run produced whitlockite crystals with U contents below the detection limit of the microprobe (<0.005 cation % U).

between these extremes in U concentration, 2) the liquid structure being significantly affected by the addition approximately one cation percent of U, or 3) the ratio of the U solute-solute activity coefficients whitlockite/liquid being increased by a factor of 1.5 (or some combination of these possibilities). A small change in the ratio of the activity coefficients is very plausible; however, evidence (presented below) exists for the U induced structural change in the melt and, possibly, for an unusual U substitution mechanism, at least at high U concentrations.

Microprobe analyses of the synthetic Ca-phosphates have been used to test the suitability of various U-bearing, coupled substitution, end members. Only the data for $fO_2 \cong 10^{-9}$ have been considered. Table 22 summarizes the U-free and U^{+4}-bearing end members, all selected by analogy to the various crystallographic sites in Ca-phosphate following Dowty (1977). Using the constrained least-squares analysis calculations described by Reid et al. (1973), the best description of the U-free Ca-phosphate compositions in terms of the end members on Table 22 is: C:9.6%; M:78.3%; N:2.5%; S:9.5%. A priori a plausible substitution for large ions is a substitution for Ca in the end member formulae. U charge balance can be maintained by an increase in the vacancy fraction of the IIA site (end member 2) or by a coupled Na, Si substitution (end member 3). The only analytically significant compositional change accompanying the addition of 0.25 cation fraction of U to the whitlockite is an increase of similar magnitude in the Si cation fraction. As discussed below, the Mg(whit) partition coefficients differ with U content; however, the difference is in the liquid composition, not the whitlockite. The increase in Si would favor substitutions represented by end members 1 or 3. However, combinations of either 1 or 3 with the

TABLE 22

End Members Utilized in Solid Solution Modeling of Synthetic Ca-phosphates

I. U-free end members (from Dowty, 1977)

C. $[Ca\ \square\ ]Ca_{18}Ca_2(PO_4)_{14}$

M. $[Ca\ \square\ ]Ca_{18}Mg_2(PO_4)_{14}$

N. $[NaNa]Ca_{18}Mg_2(PO_4)_{14}$

S. $[NaCa]Ca_{18}Mg_2(SiO_4)(PO_4)_{13}$

$\square$ = Site vacancy

[ ] = IIA site (octahedral)

II. Possible U^{+4}-bearing end members considered

1. $[U\ \square\ ]Ca_{18}Mg_2(SiO_4)_2(PO_4)_{12}$

2. $[\ \square\square\ ]UCa_{17}Mg_2(PO_4)_{14}$

3. $[Na\ \square\ ]UCa_{17}Mg_2(SiO_4)(PO_4)_{13}$

4. $[NaCa]Ca_{18}Mg_2(UO_4)(PO_4)_{13}$

5. $[Na\ \square\ ]UCa_{17}Mg_2(UO_4)(PO_4)_{13}$

U-free end members do not give particularly good fits to the total phosphate composition. Reduced chi-squared (Bevington, 1969) values of 7 to 9 are obtained for a typical analysis where values of 1-2 are expected for good fits. Somewhat surprisingly, the best fit (chi-squared = 1.75) occurs for end member 4 with U substituting for P (C:13.4%; M:62.8%; N:0%; S:14.8%; 4:9.0%). For 10 U-rich whitlockite analyses, end member 4 gives best fit in 8 cases; end member 5 is the best fit for the other two cases. However, these substitutions are a priori implausible given the large ionic size difference between U and P; consequently additional checking is needed to determine that this result is not just an artifact of the microprobe or least squares analysis. Mysen et al. (in press) have demonstrated that ($AlPO_4^\circ$) is a common species in P-bearing aluminous melts, so it is conceivable that, during crystal growth, a UPO_5^-, UPO_4^+, etc. structure is incorporated from the melt. A substitution utilizing end member four suggests that U partitioning may be fairly sensitive to melt Na content, a result which could be checked experimentally. In any case, the fact that the D_U(whit) differs between 20 ppm and percent level U concentrations implies that the substitution occurring at percent levels may not be valid at trace levels. Alternatively, as discussed below, the overall whitlockite composition changes for U-rich systems may be interpreted in terms of melt structural changes.

A possible indicator of a change in the melt structure with the addition of percent levels of U can be seen in the minor element data for whitlockite (Table 16) which do not appear, following the above discussion, to be involved in coupled substitutions with U. Although the Na partition coefficients are indistinguishable between the UTh20

and U23+U23' (which nominally differ only U content; Appendix III), the Mg and more noticably, Si, partition coefficients are higher for the U-rich compositions. For fO_2=air, U is primarily +6 and U-free phosphates are formed (footnote Table 21). These give a best fit: C:12.4%; M:69.5%; N:11.1%; S:7.0% which is very different from phosphates grown from low U systems, and further illustrates the differences due to percent levels of U. As discussed in Sections III-F, G, and H, an increase in the 'basic' nature of a melt due to addition of a network modifier element, will tend to increase the partition coefficients of the compatible elements while decreasing the incompatible (U, Th, Pu) element partition coefficients. Mg is different in that Watson (1976) found Mg to be slightly enriched in basic melts relative to coexisting, immiscible, acidic melts. Resolution of this observation with the Mg partitioning results (Table 16) requires more experimentation as the system studied by Watson (1976) was Fe-rich and the complex interactions of phosphorus in melts are just beginning to be elucidated (Mysen et al., 1980). If the observed effects on the Mg, Si, and U partition coefficients are due to structural changes in the melt (instead of activity coefficient changes for U or coupled substitutions for Mg and Si), then U appears to behave as a network modifier.

The sealed in air synthesis runs (Table 21) were attempts to compare trace element (D_U=0.002) and high U concentration partition coefficients for U^{+6}. The results are reproducible but higher than the corresponding results at $fO_2=10^{-8.5}$. These runs, and other 1 bar trace element runs (e.g., 20A-5A, Table 11), appear to be buffered by a contaminant more reducing than Co-CoO. The sooty material ubiquitous to the Caltech ventilation system is the most likely source. A follow-up high U run in a capsule left open to air produced whitlockite

crystals with U contents below the detection limit of the microprobe (<0.005 cation percent), confirming the low D_U(whit) values obtained from the trace element experiments that were also run open to air (20A-9A and 20A-11A, Table 11). To avoid this problem, as well as the problem of volitilization of Na and P inherent to open air runs, an oxidizing buffer such as hematitie-magnetite (Appendix II) must be used (e.g., 14A-2HM, Table 12).

J. Apatites

Several of the 20 composition, 20 kilobar, runs produced needles of apatite in addition to the whitlockite and clinopyroxene (Table 2). Apatite crystallization was induced by the presence of Cl, the most likely source being the actinide chloride spike solution. The melt is nearly Cl free after apatite crystallization, which probably precedes whitlockite crystallization (Table 6), and all the Cl in the starting material (Appendix III-4) is accounted for by the apatite. Only three runs yielded apatite crystals sufficiently large for reliable trace element partition coefficients to be measured (Table 10). The U partition coefficients agree, within errors, for the three samples. The ratio of the synthetic apatite to whitlockite D_U values (D_U(ap)/ D_U(whit)=3; Table 19) is lower than the observed ratio of 6-25 between chlorapatite and whitlockite in chondrites (Crozaz, 1974; Pellas and Storzer, 1975; Jones and Burnett, 1979). However, the appliciability of these data is questionable because, although all three samples of crystallized apatites have compositions nearly identical to that given in Table 6, the apatites are Si and Al rich and, more significantly, very halogen poor. The chlorapatite end member, $Ca_5(PO_4)_3Cl$, contrasts

with the average synthetic apatite composition, $(Ca_{4.68}Mg_{0.10}Na_{0.08}Si_{0.10}Al_{0.04})(PO_4)_{2.72}(SiO_4)_{0.28}(O_{0.33}[\ ]_{0.33}Cl_{0.33})$. The Al substitution for Ca is documented (Fisher and McConnell, 1969) and the Si substitution is made by analogy to Al and with the known characteristics of apatites to substitute most of the periodic table into their structures (McConnell, 1973; Kreidler and Hummel, 1970). This exotic Si substitution is required because there is more Si+P than can be accommodated in the tetrahedral sites. The anhydrous conditions of the 20 kilobar experiments should rule out the presence of an hydroxyapatite component replacing the $O_{0.33}$ and vacancy ($[\ ]_{0.33}$) with the obviously more attractive $OH_{0.67}$; however, without further characterization such as spectroscopically checking for the O-H stretching mode, the possibility of H_2 diffusion through the Pt capsule cannot be discarded.

K. Summary

Figures 19 and 20 summarize the magnitudes and relationships of the adopted partition coefficients (Tables 18 and 19). The valence state assignments are interpretive and are the best estimates, at present, of the dominant valence state under the conditions of the experimental synthesis runs (Section III-G, Appendix VI).

In addition to summarizing the actinide partition coefficients for clinopyroxene, Figure 19 is also a comparison with the lanthanide partition coefficients, as a function of ionic radii, for clinopyroxenes synthesized by Grutzeck et al. (1974) and for natural clinopyroxene phenocrysts analyzed by Schnetzler and Philpotts (1970). The Pu^{+3} partition coefficients are similar to the equivalent lanthanide partition coefficients, whereas the tetravalent actinide partition coefficients

FIGURE 19

The actinide (this work) and lanthanide (literature) partition coefficients for diopsidic clinopyroxene are compared as a function of ionic radius. The dashed line connects the lanthanide D values for synthetic diopsides as measured by Grutzeck et al. (1974). The solid lines connect two D patterns, representing the range of natural diopside phenocryst-matrix D values, as measured by Schnetzler and Philpotts (1970). The ionic radii (6-fold co-ordination) are taken from Shannon (1976). No appreciable relative differences would result for other choices of ionic or crystal radii, although 8-fold co-ordination radii would be appropriate for the M2 site in diopside (Table 20). Data points are plotted assuming trivalent Pu and tetravalent U and Th for our measurements at $fO_2=10^{-9}$. For reference the ionic radius locations of U^{+3}, Pu^{+4} and Ca^{+2} are indicated on the upper scale. Clinopyroxene shows a strong preference for partitioning trivalent, as opposed to tetravalent ions, presumably because of easier charge compensation. The strong dependence of P content for the +4 ions is clearly illustrated. The similarity in D values between Pu^{+3} and light lanthanides gives support to the use of Pu/Nd for chronology purposes. (See Tables 18 and 19 for errors).

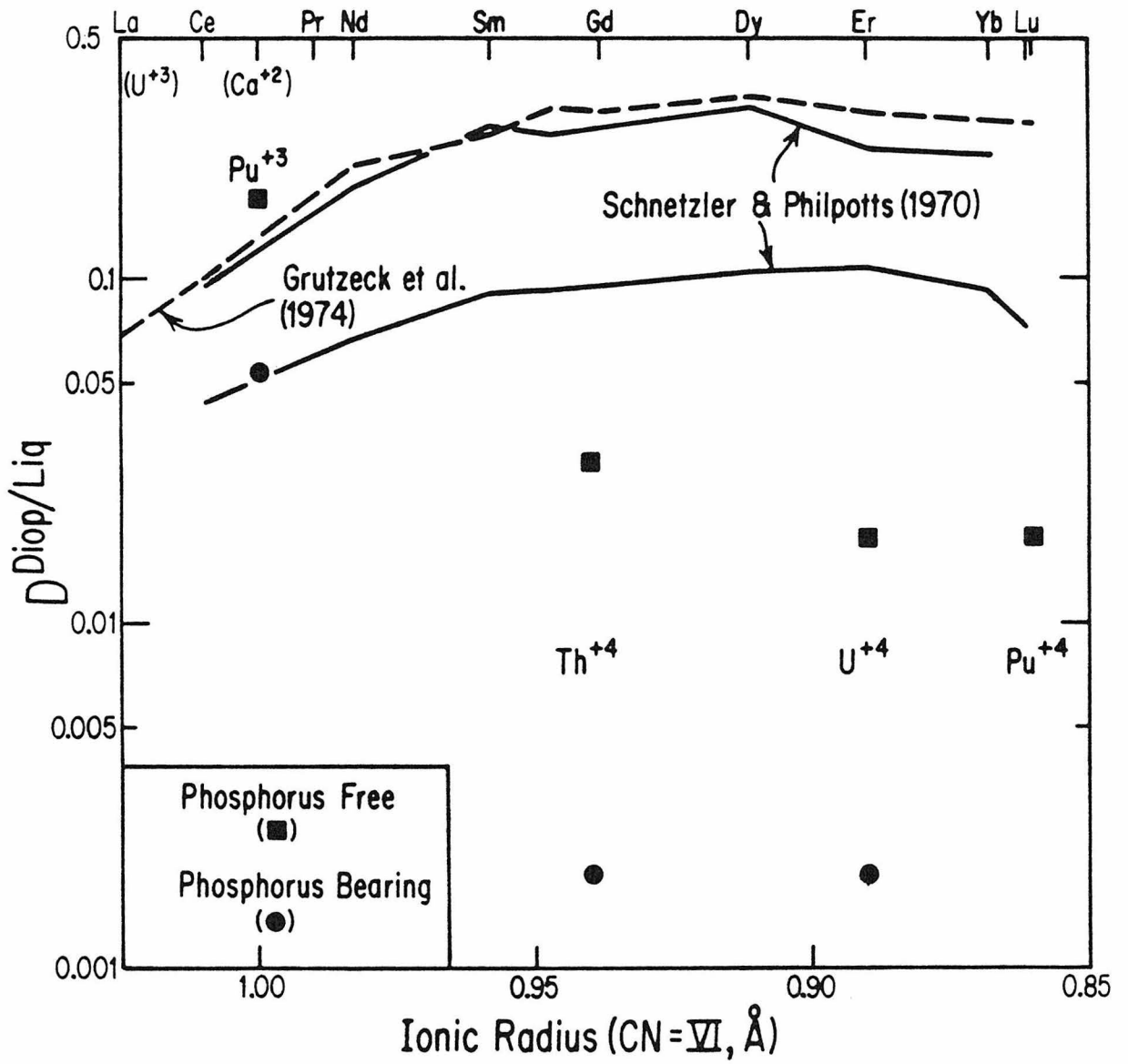
La
Ce
Pr
Nd
Sm
Gd
Dy
Er
Yb
Lu
0.5
0.1
0.05
0.01
0.005
0.001
(U+3)
(Ca+2)
Pu+3
Schnetzler & Philpotts (1970)
Grutzeck et al. (1974)
Th+4
U+4
Pu+4
Phosphorus Free (■)
Phosphorus Bearing (●)
D Diop/Liq
1.00
0.95
0.90
0.85
Ionic Radius (CN = VI, Å)

FIGURE 20

Experimental actinide crystal/liquid partition coefficients, $D^{Xl/Liq}$, are plotted in order of increasing atomic number. Data points are the best values from Tables 18 and 19. Data for both high phosphorus and phosphorus-free bulk composition experiments are plotted. In general the partition coefficients for whitlockite are much higher than those for diopsidic clinopyroxene. Valence state assignments for the various experimental conditions are indicated. The "+3" symbols for Pu imply only that the observed D value is dominated by the presence of Pu^{+3}. The measured D values at $fO_2=10^{-9}$ are strictly lower limits to the Pu^{+3} partition coefficients. Similarly, the 1 bar D_{Pu}^{+4}(whit) is an upper limit for the Pu^{+4} partition coefficient (see Section III-G and Appendix VI). A relatively smooth "D-pattern" (solid line) for the tetravalent actinides is observed. However, for natural (low) fO_2 conditions trivalent Pu will be important for $fO_2 \leq 10^{-9}$, whereas U and Th will probably remain tetravalent. (See Tables 18 and 19 for errors).

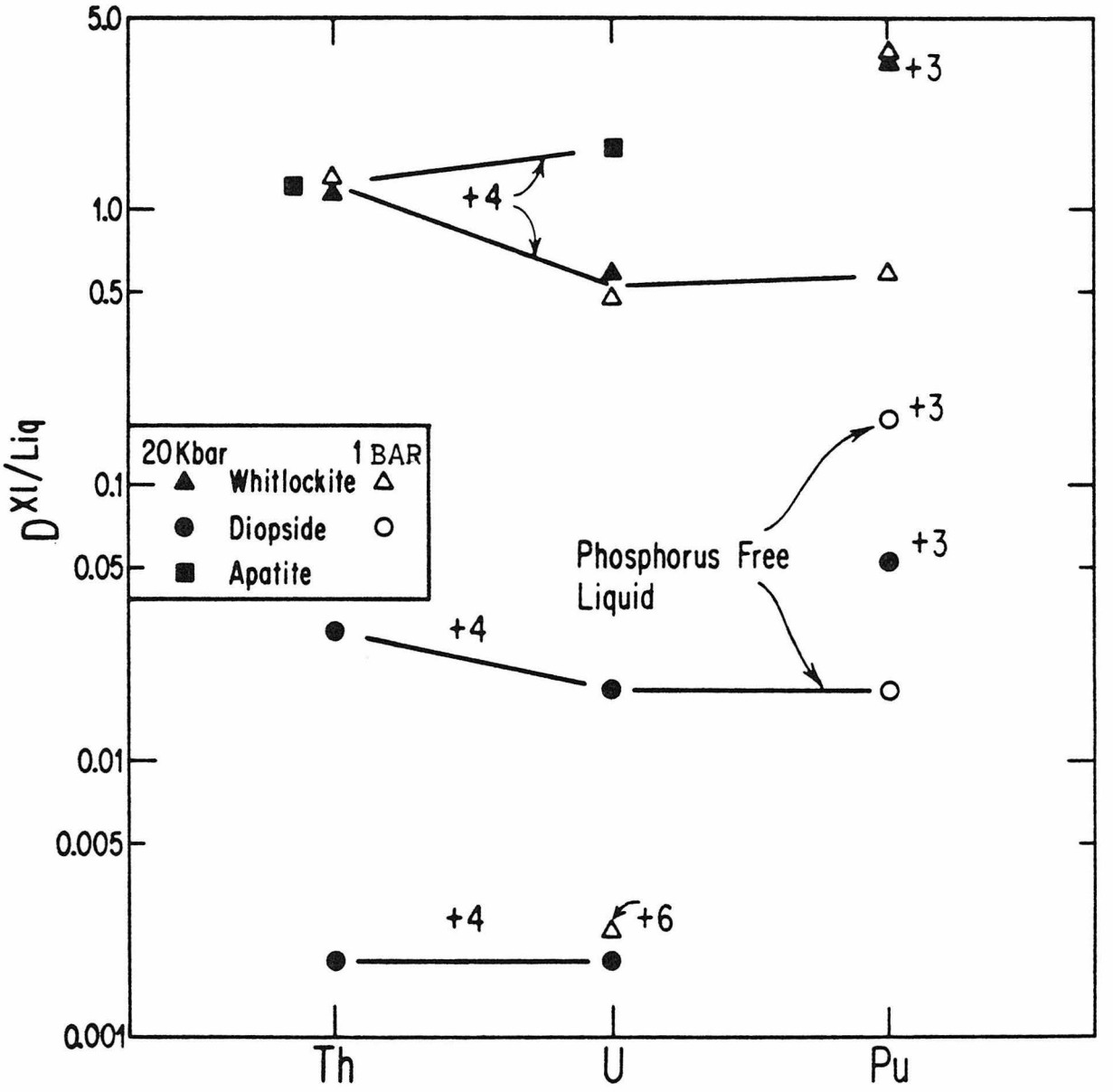
5.0
1.0
0.5
0.1
0.05
0.01
0.005
0.001
$D^{Xl/Liq}$
20 Kbar
1 BAR
Whitlockite
Diopside
Apatite
+3
+4
+3
Phosphorus Free
Liquid
+3
+4
+4
+6
Th
U
Pu

are one to two orders of magnitude lower, depending on bulk composition (i.e., P content). The similarity between the D_{Pu}+3(cpx) and those for the light lanthanides gives support to the use of Pu/Nd for chronology purposes (Section I-A).

Figure 20 summarizes the actinide whitlockite and apatite partitioning data along with the clinopyroxene data from Figure 19 as a function of increasing atomic number. For the +4 valence state, the partitioning patterns are similar in shape (but not magnitude) for whitlockite and clinopyroxene and for the different bulk compositions. The apatite data are incomplete and further experimentation is required to confirm the apparent difference between apatite and the other phases. Pressure has little effect on the partition coefficients. In contrast, fO_2 is important. For meteoritic and lunar (low) fO_2 conditions, trivalent Pu coexists with tetravalent U and Th; a condition where chemical fractionation of Pu from U and Th is likely to occur.

IV. APPLICATIONS AND CONCLUSIONS

A. Pu/Sm Partitioning

Laboratory measurements of crystal-liquid partition coefficients (D) for actinide elements (Pu, U, Th) and Sm for Ca-phosphate and diopsidic clinopyroxene permit a discussion of the possibility of relative age determinations for ancient objects utilizing the Pu/Nd ratio. As discussed in more detail below, from measured Sm partition coefficients (Benjamin et al., 1979), those for Nd can be estimated with the most significant result being that $D_{Pu}(cpx)/D_{Nd}(cpx) \cong D_{Pu}(phos)/D_{Nd}(phos) \cong 0.6$ (Table 23). Since D_{Pu} and D_{Nd} are not equal, the possibility of Pu/Nd chemical fractionation exists at $fO_2 \cong 10^{-9}$. At lower fO_2 conditions ($\sim 10^{-12}$), the D_{Pu}/D_{Nd} values may be closer to 1 (see Section III-G) for both whitlockite and clinopyroxene. For this case, Pu/Nd chemical fractionation would be negligible for most igneous differation models.

The Sm partition coefficients were determined by ^{151}Sm beta-radiography (Mysen and Seitz, 1975) by J. Jones. Nuclear emulsions (Ilford K5, 25 micron) were exposed to polished sections of the synthesis products (compositions 14 and 15, Appendix III-4, 50 ppm ^{151}Sm). Partition coefficients were measured by counting (15 KeV) electron-induced Ag L-alpha x-rays using either an electron microprobe or a scanning electron microscope equipped with a semiconductor detector (Si(Li)) (Holloway and Drake, 1975; Benjamin et al., 1977). Both the Pu and Sm partition coefficients were measured on the same samples to avoid problems due to differing bulk compositions. The necessity of this can be seen in both the actinide and lanthanide data presented in

TABLE 23

Pu/Sm Partitioning Summary

$fO_2 = 10^{-8.5}$

	Clinopyroxene (Phosphorus=0)	Whitlockite
D_{Pu} *	0.17±0.01	3.7±0.3
D_{Sm} **	0.36±0.03	6±1
D_{Sm}/D_{Nd}	1.25†	1.0††
D_{Pu}/D_{Nd}	0.59	0.62

* Table 18

** Benjamin et al., 1974

† Grutzeck et al., 1974

†† Estimated from Irving, 1978

Figure 19. The natural phenocryst/matrix lanthanide partition coefficients vary by a factor of five but the relative values vary by less than a factor of two. The same relationships exist for the actinide data, the relative values are more constant than the absolute values between different bulk compositions. The most important quantity is the relative D values for Pu and Sm.

As summarized in Table 23, the preliminary D_{Sm} values, under both reducing ($fO_2 \cong 10^{-9}$) and oxidizing conditions, are 6±1 for whitlockite and 0.36±0.03 for clinopyroxene (Benjamin et al., 1979). With these data, the D_{Pu} values from Table 19, and using D_{Sm}/D_{Nd} from Grutzeck et al. (1974), a $D_{Pu}(cpx)/D_{Nd}(cpx) = 0.59$ is inferred. There are no D patterns published for lanthanides in $Ca_3(PO_4)_2$ but, by analogy with data for apatites summarized by Irving (1978), we estimate $D_{Sm}(phos) \cong D_{Nd}(phos)$ which gives $D_{Pu}(phos)/D_{Nd}(phos) = 0.62$, in good agreement with the equivalent ratio for clinopyroxene.

The possibility of Pu/Nd chronology was proposed as a result of measurements on AdoR (Angra dos Reis) by Lugmair and Marti (1977) and Wasserburg et al. (1977), who found that the concentration ratio of ^{244}Pu to Nd was the same in clinopyroxene and $Ca_3(PO_4)_2$. The ratios of ^{244}Pu to either Th or U however, differed in the two phases. These results were interpreted as indicating that Pu and Nd tend not to fractionate, whereas considerable fractionation of Pu from Th or U can occur. Since relative D values for a set of chemically similar elements (lanthanides and trivalent Pu in this case) for a given mineral are expected to be comparatively insensitive to either bulk or phase chemical compositions, it is reasonable to assume - at least as a working hypothesis - that the laboratory D_{Pu}/D_{Nd} for a given phase applies

to AdoR, even though the absolute D values may not because of compositional differences between the two systems, particularly in Fe and Ti. This assumes that the lower fO_2 (10^{-12}, Brett et al., 1977) for AdoR would not significantly change D_{Pu}. It is equally (perhaps more) plausible to assume that the measured equality of D_{Pu}/D_{Nd} in clinopyroxene and whitlockite (Table 23) also applies to the AdoR system. The data in Tables 18 and 19 show, however, that constancy of relative D values as a function of composition is not maintained for elements in different valence states because the effect of adding 5.3 cation percent phosphorus on D(cpx) was a factor of ten decrease for U and Th but only a factor of three decrease for Pu.

In general, the fact that D_{Pu} and D_{Nd} are not equal permits fractionation of these elements in the crystallization of AdoR from its parent liquid. However, the degree of fractionation depends on the igneous differentiation model assumed. The petrographic observations of Prinz et al. (1977) convincingly establish AdoR as a cumulate rock; however, this conclusion is not sufficient in that additional assumptions must be made to interpret the actinide and lanthanide data.

A simple model by which to compare the partitioning data with AdoR involves the additional assumption that clinopyroxene and whitlockite were co-crystallizing phases. Although consistent with the petrographic observations, this assumption is, a priori, relatively implausible. However, this is a useful model for discussion. With these assumptions, the measured Pu/Nd concentration ratio in any phase i is related to the crystal-liquid partition coefficients, D:

$$(1) \quad (Pu/Nd)_i = D_{Pu}(i)/D_{Nd}(i) \; (Pu/Nd)_o \cdot f \text{ (composition, X)}$$

where $(Pu/Nd)_o$ refers to the original liquid from which crystallization has occured, and X is the fraction crystallized. Depending on the form of the function f (e.g., $(1-X)^{D_{Pu}-D_{Nd}}$ for fractional crystallization or $\frac{(1+X(D_{Nd}-1))}{(1+X(D_{Pu}-1))}$ for equilibrium crystallization), Equation (1) is valid for all degrees of crystallization and for both equilibrium and fractional crystallization. Alternatively, Equation (1) holds if Pu and Nd have re-equilibrated subsolidus, or if the clinopyroxene equilibrated with a late-stage liquid at the time of phosphate crystallization. The important point is that f is the same for all phases. Thus, <u>for these models</u>, the observed equality of Pu/Nd value in whitlockite and clinopyroxene requires only that the <u>ratio</u> of the partition coefficients for Pu and Nd be equal for these two phases but does not require $D_{Pu}(i) = D_{Nd}(i)$ where i = clinopyroxene or whitlockite. The required equality of D_{Pu}/D_{Nd} for clinopyroxene and whitlockite is in quantitative accord with the meteorite measurements. Quantitatively, if our observed $D_{Pu}/D_{Nd} = 0.6$ value applies to AdoR, which is a reasonable assumption, then for f ~1 the Pu/Nd in AdoR is lower by a factor of about 1.7 than in the parent liquid, leading to an error in a Pu/Nd relative age of 60 m.y. If phosphate is not a major reservoir for Pu and Nd, this factor of two fractionation is approximately correct even for amounts of crystallization up to ~90%. The assumptions of this model can be challenged, but it points to a general conclusion that the AdoR (Pu/Nd) data do not require $D_{Pu} = D_{Nd}$, but can be understood in terms of a constancy of the ratio D_{Pu}/D_{Nd} for the relevant phases. This model calculation also illustrates another general point in that, because both D_{Pu} and D_{Nd} are less than one for clinopyroxene, solid residues from igneous differentiation, such as AdoR, can have significantly different

Pu/Nd ratios from the initial magma and are the least suitable materials for Pu/Nd chronology in that the largest fractionation corrections would be required.

B. The Bracketing Theorem

In Benjamin et al. (1978) a 'bracketing theorem' was proposed based on the experimentally determined partition coefficients obtained during the course of this study. These results indicated that Pu was intermediate in its partitioning behavior (at least for $fO_2 \geq 10^{-9}$) between the tetravalent actinides, U and Th, and the middle lanthanides, Sm or Nd. That is, for clinopyroxene and whitlockite, a sequence is defined: $D_{Sm} > D_{Pu} > D_{Th} \geq D_U$ so Pu is bracketed between Sm (and therefore Nd, Grutzeck et al., 1974) and Th or U. Further experimentation is required to see if this relationship is valid for other minerals that are potentially significant reservoirs for the actinides. If generally valid, a consequence of this bracketing theorem is that any meteoritic/lunar sample which has an unfractionated whole-rock lanthanide-U-Th abundance, relative to Cl chondrites, would be expected to have both Pu/Nd and Pu/U ratios that could be interpreted chronologically.

If the Pu^{+3} partition coefficents calculated in Section III-G are significant for lower fO_2 values (e.g., $fO_2 = 10^{-12}$ for Angra dos Reis, Brett et al., 1977), then the bracketing theorem still applies essentially because Pu^{+3} behaves, geochemically, as a lanthanide. Even if U^{+3} is important under more reducing conditions, the above sequence should still hold. But under oxidizing conditions (all tetravalent actinides) the correlation with the lanthanides and therefore the bracketing theorem may not hold.

Few meteorites have Nd, Th, and U measured on the same specimen; however, it is likely that basaltic achondrites will satisfy the bracketing theorem. For the specific case of AdoR, it appears that, in addition to light rare earth depletion (Nd/La $\simeq$ 1.8 chondritic), U and Th are also depleted relative to Nd. Determination of the exact depletion factor (on a whole rock basis) is complicated by variability in literature U and Th concentrations (compare Tatsumoto et al., 1973 and Wasserburg et al., 1972) probably reflecting variable amounts of phosphate. However, accepting clinopyroxene as the major reservoir for U and Th in AdoR, and using the (>3.3) density fractions of Wasserburg et al., the (U/Nd) for AdoR is estimated to be 0.5xC1. Consequently, the cumulative effects of all chemical fractionation, in the evolution of AdoR relative to average solar system material, would be expected to increase Pu/U and decrease Pu/Nd for AdoR, but by no more than a factor of two. Comparison with the previous discussion, based on D_{Pu}/D_{Nd}, indicates that this fractionation could have occurred in the final step of separation of AdoR from its parent liquid. This conclusion is unfortunately tentative because the deviations of the AdoR lithophile abundance patterns from C1 are not large (less than a factor of two) and the significance of the C1 pattern, particularly Nd/U, at this level requires further study.

C. Application to Meteorite/Lunar Chronology

The data presented in this study (Tables 18 and 19; Figures 19 and 20) clearly demonstrate pronounced chemical fractionation of Pu from U or Th at fO_2 values ($10^{-8.5}$) representative of natural systems. If anything, these fractionations will probably be enhanced at lower fO_2

values characteristic of lunar rocks and most meteorites. Relative to the liquid, Th and U are also strongly fractionated by whitlockite and somewhat less fractionated by apatite and clinopyroxene. Interestingly, the Th/U fractionation factors (D_{Th}/D_U) are >1 for whitlockite and clinopyroxene and <1 for apatite. The unusual apatite composition (Section III-J) may be responsible for this difference, although Th/U ratios are higher in chondritic whitlockites relative to coexisting chlorapatites (Crozaz, 1974, 1978). The actinide partition coefficients are sensitive to bulk composition although the effects of Fe and Ti are unexplored. Fortunately, the correlated pressure and temperature changes do not appear to affect the partition coefficients greatly over the range studied (<1%/kilobar).

These results reiterate the necessity of applying a chemical fractionation correction to measured Pu/U or Pu/Th values obtained on mineral separates for chronological purposes. The compositional dependence of the partition coefficients and the limited quantification of that dependence at this time prevents quantitative application of these experimental fractionation factors. Pu/Th/U fractionation due to major phases (of which clinopyroxene is the most important actinide reservoir) is likely to be small because the fractionation factor is near unity for Th and U (≤1.6) and, more importantly, the partition coefficients are low (≤0.17). Major changes in relative actinide abundances must either be due to extreme fractionation processes or, more likely, due to a minor phase (or phases) that combine a fractionation factor different than unity and relatively large partition coefficients. Based on these experiments, whitlockite would be much more efficient than apatite in Pu/Th/U fractionation because whitlockite has

greater fractionation factors and in particular D_{Pu}(whit) and D_{Th}(whit) are >1 while D_U(whit) is <1.

The chemical coherence of Pu and the lanthanides has been experimentally demonstrated (Sections III-K and IV-A). The extent of Pu/Nd fractionation is not only dependent on the fractionation model assumed but also on the fO_2 of the system if Pu^{+4} is still important at $fO_2 = 10^{-8.5}$. Although the foregoing discussion (Section IV A and B) has focussed on situations where Pu and Nd can be fractionated, it should be emphasized that, because the bulk D values for both Pu and Nd are small, in many igneous differentiation processes, this fractionation will not be large; consequently, overall, the results presented in this thesis support the hypothesis of Pu/Nd dating.

Although quantitative discussions are premature, it is possible to evaluate the available meteoritic and lunar actinide (and lanthanide) data to determine which sample types are suitable for relative age measurements. Because many meteorites have essentially identical ages based on long-lived nuclei, those objects suitable for ^{244}Pu geochronology are likely to also be suitable for the cosmochronologically important determination of the solar-system actinide abundances.

The unequilibrated chondrites do not appear to be useful sources for whole rock Pu abundance determinations because of the high trapped gas content, particularly the anomalous heavy Xe component. This Xe may be of fission origin but not related to ^{244}Pu (Lewis et al., 1975) which makes the ^{244}Pu fission Xe determination extremely difficult. The classical source of cosmic abundances, the C1 and C2 chondrites, have very complex rare gas patterns (Pepin and Phinney, 1979; Frick and Moniot, 1977) and furthermore show relatively large variations in Th/U

(Morgan and Lovering, 1968; Stapanian et al., 1978).

The equilibrated chondrites are volatile poor, so ^{244}Pu fission Xe can be measured, with difficulty, in whole rock samples. Using the bracketing theorem discussed in Section IV-B, the whole rock abundances of the actinides should be unfractionated provided that these objects have essentially solar-system (i.e., C1) abundances for all lithophile refractory elements. A whole rock 'solar-system' $^{244}Pu/^{238}U$ value of 0.015 was obtained from St. Severin (LL6, Podosek, 1972) which is in agreement with the 0.016 value obtained from an Allende coarse-grained inclusion (Drozd et al., 1977). Mineral separates of phosphates (whitlockite and apatite) yield better Xe data (Wasserburg et al., 1969a; Lewis, 1975; Kirsten et al., 1977) but these phases have fractionated Th/U values (Crozaz, 1974) and variable Pu/U between coexisting apatite and whitlockite (Pellas and Storzer, 1975, 1979). The measured $^{244}Pu/^{238}U$ values from whitlockites have recently been used for relative chronology (Pellas and Storzer, 1979). This assumes that the Pu/U fractionation factor for whitlockites are constant and that these meteorites are equilibrated with respect to the actinides. The whitlockite/apatite variability is assumed to be a function of the apatite; a reasonable assumption considering the known variability in natural and synthetic apatites (McConnell, 1973). However, actinide disequilibrium must still be considered a possibility (Jones and Burnett, 1979).

The experimentally determined $D_U(ap)/D_U(whit)$, solid-solid, partition coefficient value of ~3 differs greatly from the range of values (6-23) measured on coexisting phosphates from equilibrated chondrites (Pellas and Storzer, 1974). This difference may be due to: 1) the lower temperatures (600-900°C) of meteorite equilibration

relative to the synthesis experiment, 2) difference in bulk composition or apatite composition, or 3) disequilibrium of the actinides between coexisting phosphates in meteorites, a real possibility in light of the spread in U concentrations between individual whitlockites and between individual apatites from a given chondrite (Pellas and Storzer, 1974).

The achondrites are igneous rocks (breccias), therefore crystal-liquid partition coefficients are directly applicable (see the discussion of AdoR in the preceding sections). These rocks are volatile poor and refractory lithophile rich which permits whole rock fission Xe measurements. Although not measured on the same samples, these objects may obey the bracketing theorem because unfractionated lanthanide (Schnetzler and Philpotts, 1968) and Th/U (Tatsumoto et al., 1973) values are observed. This implies that the low Pasamonte $^{244}Pu/^{238}U$ value (0.008; Hohenberg et al., 1966) is a result of an 80 m.y. time difference relative to St. Severin (0.015) or the Allende coarse-grained inclusion (0.016). The data presented in this thesis support the interpretation of the Pu/Nd variations between the basaltic achondrites (Marti et al., 1977) as age differences.

The coarse-grained Allende inclusions are both very interesting and complicated (see Grossman, 1980). The question of the genesis of these inclusions, whether vapor-solid condensation, vapor-liquid-solid condensation and crystallization, or vapor-solid-liquid-solid condensation followed by remelting and crystallization, is unresolved. In any case, Grossman and Ganapathy (1976) have proposed that Type A and B, (Grossman, 1975) inclusions are the best source of solar system actinide abundances because, on the average, these inclusions show no relative fractionation of refractory lithophile elements. This con-

clusion is probably valid as Boynton (1978) calculated that Pu is intermediate in volatility between Th and U during condensation. However, there is disagreement on the interpretation of the U and Th/U analytical data in terms of possible fractionation (Boynton, 1978). The experimentally determined bracketing theorem also supports the Grossman and Ganapathy conclusion. On other than a whole rock basis, the crystal-liquid (or crystal-crystal) partition coefficients are only of value if the inclusions crystallized from a melt or equilibrated subsolidus. The large intra and intercrystal U and Pu variabilities in clinopyroxenes and melilites from a single Type B inclusion argue against actinide equilibration (Shirck, 1974).

The Th/U ratio in lunar rocks is relatively constant at the accapted solar-system value of 3.8 (see e.g., Töksoz and Johnston, 1977). It would appear that Th and U have totally partitioned into the liquid phase and, only at the last instant of crystallization in mesostasis areas, has any fractionation occurred (Burnett et al., 1971). However, there are reported variations in Th/U ranging from 2 to 5, most spectacularly in adjoining depths in the 70008 core (Fruchter et al., 1975). Of particular interest are the low Th/U ratios observed in some Apollo 17 basalts, e.g., 71155 and 70255 (Keith et al., 1974; Laul and Fruchter, 1976). This problem was treated by Laul and Fruchter, but their conclusions are compromised because they guessed, incorrectly, at the relative partition coefficients required for their calculations. Because of the small fractionations and near zero partition coefficients of the major phases, which clinopyroxene should dominate, any Th/U variations are probably due to minor phases, the phosphates being likely candidates.

Evidence for ^{244}Pu decay products in lunar samples is quite strong (Drozd et al., 1972; Marti et al., 1973; Hutcheon and Price, 1972; Haines et al., 1975; Braddy et al., 1975), and the latter four papers give evidence of in situ Pu decay in rocks of 3.95×10^9 year age. One line of interpretation for lunar Pu/U ratios is to compare with meteoritic ratios at some fixed reference time to see if evidence for Pu/U fractionation - perhaps in the formation of the moon - can be found (Hutcheon and Price, 1972). The precise relative ages between meteorites and lunar rocks, which are required for this application, are not known. Although the experimental partition coefficients would be applicable to the crystalline phases in these objects, their application cannot solve this problem.

An alternative approach to the interpretation of lunar ^{244}Pu data - as yet unused - is to assume no Pu/U fractionation for the moon as a whole, by analogy with the apparent lack of Th/U fractionation. (A complication is that it cannot be proven that the moon has an unfractionated lanthanide pattern). Then, knowing a meteorite Pu/U at some reference time (e.g., time of fission Xe retention in St. Severin) and assuming no chemical fractionation, ages for lunar samples relative to St. Severin or relative ages of lunar samples among themselves could be calculated fairly precisely. Such relative ages would be of great interest in assessing the time spread of the period of intense bombardment. The key problem, of course, is again to correct any Pu/U fractionation that may have occurred, and the experimental data would be directly relevant in this case. However, even given accurate knowledge of partition coefficients, there are serious problems with this approach, e.g., whole-rock Pu/U fractionation must be evaluated in terms

of a model for the formation of the sample in question.

D. Application to Cosmochronology

Chondrites are the closest approximation to solids of average solar system composition so, if possible, the solar-system Pu/U/Th abundances should be derived from these meteorites. The experimental partition coefficients show that Pu is chemically intermediate between Nd and U or Th in igneous processes, and the calculations of Boynton (1978) predict that Pu is also of intermediate volatility relative to these elements. Thus, the equilibrated chondrites should have unfractionated Pu/U/Th abundances provided they show the Cl Nd/Th/U relative abundances. The factor of two scatter in Nd/U/Th chondritic abundances may be due to analytical and sampling errors. If the Nd/U/Th abundances prove to be unfractionated then the whole rock $^{244}Pu/^{238}U$ value of 0.015 for St. Severin should represent the true solar system ratio at the time of formation of St. Severin (Jones and Burnett, 1979). Taken at face value, $^{244}Pu/^{238}U$ values >0.015 require an increase in the rate of r-process nucleosynthesis just prior to the isolation of the solar system (Schramm and Wasserburg, 1970; Fowler, 1977). Consequently, knowledge of the solar system Pu abundance to better than a factor of two is important.

As noted in Section IV-C, the pronounced Pu/U fractionation, e.g., as measured in this thesis relative to a basaltic liquid ($D_{Pu}/D_U \sim 7$ for whitlockite, ≥ 9 for clinopyroxene), implies that the interpretation of Pu/U from mineral separates, as opposed to whole rock values, is complex. Specifically, $^{244}Pu/^{238}U$ values (0.03-0.130) in whitlockite (Wasserburg et al., 1969a; Lewis, 1975; Kirsten et al., 1977) undoubtedly

reflect the preferential incorporation of trivalent Pu.

The whitlockite partition coefficients presented in this study ($D_{Pu}>D_{Th}>D_U$) suggest that the measured $^{244}Pu/^{238}U$ values from whitlockites are upper limits for the solar-system abundance ratio. The constancy of $D_{Pu}/D_{Th}/D_U$(whit) must be investigated, experimentally, for fO_2 and bulk compositions relevant to the chondrites. (Note that the ratios of the whitlockite partition coefficients are not constant between $fO_2=10^{-8.5}$ and fO_2=air [Table 19]).

As discussed by Kelly and Wasserburg (1978), a recent nucleosynthetic event, required by the discovery of in situ ^{26}Al and (probably) ^{107}Pd, complicates the chronology of earlier periods of nucleosynthesis. The relative abundances of these short lived nuclides are a few times 10^{-5} that of a stable isotope of the corresponding element (Esat et al., 1979; Kelly and Wasserburg, 1978). The $^{244}Pu/^{238}U$ abundance is $1.5x10^{-2}$; unless the most recent event had an anomolously high yield of ^{244}Pu relative to the other nuclides from this event, then most of the ^{244}Pu must be ascribed to an earlier period (event). The crux of the problem is ^{129}I which has an abundance, relative to ^{127}I, of 10^{-4} (Hohenberg et al., 1967). If none of the ^{129}I was produced in the most recent event, then the $^{129}I/^{127}I$ data alone can set the order of magnitude ($2x10^8$ years) of the interval between the 'next-to-last' event and condensation (Schramm and Wasserburg, 1970). It is possible that all the ^{129}I was produced in the ^{26}Al and ^{107}Pd nucleosynthetic event, consequently the interval to the 'next-to-last' event could be relatively long. An upper limit of $5x10^8$ years is set by assuming that all of the solar system ^{244}Pu and ^{232}Th was produced by the 'next-to-last' event. However, as pointed out by Schramm and Wasserburg (1970), if

only ten percent of the ^{129}I came from the earlier era, then the isolation interval between the 'next-to-last' event and meteorite formation would still be well-defined and increased by only 0.6×10^8 years, compared to the 2×10^8 year value calculated by Schramm and Wasserburg prior to the discovery of ^{26}Al.

E. Application to Petrogenesis

The low and nearly equal U and Th partition coefficients for clinopyroxene, when applied to models of fractional crystallization and melting, will not produce significant fractionation of Th from U in most cases. Extreme degrees of fractionational melting or crystallization or multistage combinations can result in clinopyroxene controlled Th/U fractionation; however, this fractionation is much more easily done by the minor phases. The whitlockite and the apatite synthesized in this study concentrate the actinides by one to two orders of magnitude relative to clinopyroxene so small modal proportions of these phases will control a significant part, if not nearly all, of the total amount of actinide in the system. Similar roles might be played by baddelyite, zircon or sphene. As discussed in Section IV-C, whitlockite should be very effective in fractionating Th from U because the partition coefficients are on opposite sides of unity. The apatite partition coefficients are both greater than unity so Th and U fractionation would be less easily achieved.

In terms of the oceanic basalts (Tatsumoto, 1978) and Apollo 17 basalts (Laul and Fruchter, 1976) that have Th/U values different (higher and lower) than the accepted value of 3.8, minor phases such as the phosphates or extremes in fractionation appear necessary. The major

phases (i.e., clinopyroxene) could not produce these fractionations unless the fractionation occurred at a very late stage in the evolution of the liquid (provided the range of clinopyroxene partition coefficients in natural systems is not an order of magnitude greater than that observed experimentally in the P-free systems).

The problems of fO_2, bulk composition, cooling rate, and 'trace element' concentration have all been presented and discussed in the text. The effects of these have been shown to be, at least potentially, significant. The creators of petrogenetic models based on trace elements as well as the experimental petrologists are forced to concern themselves with these aspects of partitioning. Further experimental work on natural compositions, if attention is given to the other important parameters, will determine the sensitivity and therefore the criticality in the selection and modelling of trace element data.

F. Application to Radioactive Waste Disposal

The parameters of fO_2, bulk composition, cooling rate, and 'trace element' concentration have been demonstrated to have a significant influence on the partition coefficients for incompatible elements. Although the readily soluble phosphates are not good candidates for waste storage, the major effect of bulk composition and fO_2 (for multivalent cations) on clinopyroxene partitioning suggests that tailoring of synthesis conditions can increase the efficiency and economy of permanent storage of radioactive waste in stable crystalline structures.

For example, the fO_2 conditions could be used to regulate the valence state of multivalent elements. This would either enhance (as for Pu^{+3} relative to Pu^{+4}) or decrease (as for U^{+6}) the partitioning in

a particular phase to yield synthetic crystals with the desired element at the desired activity (which must be regulated to insure stability of the crystalline phases over geologic time). Reduction of Pu to Pu^{+2} would make end member phase compositions such as $PuMgSi_2O_6$ or $PuAl_2Si_2O_8$ easily possible. Bulk composition not only determines the phases that crystallize and the sequence of crystallization, but also affects the magnitudes of the partition coefficients of the trace and minor elements. The range of experimental compositions used in this work is not extensive, but the possibilities are clear.

Cooling rate and initial 'trace element' concentrations have much smaller effects than the variables of fO_2 and bulk composition; however, these smaller effects (for the elements and systems studied in this work) may be significant in incorporating very large, incompatible, elements like ^{137}Cs or ^{129}I in stable crystal structures.

REFERENCES

Ackermann, R. J. and Chandrasekharaiah, M. S. (1974) Systematic thermodynamic properties of actinide metal-oxygen systems at high temperatures. In Thermodynamics of Nuclear Materials II, 3-26. International Atomic Energy Agency, Vienna.

Ahrens, L. H. (1952) The use of ionization potentials, Part 1. Ionic radii of the elements. Geochim. Cosmochim. Acta 2, 155-169.

Albarede, F. and Bottinga, Y. (1972) Kinetic disequilibrium in trace element partitioning between phenocrysts and host lava. Geochim. Cosmochim. Acta 36, 141-156.

Alexander, E. C., Jr., Lewis, R. S., Reynolds, J. H. and Michel, M. C. (1971) Plutonium-244: Confirmation as an extinct radioactivity. Science 172, 837-840.

Ando, J. (1957a) Tricalcium phosphate and its variations. Bull. Chem. Soc., Japan, 31, 196-201.

Ando, J. (1957b) Phase diagrams of $Ca_3(PO_4)_2$-$Mg_3(PO_4)_2$ and $Ca_3(PO_4)_2$-$CaNaPO_4$ systems. Bull. Chem. Soc., Japan, 31, 201-205.

Arden, J. W. (1977) Isotopic composition of uranium in chondritic meteorites, Nature 269, 788-789.

Bell, P. M. and England, J. L. (1967) High-pressure experimental techniques. In Researches in Geochemistry (ed. P. Abelson), 2, 619-638. Wiley, New York.

Bence, A. E. and Albee, A. L. (1968) Empirical correction factors for the electron microanalysis of silicates and oxides. J. Geol. 76, 382-403.

Benjamin, T. M., Arndt, N. T. and Holloway, J. R. (1977) Instrumental techniques for beta-track mapping. Carnegie Inst. Wash., Year. 76, 658-660.

Benjamin, T. M., Heuser, W. R. and Burnett, D. S. (1978) Laboratory studies of actinide partitioning relevant to ^{244}Pu chronometry. Proc. 9th Lunar and Plan. Sci. Conf., Geochim. Cosmochim. Acta Suppl. 10, 1, 1393-1406. Pergamon, New York.

Benjamin, T. M., Jones, J. H. and Burnett, D. S. (1979) Laboratory partitioning studies testing the validity of ^{244}Pu-rare earth chronology (Abstract). In Lunar Plan. Sci. X, 98-100. Lunar and Planetary Inst., Houston.

Beswick, A. E. and Carmichael, I. S. E. (1978) Constraints on mantle source compositions imposed by phosphorus and the rare-earth elements. Contrib. Min. Pet. 67, 317-330.

Bevington, P. R. (1969) Data Reduction and Error Analysis for the Physical Sciences. McGraw-Hill, San Francisco.

Bottinga, Y. and Weill, D. F. (1972) The viscosity of magmatic silicate liquids: A model for calculation. Am. J. Sci. 272, 438-475.

Bowen, N. L. (1915) The crystallization of haplobasaltic, haplo-dioritic and related magmas. Am. J. Sci. XL, 161-185.

Boynton, W. V. (1978) Fractionation in the solar nebula, II. Condensation of Th, U, Pu and Cm. Earth Planet. Sci. Lett. 40, 63-70.

Braddy, D., Hutcheon, I. D. and Price, P. B. (1975) Crystal chemistry of Pu and U and concordant fission track ages of lunar zircons and whitlockites. Proc. 6th Lunar Sci. Conf., Geochim. Cosmochim. Acta Suppl. 6, 3, 3587-3600. Pergamon.

Brett, R., Huebner, J. S. and Sato, M. (1977) Measured oxygen fugacities of the Angra dos Reis achondrite as a function of temperature. Earth Planet. Sci. Lett. 35, 363-368.

Burnett, D. S., Monnin, M., Seitz, M., Walker, R. and Yuhas, D. (1971) Lunar astrology-U-Th distributions and fission-track dating of lunar samples. Proc. 2nd Lunar Sci. Conf., Geochim. Cosmochim. Acta Suppl. 2, 2, 1503-1519. MIT, Cambridge.

Calas, G. (1979) Etude expérimentale du comportement de l'uranium dans les magmas: Etats d'oxydation et coordinance. Geochim. Cosmochim. Acta 43, 1521-1531.

Calvo, C. and Gopal, R. (1975) The crystal structure of whitlockite from the Palermo quarry. Am. Min. 60, 120-133.

Cantelaube, Y., Maurette, M. and Pellas, P. (1967) Traces d'ions lourds dans les minéraux de la chondrite de St. Severin. In Radioactive Dating and Methods of Low Level Counting, 215-229. International Atomic Energy Agency, Vienna.

Champion, D. E., Albee, A. L. and Chodos, A. A. (1974) Reproducibility and operator bias in a computer-controlled system for quantitative electron microprobe analysis. Proc. 10th Nat. Conf. Electron Probe Assn.55A,

Chen, J. H. and Tilton, G. R. (1979) Preliminary studies of uranium isotopic composition in chondritic meteorites. (Abstract). In Lunar Plan. Sci. X, 192-194. Lunar and Planetary Inst., Houston.

Crozaz, G. (1974) U, Th, and extinct ^{244}Pu in the phosphates of the St. Severin meteorite. Earth Planet. Sci. Lett. 23, 164-169.

Crozaz, G. (1979) Uranium and thorium microdistributions in stony meteorites. Geochim. Cosmochim. Acta 43, 127-136.

Donaldson, C. H. (1975) Calculated diffusion coefficients and the growth rate of olivine in a basaltic magma. Lithos 8, 163-174.

Donaldson, C. H., Williams, R. J. and Lofgren, G. (1975) A sample holding technique for study of crystal growth in silicate melts. Am. Min. 60, 324-326.

Dowty, E. (1977) Phosphate in Angra dos Reis: Structure and composition of the $Ca_3(PO_4)_2$ minerals. Earth Planet. Sci. Lett. 35, 347-351.

Drozd, R. J., Hohenberg, C. M. and Ragan, D. (1972) Fission xenon from extinct ^{244}Pu in 14301. Earth Planet. Sci. Lett. 15, 338-346.

Drozd, R. J., Morgan, C. J., Podosek, F. A., Poupeau, G., Shirck, J. R. and Taylor, G. J. (1977) ^{244}Pu in the early solar system? Ap. J. 212, 567-580.

Esat, T. M., Lee, T., Papanastassiou, D. A. and Wasserburg, G. J. (1978) Search for ^{26}Al in the Allende FUN inclusion C1. Geophys. Res. Lett. 5, 807-810.

Finger, L. W. and Ohashi, Y. (1976) The thermal expension of diopside to 800 ^{o}C and a refinement of the crystal structure at 700 ^{o}C. Am. Min. 61, 303-310.

Fisher, D. J. and McConnell, D. (1969) Aluminum-rich apatite. Science 164, 551-553.

Fleischer, R. L., Price, P. B. and Walker, R. M. (1975) Nuclear Tracks in Solids. University of California, Los Angeles.

Fowler, W. A. (1971) New observations and old nucleocosmochronologies. Ch 7, In Cosmology, Fusion and Related Matters: A memorial to George Gamow (ed. F. Reines). Colorado Associated University Press, Boulder.

Fowler, W. A. (1977) Nuclear cosmochronology. Ch III, In Proc. of The Robert A. Welch Foundation Conferences on Chemical Research, XXI. Cosmochemistry.

Frick, U. and Moniot, R. K. (1977) Planetary noble gas components in Orgueil. Proc. 8th Lunar Sci. Conf., Geochim. Cosmochim. Acta Suppl. 8, 1, 229-261.

Friedlander, G., Kennedy, J. W. and Miller, J. M. (1964) Nuclear and Radiochemistry. Wiley, New York.

Fruchter, J. S., Rancitelli, L. A. and Perkins, R.W. (1975) Primordial Radionuclide variations in the Apollo 15 and 17 deep core samples and in Apollo 17 igneous rocks and breccias. Proc. 6th Lunar Sci. Conf., Geochim. Cosmochim. Acta Suppl. 6, 2, 1399-1406.

Ganapathy, R. and Grossman, L. (1976) Trace elements in the Allende meteorite-I. Coarse-grained, Ca-rich inclusions. Geochim. Cosmochim. Acta 40, 331-344.

Garrels, R. M. and Christ, C. L. (1965) Solutions, Minerals, and Equilibria. Harper and Row, New York.

Gast, P. W. (1968) Trace element fractionation and the origin of tholeiitic and alkaline magma types. Geochim. Cosmochim. Acta 32, 1057-1086.

Gray, C. M., Papanastassiou, D. A. and Wasserburg, G. J. (1974) The identification of early condensates from the solar nebula. Icarus 20, 213-239.

Gray, C. M. and Compston, W. (1974) Excess ^{26}Mg in the Allende meteorite. Nature 251, 495-497.

Grossman, L. (1975) Petrology and mineral chemistry of Ca-rich inclusions in the Allende meteorite. Geochim. Cosmochim. Acta 39, 433-454.

Grossman, L. and Ganapathy, R. (1976) The case for an unfractionated $^{244}Pu/^{238}U$ ratio in high-temperature condensates. Earth Planet. Sci. Lett. 31, 386-392.

Grossman, L. (1980) Refractory inclusions in the Allende meteorite. Submitted to Ann. Rev. Earth Planet. Sci.

Grutzeck, M., Kreidelbaugh, S. and Weill, D. (1974) The distribution of Sr and REE between diopside and silicate liquid. Geophys. Res. Lett. 1, 273-275.

Haines, E. L., Hutcheon, I.D. and Weiss, J. R. (1975) The fission track record of Appenine Front KREEP basalts. Proc. 6th Lunar Sci. Conf., Geochim. Cosmochim. Acta Suppl. 6, 3, 3527-3540.

Harrison, W. J. (1977) An experimental study of the partitioning of samarium between garnet and liquid at high pressures (Abstract). In International Conference on Experimental Trace Element Partitioning, Sedona, 41-42.

Hazen, R. M. and Finger, L. W. (1977) Crystal structure and compositional variation of Angra dos Reis fassaite. Earth Planet. Sci. Lett. 35, 357-362.

Hofmann, A. W. and Magaritz, M. (1977) Diffusion of Ca, Sr, Ba, and Co in a basalt melt: Implications for the geochemistry of the mantle. J. Geophys. Res. 82, 5432-5440.

Hohenberg, C. M., Munk, M. N. and Reynolds, J. H. (1967) Spallation and fissiogenic xexon and krypton from stepwise heating of the Pasamonte achondrite; The case for extinct plutonium 244 in meteorites; Relative ages of chondrites and achondrites. J. Geophys. Res. 72, 3139-3177.

Hohenberg, C. M. (1969) Radioisotopes and the history of nucleosynthesis in the galaxy. Science 166, 212-215.

Hollister, L. S. (1966) Garnet zoning: An interpretation based on the Rayleigh fractionation model. Science 154, 1647-1651.

Holloway, J. R. and Drake, M. J. (1977) Quantitative microautoradiography by x-ray emission micro-analysis. Geochim. Cosmochim. Acta 41, 1395-1397.

Huebner, J. S. (1971) Buffering techniques for hydrostatic systems at elevated pressures. Ch 5 IN Research Techniques for High Pressure and High Temperature (ed. G. C. Ulmer), 123-177. Springer-Verlag, New York.

Huebner, J. S. (1975) Oxygen fugacity values of furnace gas mixtures. Am. Min. 60, 815-823.

Huneke, J. C., Smith, S. P., Rajan, R. S., Papanastassiou, D. A. and Wasserburg, G. J. (1977) Comparison of the chronology of the Kapoeta parent planet and the moon (Abstract). In Lunar Sci. VIII, 484-486. Lunar Science Institute, Houston.

Hutcheon, I. D. and Price, P. B. (1972) Plutonium-244 fission tracks: Evidence in a lunar rock 3.95 billion years old. Science 176, 909-911.

Irving, A. J. (1978) A review of experimental studies of crystal/liquid trace element partitioning. Geochim. Cosmochim. Acta 42, 743-770.

Ito, J. (1968) Silicate apatites and oxyapatites. Am. Min. 53, 890-907.

Johnson, R. (1969) Cast your own-Why not? Strategy and Tactics III, 12-13.

Johnston, W. D. (1965) Oxidation-reduction equilibria in molten $Na_2O \cdot 2SiO_2$ glass. J. Am. Ceram. Soc. 48, 184-190.

Joiner, B. L. (1969) Student-t deviate corresponding to a given normal deviate. J. Res. Nat. Bur. Stand. 73c,15-16.

Jones, J. H. and Burnett, D. S. (1979) The distribution of U and Pu in the St. Severin chondrite. Geochim. Cosmochim. Acta 43, 1895-1905.

Katz, J. J. and Rabinowich, E. (1951) The Chemistry of Uranium: The Element, Its Binary and Related Compounds. Dover, New York.

Keith, J. E., Clark, R. S. and Bennett, L. J. (1974) Determination of natural and cosmic ray induced radionuclides in Apollo 17 lunar samples. Proc. 5th Lunar Sci. Conf., Geochim. Cosmochim. Acta Suppl. 5, 2, 2121-2138.

Kelly, W. R. and Wasserburg, G. J. (1978) Evidence for the existence of ^{107}Pd in the early solar system. Geophys. Res. Lett. 5, 1079-1082.

Kirkpatrick, R. J. (1974) Kinetics of crystal growth in the system $CaMgSi_2O_6$-$CaAl_2SiO_6$. Am. J. Sci. 274, 215-242.

Kirkpatrick, R. J., Robinson, G. R. and Hays, J. F. (1976) Kinetics of crystal growth from silicate melts: Anorthite and diopside. J. Geophys. Res. 81, 5715-5720.

Kirsten, T., Jordan, J., Richter, H., Pellas, P. and Storzer, D. (1977) Plutonium in phosphates from ordinary chondrites inferred from xenon and track data. Meteoritics 12, 279-281.

Kreidler, E. R. and Hummel, F. A. (1970) The crystal chemistry of apatite: Structure fields of fluor- and chlorapatite. Am. Min. 55, 170-184.

Kushiro, I. (1976) Changes in viscosity and structure of melt of $NaAlSi_2O_6$ composition at high pressures. J. Geophys. Res. 81, 6347-6350.

Kushiro, I., Yoder, H. S., Jr. and Mysen B. O. (1976) Viscosities of basalt and andesite melts at high pressures. J. Geophys. Res. 81, 6351-6356.

Laul, J. C. and Fruchter, J. S. (1976) Thorium and uranium in Apollo 17 basalts, and K-U systematics. Proc. 7th Lunar Sci. Conf., Geochim. Cosmochim. Acta Suppl. 7, 2, 1545-1559.

Lee, T. and Papanastassiou, D. A. (1974) Mg isotopic anomalies in the Allende meteorite and correlation with O and Sr effects. Geophys. Res. Lett. 1, 225-228.

Lee, T., Papanastassiou, D. A. and Wasserburg, G. J. (1976) Demonstration of ^{26}Mg excess in Allende and evidence for ^{26}Al. Geophys. Res. Lett. 3, 41-44. Correction: 3, 109-112.

Lee, T., Papanastassiou, D. A. and Wasserburg, G. J. (1977) Calcium isotopic anomalies in the Allende meteorite. Ap. J. (Lett.) 211, L107.

Lee, T., Russell, W. A. and Wasserburg, G. J. (1979) Calcium isotopic anomalies and the lack of aluminum-26 in an unusual Allende inclusion. Ap. J. 228, L93-L98.

Lewis, P. S. (1975) Rare gases in separated whitlockite from the St. Severin chondrite: Xenon and krypton from fission of extinct ^{244}Pu. Geochim. Cosmochim. Acta 39, 417-432.

Lewis, R. S., Srinivasan, B. and Anders, E. (1975) Host phase of a strange xenon component in Allende. Science 190, 1251-1262.

Lindstrom D. J. and Weill, D. F. (1978) Partitioning of transition metals between diopside and coexisting silicate liquids-I. Nickel, cobalt, and manganese. Geochim. Cosmochim. Acta 42, 817-832.

Lugmair, G. W. and Marti, K. (1977) Sm-Nd-Pu timepieces in the Angra dos Reis meteorite. Earth Planet. Sci. Lett. 35, 273-284.

Lugmair, G. W., Marti, K. and Scheinin, N. B. (1978) Incomplete mixing of products from R-, P-, and S-process nucleosynthesis: Sm-Nd systematics in Allende inclusion EK 1-04-1 (Abstract). In Lunar Plan. Sci. IX 2, 672-674. Lunar Plan. Sci. Inst., Houston.

Mao, H.-K., Bell, P. M. and England, J. L. (1971) Tensional errors and drift of thermocouple electromotive force in the single-stage, piston-cylinder apparatus. Carnegie Inst. Wash., Year. 70, 281-287.

Marti, K., Lightner, B. D. and Lugmair, G. W. (1973) On ^{244}Pu in lunar rocks from Fra Mauro and implications regarding their origin. The Moon 8, 241-250.

Marti, K., Lugmair, G. W. and Scheinin, N. B. (1977) Sm-Nd-Pu systematics in the early solar system (Abstract). In Lunar Sci. VIII, 619-621. Lunar Sci. Inst., Houston.

Matsui, Y., Onuma, N., Nagasawa, H., Higuchi, H. and Banno, S. (1977) Crystal structure control in trace element partition between crystal and magma. Bull. Soc. fr. Mineral. Cristallogr. 100, 315-324.

Mattinson, J. M., Tilton, G. R., Todt, W. and Chen, J. H. (1977) Lead isotope studies of mare basalt 70017. Proc. 8th Lunar Sci. Conf., Geochim. Cosmochim. Acta Suppl. 8, 2, 1473-1487.

McConnell, D. and Hey, M. H. (1969) The oxyapatite (voelckerite) problem. Min. Mag. 37, 301-303.

McConnell, D. (1973) Apatite: Its Crystal Chemistry, Mineralogy, Utilization, and Geologic and Biologic Occurrences. Springer-Verlag, New York.

McCulloch, M. T. and Wasserburg, G. J. (1978a) Barium and Neodymium isotopic anomalies in the Allende meteorite. Ap. J. (Lett.) 220, L15-L19.

McCulloch, M. T. and Wasserburg, G. J. (1978b) More anomalies from the Allende meteorite: Samarium. Geophys. Res. Lett. 5, 599-602.

McSween, H. Y., Jr. (1976) A new type of chondritic meteorite found in lunar soil. Earth Planet. Sci. Lett. 31, 493-499.

Morgan, J. W. and Lovering, J. F. (1968) Uranium and thorium abundances in chondritic meteorites. Talanta 15, 1079-1095.

Morris, R. V. and Haskin, L. A. (1974) EPR measurement of the effect of glass composition on the oxidation states of europium. Geochim. Cosmochim. Acta 38, 1435-1445.

Morris, R. V., Haskin, L. A., Biggar, G. M. and O'Hara, M. J. (1974) Measurement of the effects of temperature and partial pressure of oxygen on the oxidation states of europium in silicate glasses. Geochim. Cosmochim. Acta 38, 1447-1459.

Mory, J., DeGuillebon, D. and Delsarte, G. (1970) Measurement or the mean range of fission fragments using mica as a detector-Influence of the crystalline structure. Radiation Effects 5, 37-40.

Myers, J. and Gunter, W. D. (1979) Measurement of the oxygen fugacity of the colbalt-cobalt oxide buffer assemblage. Am. Min. 64, 224-228.

Mysen, B. O. and Seitz, M. G. (1975) Trace element partitioning determined by beta track mapping: An experimental study using carbon and samarium as examples. J. Geophys. Res. 80, 2627-2635.

Mysen, B. O. (1978) Limits of solution of trace elements in minerals according to Henry's Law: Review of experimental data. Geochim. Cosmochim. Acta 42, 871-886.

Mysen, B. O., Virgo, D., Hoover, J. and Sharma, S. K. (1978) Experimental data bearing on Eu^{+2}/Eu^{+3} in silicate melts and crystals. Carnegie Inst. Wash., Year. 77, 677-682.

Mysen, B. O., Ryerson, F. J. and Virgo, D. (1980) The structural role of phosphorus in silicate melts. Submitted to: Am. Min.

Northcliffe, L. C. and Schilling, R. F. (1970) Range and stopping-power tables for heavy ions. Nuclear Data Tables A7, 233-463.

Papanastassiou, D. A. and Wasserburg, G. J. (1978) Strontium isotopic anomalies in the Allende meteorite. Geophys. Res. Lett. 5, 595-598.

Paul, A. and Douglas, R. W. (1965) Cerous-ceric equilibrium in binary alkali borate and alkali silicate glasses. Phys. Chem. Glasses 6, 212-215.

Pellas, P. and Storzer, D. (1975) Uranium and plutonium in chondritic phosphates. Meteoritics 10, 471-473.

Pellas, P. and Storzer, D. (1980) ^{244}Pu fission track thermometry and its application to stony meteorites. Submitted to: Trans. Royal Soc.

Pepin, R. O. and Phinney, D. (1979) Components of Xe in the solar system. Submitted to: Geochim. Cosmochim. Acta.

Podosek, F. A. (1970a) Dating of meteorites by the high-temperature release of iodine correlated ^{129}Xe. Geochim. Cosmochim. Acta 34, 341-365.

Podosek, F. A. (1970b) The abundance of ^{244}Pu in the early solar system. Earth Planet. Sci. Lett. 8, 183-187.

Podosek, F. A. (1972) Gas retention chronology of Petersburg and other meteorites. Geochim. Cosmochim. Acta 36, 755-772.

Podosek, F. A. and Lewis, R. S. (1972) ^{129}I and ^{244}Pu abundances in white inclusions of the Allende meteorite. Earth Planet. Sci. Lett. 15, 101-109.

Portnov, A. M., Dubinchuk, V. T. and Stolyarova, T. I. (1970) A natural rare-earth oxy-apatite. Doklady Akademii Nauk SSSR 192, 114-116.

Prinz, M., Keil, K., Hlava, P. F., Berkley, J. L., Gomes, C. B. and Curvello, W. S. (1977) Studies of Brazilian meteorites III. Origin and history of the Angra dos Reis achondrite. Earth Planet. Sci. Lett. 35, 317-330.

Reed, S. J. B. and Long, J. V. P. (1963) Electron-probe measurements near phase boundaries. In X-Ray Optics and X-Ray Microanalysis (eds. H. H. Pattee, V. E. Cosslett and A. Engstrom), 317-327. Academic, New York.

Reid, M. J., Gancarz, A. J. and Albee, A. L. (1973) Constrained least-squares analysis of petrologic problems with an application to lunar sample 12040. Earth Planet. Sci. Lett. 17, 433-445.

Reynolds, J. H. (1960) Determination of the age of the elements. Phys. Rev. Lett. 4, 8-10.

Ringwood, A. E. (1978) Safe Disposal of High Level Nuclear Reactor Wastes: A New Strategy. Australian National University Press, Canberra.

Rowe, M. W. and Kuroda, P. K. (1965) Fissiogenic xenon from the Pasamonte meteorite. J. Geophys. Res. 70, 709-714.

Ryerson, F. J. and Hess, P. C. (1978) Implications of liquid-liquid distribution coefficients to mineral-liquid partitioning. Geochim. Cosmochim. Acta 42, 921-932.

Sato, M. (1970) An electrochemical method of oxygen fugacity control of furnace atmosphere for mineral synthesis. Am. Min. 55, 1424-1431.

Schnetzler, C. C. and Philpotts, J. A. (1968) Genesis of the calcium-rich achondrites in light of rare-earth and barium concentrations. Ch 19 In Meteorite Research (ed. Millman), 206-216. Springer-Verlag, New York.

Schnetzler, C. C. and Philpotts, J. A. (1970) Partition coefficients of rare-earth elements between igneous matrix material and rock-forming mineral phenocrysts-II. Geochim. Cosmochim. Acta 34, 331-340.

Schramm, D. M. and Wasserburg, G. J. (1970) Nucleochronologies and the mean age of the elements. Ap. J. 162, 57-69.

Schreiber, H. D. (1977) Redox states of Ti, Zr, Hf, Cr, and Eu in basaltic magmas: An experimental study. Proc. 8th Lunar Sci. Conf., Geochim. Cosmochim. Acta Suppl. 8, 2, 1785-1807.

Schreiber, H. D., Thanyasiri, T, Lach, J. J. and Legere, R. A. (1978) Redox equilibria of Ti, Cr, and Eu in silicate melts: Reduction potentials and mutual interactions. Submitted to: Phys. Chem. Glasses.

Seeger, P. A. and Schramm, D. N. (1970) R-process production ratios of chronologic importance. Ap. J. 160, L157-L160.

Seitz, M. G. (1973) Uranium and thorium diffusion in diopside and fluorapatite. Carnegie Inst. Wash., Year. 72, 586-588.

Seitz, M. G. (1974) Promotion of kinetic disequilibrium of trace thorium. Carnegie Inst. Wash., Year. 73, 551-553.

Seitz, M. G., Burnett, D. S. and Bell, P. M. (1974) U, Th, Pu fractionation in geologic systems: Early Pu/U abundance in meteorites. Carnegie Inst. Wash., Year. 73, 451-454.

Shannon, R. D. (1976) Revised effective ionic radii and systematic studies of interatomic distances in halides and chalcogenides. Acta Cryst. A32, 751-767.

Shirck, J. (1974) Fission tracks in a white inclusion of the Allende chondrite-Evidence for ^{244}Pu. Earth Planet. Sci. Lett. 23, 308-312.

Stapanian, M. I., Burnett, D. S., Eggers, R. and Namboodiri, N. (1978) Solar system actinide abundances: III. Th/U fractionation in carbonaceous chondrites (Abstract). In Lunar Plan. Sci. IX, 2, 1095-1097. Lunar Plan. Sci. Inst., Houston.

Tatsumoto, M., Knight, R. J. and Allegre, C. J. (1973) Time differences in the formation of meteorites as determined from the ratio of lead-207 and lead-206. Science 180, 1279-1283.

Tatsumoto, M. (1978) Isotopic composition of lead in oceanic basalt and its implication to mantle evolution. Earth Planet. Sci. Lett. 38, 63-87.

Toksoz, M. N. and Johnston, D. H. (1977) The evolution of the moon and the terrestrial planets. In The Soviet-American Conference on Cosmochemistry of the Moon and Planets (eds. J. Pomeroy and N. Hubbard), 295-328. NASA, Washington D.C.

Unruh, D. M., Hutchison, R. and Tatsumoto, M. (1979) U-Th-Pb systematics and uranium isotopic composition of chondrites. In Lunar Plan. Sci. X, 3, 1256-1258. Lunar Plan. Sci. Inst., Houston.

Walker, D., Powell, M. A., Lofgren, G. E. and Hays, J. F. (1978) Dynamic crystallization of a eucrite basalt. Proc. 9th Lunar Plan. Sci. Conf., Geochim. Cosmochim. Acta Suppl. 10, 1, 1369-1391.

Wasserburg, G. J., Huneke, J. C. and Burnett, D. S. (1969a) Correlation between fission tracks and fission type xenon in meteoritic whitlockite. J. Geophys. Res. 74, 4221-4232.

Wasserburg, G. J., Schramm, D. N. and Huneke, J. C. (1969b) Nuclear chronologies for the galaxy. Ap. J. 157, L91-L96.

Wasserburg, G. J., Tera, F., Papanastassiou, D. A. and Huneke, J. C. (1977) Isotopic and chemical investigations on Angra dos Reis. Earth Planet. Sci. Lett. 35, 294-316.

Watson, E. B. (1976) Two-liquid partition coefficients: Experimental data and geochemical implications. Contrib. Min. Pet. 56, 119-134.

Wetherill, G. W. (1975) Radiometric chronology of the early solar system. Ann. Rev. Nuc. Sci. 25, 283-328.

Williams, R. J. and Mullins, O. (1976) A system using solid ceramic oxygen electrolyte cells to measure oxygen fugacities in gas-mixing systems. NASA Technical Memorandum, JSC-09909, NASA TMX-58167.

Wittry, D. B. (1959) Metallurgical applications of electron microprobe microanalysis. In Advances in X-Ray Analysis, 3 (ed. W. M. Mueller), 197-212. Plenum, New York.

Woolum, D. S., Bies-Horn, L., Burnett, D. S. and August, L. S. (1979) Bismuth and ^{208}Pb microdistributions in enstatite chondrites. Geochim. Cosmochim. Acta 43, 1819-1828.

Young, E. J. and Munson, E. L. (1966) Fluor-chlor-oxy-apatite and sphene from Crystal Lode pegmatite near Eagle, Colorado. Am. Min. 51, 1476-1493.

Young, E. J., Myers, A. T., Munson, E. L. and Conklin, N. M. (1969) Mineralogy and geochemistry of fluorapatite from Cerro de Mercado, Durango, Mexico. USGS Prof. Paper 650-D, D84-D93.

APPENDIX I

Preparation of Starting Materials

The following brief description concerns the starting material preparations of Seitz et al. (1974). The additional ones prepared in this study are augmented by a detailed 'recipe'.

The original preparations of Seitz et al. combined equal weights of a natural diopside ($CaMgSi_2O_6$-Di, Twin Lakes, Ca. and a ^{239}Pu spiked feldspar glass. The unspiked feldspar glass was synthesized by I. Kushiro to have equimolar amounts of albite ($NaAlSi_3O_8$-Ab) and anorthite ($CaAl_2Si_2O_8$-An). This mixture of approximately Di_2AbAn was fused for one hour at 1260°C. This yielded the 'haplobasaltic' base composition (located in the pseudo-ternary Di:Ab:An, Figure 1) to which the phosphate components were subsequently added.

Addition of 25 weight percent $Ca_3(PO_4)_2$ to the 'haplobasalt' was intended to result in the whitlockite as liquidus phase starting material (#10); however, this is the case only at 1 bar, at 20 kilobars clinopyroxene also appears on or very near the liquidus (Figure 10). Similarly, the 25 weight percent natural fluorapatite (Cerro de Mercado, Durango, Mexico; ideally $Ca_5(PO_4)_3F$, Young et al., 1969) starting material (#11) has apatite on the liquidus at 1 bar and also clinopyroxene at 20 kilobars. The 15 weight percent $Ca_3(PO_4)_2$ starting material (#12) has clinopyroxene on the liquidus only at 20 kilobars; at 1 bar, whitlockite is the sole liquidus phase.

These compositions were fused in Pt crucibles for one-half hour at 1260°C. The low fusion temperature (liquidus was later determined to be near 1330 °C) and short times did not completely homogenize these

preparations and a few relict diopside (and fluorapatite) crystals were subsequently observed. Care was taken during the actual synthesis runs to melt and homogenize the individual charges although slight run-to-run compositional differences are probable.

Other than these three original starting materials, all preparations followed the procedures given below, using only oxides and carbonate reagents. (Excepting compositions 14 and 15 which used the ^{239}Pu spiked feldspar glass).

Oxide Preparation [Compositions 14, 15, 20, 23, 23', 30, 31, 32, 40]

SiO_2	Silicic Acid ($H_2SiO_3 \cdot nH_2O$) Reagent Dehydrate slowly on Bunsen burner; Follow with 1 hour at 1500°C.	Bluish cristobalite (SiO_2) formed with a volume reduction; quartz treated in the same manner expands on heating, possibly rupturing Pt crucible.
MgO	MgO dried 1½ hour at 1400°C.	
Al_2O_3	$Al_2O_3 \cdot 3H_2O$ Dehydrate slowly on Bunsen burner to red heat; follow with 1 hour at 1400°C.	Slow heating required to prevent explosive evolution of H_2O. Reagent hydrate has lower alkali content than commercial Al_2O_3.
CaO	$CaCO_3$ dried 5 hours at 380°C; decarbonation in later step.	Simpler to use and store than CaO.
$Ca_3(PO_4)_2$	Reagent $Ca_3(PO_4)_2$ dried 16 hours at 340°C.	Reagent may be mixture of Ca phosphates, contains 7 weight % H_2O.

Na_2O	Na_2CO_3 dried 45 hours at 120°C. Decarbonation in later step.	Simpler to use and store than Na_2O.

All materials must be ground in a ball mill and redried at 120°C (24 hours). Intermediate composition Di_2An ($2\text{-}CaMgSi_2O_6 + CaAl_2Si_2O_8$) is prepared by sintering and decarbonating the appropriate weight proportions of the above, dried, materials at 960°C (24 hours) in a loosely-covered Pt crucible. Intermediate composition $Na_2Si_2O_5$ is prepared by sintering and decarbonating the appropriate weight proportions of the above, dried, materials at 750°C (96 hours) in a loosely-covered Pt crucible.

The intermediate compositions are mixed with the oxides and $Ca_3(PO_4)_2$ and fused at 1440°C (2 hours) in Pt capsules formed from Pt tubing which has been annealed (1000+°C, 1+ hour) and cleaned (1 hour in boiling 6M HCl) prior to welding, filling, and sealing. Sealed Pt tubes minimize Na and P loss in the initial fusion.

The resultant glass is crushed and loaded into a fresh Pt capsule or crucible for addition of the radioisotope spikes. The present spikes are in chloride solutions which are added directly to the glass and brought to dryness at temperatures less than 60°C to prevent spattering followed by 24 hours at 120°C. In order to remove the Cl that remains after drying, the glass + spike must be fused open to air at temperatures just above the liquidus (1330°C in this study) to minimize Na and P loss while volatilizing the Cl.

Future spikes will be nitrate solutions which will either decompose, after drying, at 500°C or persist as does the Cl; however, the presence of a little additional N in the system is unimportant, so all fusions may be done in sealed capsules.

APPENDIX II

Figure 21

T-P-fO_2 Curves for Solid Buffers

The equations given below and plotted on Figure 21 are taken from either Huebner (1971) or Myers and Gunter (1979) and are labelled H or MG respectively. Temperatures are given in degrees Kelvin and pressures in bars. Errors in the calculated fO_2 values are on the order of 0.2 log units. The difference in fO_2 units between bars and atmospheres is negligible (0.006 log units).

1-H) Iron-Wustite: $\log fO_2 = 6.57-(27215/T)+0.055(P-1)/T$

1-MG) Iron-Wustite: $\log fO_2 = 7.184-(28040/T)$

2-H) Graphite : $\log fO_2 = -0.044-(20586/T+\log P_{total}-0.028(P-1)/T$

3-MG) Co-CoO : $\log fO_2 = 7.936-(25070/T)$

4-H) Ni-NiO : $\log fO_2 = 9.36-(24930/T)+0.046(P-1)/T$

4-MG) Ni-NiO : $\log fO_2 = 9.346-(24920/T)$

5-H) Fe_2O_3-Fe_3O_4 : $\log fO_2 = 13.996-(24634/T)+0.019(P-1)/T$

6) Air : $\log fO_2 = -0.68$

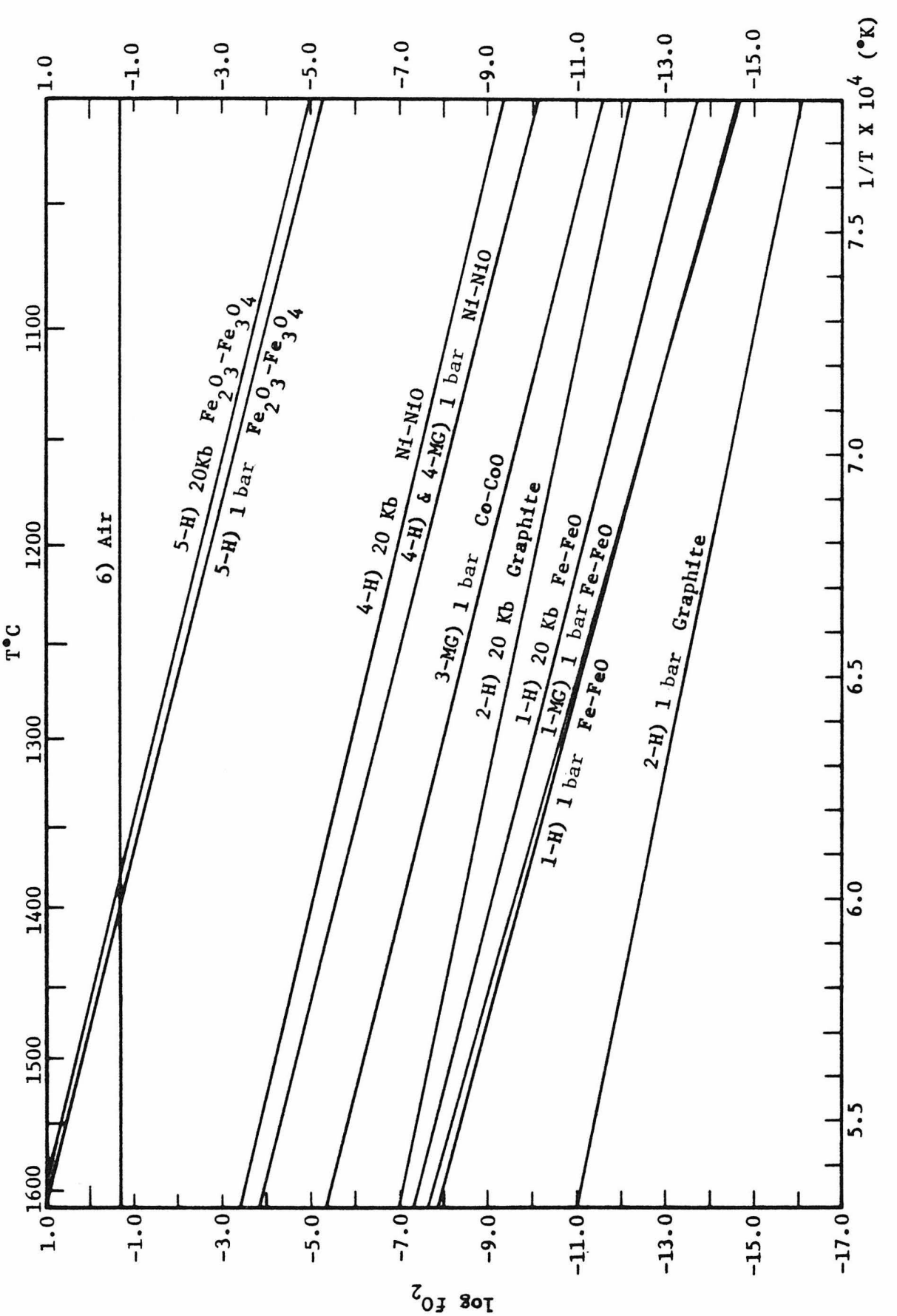
log fO_2
T°C
1/T X 10^4 (°K)
6) Air
5-H) 20Kb Fe_2O_3-Fe_3O_4
5-H) 1 bar Fe_2O_3-Fe_3O_4
4-H) 20 Kb Ni-NiO
4-H) & 4-MG) 1 bar Ni-NiO
3-MG) 1 bar Co-CoO
2-H) 20 Kb Graphite
1-H) 20 Kb Fe-FeO
1-MG) 1 bar Fe-FeO
1-H) 1 bar Fe-FeO
2-H) 1 bar Graphite

APPENDIX III

Microprobe Analyses of Quench Glasses; Reproducibility and Homogeneity

In order to assess the homogeneity of the starting materials and the quenched coexisting glasses from the experimental synthesis runs, a check on the reproducibility (precision) of Caltech's automated electron microprobe x-ray analyzer (PDP-8L on line to a MAC-5 SA3 microprobe) was performed at three different time scales (Tables III-1, 2, and 3). The work of Champion et al. (1974) defined the expected limits to microprobe precision. These authors showed that, over a period of one year, the precision on microprobe standards (assumed to be perfectly homogeneous) was 1½% (1½ times the counting statistics for the standard Caltech microprobe analysis conditions) for elements with abundances of one or more weight percent, calculated as the oxide. For less abundant elements the precision approaches three times the counting statistics (see footnote to Table III-1 for the equation used in determining the counting statistics errors).

In the following tables (as well as all data given in the text, tables, and figures) the analyses and their standard deviations (defined in the Table III-1 footnotes) are based on atomic proportions. This convention was applied for three reasons: 1) partition coefficients, for minor elements should be based on relative numbers of atoms (mole fractions) in the compared phases, not on relative weights because these are sensitive to the mean atomic weights of the phases in question; 2) formula proportions for the crystalline phases and formulation of hypothetical species in the melts can be taken directly from atomic

proportions; and 3) the standard deviations of analyses acquired on different days are reduced because varying weight percent totals, due to slight differences in day-to-day microprobe standardization, are normalized out. Normalization is reasonable because the synthetic systems are of known elemental compositions so no elements actually present will be missed in the analyses, although checks were made several times by adding Mn, Ti, K, S, Ba, Zr, and Cr to the standard element list of Na, Mg, Al, Si, Ca, Fe, P, F, Cl, and Ni, Co, U or Y, Ce, La, Nd. Additionally, a now routine part of the Caltech microprobe program consists of an across-the-board adjustment to a set of microprobe standard values to produce weight percent totals nearer to 100 percent without affecting the relative atomic proportions.

The simplest possible comparison (Table III-1) is between two consecutive analyses on a single spot without moving the position or refocussing (a significant source of error). The relatively large beam diameters used (30 microns on glass; 20 microns on crystals) minimize volatization of Na, P, F, and Cl. The small number of analyses (2) requires the multiplication of the observed standard deviations by 1.837, the critical t-value (Joiner, 1969), in order to approximate the standard deviation that would be obtained from a large sampling. The adjusted standard deviations (Table III-1), in percent, are generally lower than the errors given by counting statistics. If the standard deviations were based on the weight proportions of the elements, then they would be a few tenths of one percent larger than those standard deviations based on atomic proportions (see weight percent total standard deviations, absolute and uncorrected for small sample size, to estimate this effect).

TABLE III-1

Two Consecutive Analyses on a Single Spot,

(not refocussed between analyses)

20-30 micron spot; 0.05 microamp beam current on brass

Atomic Proportions

	Glass, 11-328Fe, 2 Nov. 1977			Clinopyroxene, 20-288, 13 Feb. 1978		
		% sd*	% cts		% sd	% cts
Na	9.320	0.2	1.1	1.888	0.2	1.7
Mg	5.024	0.0	1.0	19.783	0.0	0.8
Al	11.146	0.7	1.0	7.138	2.9	1.0
Si	35.398	0.4	0.7	47.691	0.3	0.5
Ca	18.291	0.7	0.4	23.193	0.3	0.2
Fe	18.086	0.5	1.0	0.017	BDL	BDL
P	2.630	0.8	1.5	0.265	2.6	3.8
F	1.755	14.0	15.9	BDL		
Cl	0.170	5.3	6.4	BDL		
Ce	0.048	16.2	42.2	BDL		
La	0.040	23.0	41.6	BDL		
Y	BDL†			BDL		
Nd	BDL			BDL		
Wt.% Total	100.186 ± 0.150			99.919 ± 0.053		

*% standard deviations from the spread in analyses using % sd = $100\sqrt{\frac{1}{n-1}\left[\Sigma x^2 - \frac{(\Sigma x)^2}{n}\right]}$; and in this table % sd has been multiplied by the 'critical t-value' = 1.837, (Joiner, 1969) to compensate for the small sample size.

% counting statistics from the microprobe using % cts = $\frac{100\sqrt{cts_{peak} + cts_{bkgd}}}{cts_{peak} - cts_{bkgd}}$ (all counts for equal times)

†Below Detection Limit: % cts on % sd $\geq$100%

Table III-2 is a typical comparison between the microprobe counting statistics with the standard deviations obtained during a single seven hour microprobe run. The precision is independent of standardization errors (which are present when analyses from different days are compared), but includes the errors due to refocussing, relocating the same analysis point (on zoned crystals), and any instrumental drift. The observed standard deviations have been multiplied by 1.321 to compensate for the small sample size as discussed for Table III-1. The agreement between the two error estimates is generally good.

Overall, long term precision is given in Table III-3. These data can be compared directly to the limits set by Champion et al. (1974), except for the difference between the atomic proportions used here and the weight proportions used by Champion et al. The standard deviations are not multiplied by the critical t-value (1.034) in this table. The elements with percent sd or percent cts over 100 percent have been retained, instead of being labelled BDL (except for Al which is truly BDL), to show the agreement between the two error estimates at the limits of detection; and because the errors, when taken as the error of the mean, suggest the presence of these elements although the actual abundances are questionable. The agreement is good not only between the error estimates, but the microprobe analyses also agree, within errors, with the analysis by wet chemistry (for the most part) tabulated by Young et al. (1969).

The conclusion drawn from Tables III-1, 2, and 3 is that the precision limits set by Champion et al. (1974) are met by the microprobe analyses obtained in this study. This conclusion permits discussion of the starting material analyses (Table III-4) in terms of homogeneity of

TABLE III-2

Averages of Three Analyses From Nearly the Same Spot

Taken Over a Seven Hour Period

20-30 micron spot; 0.05 microamp beam current on brass

Phase:	Whitlockite (20-266)			Clinopyroxene (20-266)		
	Atomic Proportions					
		% sd*	% cts		% sd	% cts
Na	1.295	4.5	6.4	1.968	0.1	1.6
Mg	4.750	0.3	1.0	20.337	1.6	0.8
Al	0.078	32.1	50.5	7.436	0.8	0.9
Si	0.396	4.6	2.6	46.383	0.8	0.5
Ca	54.928	0.3	0.2	23.599	0.2	0.2
Fe	BDL			BDL		
P	38.475	0.0	0.6	0.241	9.2	4.1
F	BDL			BDL		
Cl	0.010	22.9	62.8	BDL		
Ce	BDL			BDL		
Y	BDL			BDL		
La	BDL			BDL		
Nd	BDL			BDL		
Wt.% Total	101.529 ± 0.269			100.252 ± 0.238		

*See footnotes on Table III-1; critical t-value = 1.321 for three analyses.

TABLE III-3

Caltech Microprobe Standard: Durango Apatite,
Average of fifteen analyses taken from ten different
microprobe runs over a period of six months

30 micron spot; 0.05 microamp beam current on brass

	Atomic Proportions			
		% sd	% cts	Major Constituents, Wet Chemistry (Young et al., 1969)
Na	0.403	19.8	17.2	0.47
Mg	0.024	107.6	108.8	- Considered to be contaminant*
Al	BDL			- Considered to be contaminant
Si	0.264	7.1	5.1	0.36
Ca	62.834	0.7	0.4	61.40
Fe	0.033	77.9	67.1	- Considered to be contaminant
Ni	0.004	162.0	168.9	- Trace
P	36.394	1.2	0.6	36.63
F	12.429	10.0	4.0	11.85
Cl	0.719	4.4	1.7	0.74
U	0.016	94.2	128.6	- 0.001 Isotope dilution
Co	0.031	119.0	85.5	- Not analyzed

Wt.% Total 98.004 ± 1.568

*Notes are as given in Young et al. (1969)

these materials as well as the homogeneity of the synthesis charges which have been treated to superliquidus temperatures prior to the linear cooling and concommittant crystal growth.

It is known from optical examination of the initial starting materials acquired from M. G. Seitz (compositions 10, 11, and 12) that relict crystals of apatite and diopside persisted after the initial (incomplete) fusion of these materials. Other starting materials spiked with U and Th acquired at this time were rejected; new compositions were relatively easy to prepare. The 10, 11, and 12 materials (all Pu spiked) were retained, but not remelted, because of the hazards involved with manipulation of Pu^{239} spiked materials as well as excessive (compared to the initial 100-200 mg quantities acquired) losses in remelting and crushing.

These initially inhomogeneous materials permit the examination of the homogenization effect of the superliquidus treatment given to a typical, random, 10 mg sampling quenched from the superliquidus temperature (prior to any cooling and crystal growth). The analyses of single quench runs of compositions 10 and 12 given in Table III-4 do not indicate homogeneity within the limits (standard deviations from one and one-half to three times counting statistics) set by Champion et al. (1974); however, except for P in composition 10, the absolute inhomogeneities are only of a few percent in magnitude. Given the gross initial inhomogeneity, the superliquidus heating was reasonably effective. For the synthesis runs using these starting materials, some bulk compositional differences could result from sampling such inhomogeneous materials.

All the other starting materials were prepared from the oxides

(Appendix I) and are crystal free glasses. Quench runs from these glasses are also tabulated in Table III-4. For the most part (except Al in 40, P in 31 and 23) the standard deviations are either as expected (relative to counting statistics) or the absolute errors are only a few percent but appear high due to the very low counting statistics. Overall, the starting materials are acceptably homogeneous though not ideal. Since many of the analyses in Table III-4 are averages over several quench runs (see footnotes) it is reasonable to conclude that the 10 mg random sampling of the starting material gives a representative, reproducible, aliquot which, with the additional superliquidus treatment (given to all synthesis runs), yields an adequately homogeneous melt from which the crystals studied in this work are grown.

TABLE III-4

Analyses of Quench Runs; Starting Materials

Atomic Proportions

	10			11	12			14			
	Pu,25% $Ca_3(PO_4)_2$			Pu,25% $Ca_5(PO_4)_3F$	Pu,15% $Ca_3(PO_4)_2$				Pu,0% $Ca_3(PO_4)_2$		
		% sd	% cts	Calculated*		% sd	% cts			% sd	% cts
Na	3.891	2.2	1.2	4.150	4.357	2.2	1.1	Na	4.995	1.8	1.0
Mg	9.476	1.9	1.0	9.780	10.377	3.3	0.9	Mg	11.799	3.0	0.9
Al	12.520	2.9	0.9	11.661	13.316	3.3	0.9	Al	14.539	3.9	0.8
Si	39.078	1.7	0.6	39.266	42.804	0.5	0.5	Si	51.180	1.2	0.5
Ca	26.650	1.4	0.3	27.316	23.574	1.3	0.3	Ca	17.429	1.3	0.2
Fe	0.245	9.9	16.3		0.166	20.2	23.2	Fe	BDL		
P	8.115	5.2	1.0	7.828	5.370	1.9	0.9	Ni	BDL		
F	BDL			2.933	BDL			P	BDL		
Cl	0.008	82.5	90.1	0.170	0.012	72.1	60.3	F	BDL		
Ce	BDL				0.017	52.5	62.9	Cl	0.688**	1.2	1.6
Y	BDL				BDL			U	BDL		
La	BDL				BDL			Co	BDL		
Nd	BDL				BDL						
Wt.% Total	98.964 ± 0.747[a]				98.914 ± 1.194[b]				100.292 ± 1.062[c]		

TABLE III-4 (cont)

	15				20				40				30		
	Pu,25% $Ca_3(PO_4)_2$				UTh,25% $Ca_3(PO_4)_2$				UTh,25% $Ca_5(PO_4)_3F$				UTh,15% $Ca_3(PO_4)_2$		
		% sd	% cts			% sd	% cts			% sd	% cts			% sd	% cts
Na	3.731	2.1	1.2	Na	4.152	1.8	1.16		3.517	4.4	1.6		4.592	2.2	1.2
Mg	9.400	1.3	1.0	Mg	9.584	2.4	1.0		9.479	1.5	1.0		10.715	1.1	0.9
Al	11.678	1.4	0.9	Al	11.630	2.5	1.0		11.799	6.0	1.0		13.125	2.0	0.9
Si	39.776	0.8	0.6	Si	38.698	1.3	0.6		40.772	1.3	0.8		43.237	1.3	0.6
Ca	26.848	0.6	0.1	Ca	27.291	0.8	0.3		26.882	1.6	0.3		23.075	0.9	0.3
Fe	BDL			Fe	0.034	78.7	85.1		0.034	88.9	88.4		0.062	34.9	59.9
Ni	BDL			P	8.585	3.0	1.0		7.458	1.9	1.0		5.162	2.4	1.0
P	8.487	0.8	1.1	F	BDL				1.263	22.8	24.0		BDL		
F	BDL			Cl	0.060	26.3	18.0		BDL				0.017	26.4	59.0
Cl	BDL			Ce	BDL				BDL				BDL		
U	BDL			Y	BDL				BDL				BDL		
Co	BDL			La	BDL				BDL				BDL		
				Nd	BDL				BDL				BDL		
Wt.% Total	100.474 ± 0.306[d]				100.060 ± 1.185[e]				99.667 ± 1.412[f]				99.260 ± 0.265[g]		

TABLE III-4 (cont)

	31			32			23			23'		
	UTh, 10% $Ca_3(PO_4)_2$			UTh, 0% $Ca_3(PO_4)_2$			3.9U, 25% $Ca_3(PO_4)_2$			3.4U, 25% $Ca_3(PO_4)_2$		
		% sd	% cts		% sd	% cts		% sd	% cts		% sd	% cts
Na	4.528	1.7	1.1	4.846	2.4	1.1	3.792	2.2	1.2	3.831	0.9	1.2
Mg	10.816	2.1	1.0	12.074	1.3	0.9	8.597	1.1	0.9	7.223	0.4	1.0
Al	15.670	1.8	0.8	16.548	2.3	0.8	10.520	1.6	0.9	9.554	0.7	0.9
Si	46.277	0.7	0.6	48.521	0.9	0.5	36.743	1.3	0.5	37.765	0.4	0.5
Ca	19.725	1.3	0.4	17.890	1.8	0.4	29.551	0.7	0.4	31.455	0.2	0.4
Fe	BDL			0.053	90.3	57.6	BDL			0.085	7.1	40.1
P	2.934	6.2	1.2	BDL			Ni BDL			BDL		
F	BDL			BDL			P 9.917	4.1	0.9	9.320	0.5	0.9
Cl	0.134	17.8	10.8	0.034	55.6	33.2	F BDL			BDL		
Ce	BDL			0.018	89.3	58.3	Cl BDL			BDL		
Y	BDL			BDL			U 0.838	1.8	1.3	0.735	1.4	1.5
La	BDL			BDL			Co BDL			BDL		
Nd	BDL			BDL								
Wt.% Total	98.264 ± .878[h]			98.732 ± 1.080[i]			99.936 ± 0.814[j]			98.561 ± 0.075[k]		

TABLE III-4 (cont)

* No representative quench glass available for analyses.

** Average of four points of initial glass; subsequently the material was fused in air to remove Cl.

a) Average of five points from a single microprobe run on one 20 kilobar quench glass run: (5-1-1) 20 Kb.

b) Average of six points from two microprobe runs on one 20 kilobar quench glass run: (6-2-1) 20 Kb.

c) (8-1-3) 1 bar

d) (8-1-1) 1 bar

e) (16-4-4) 3-20 Kb, 1-1 bar

f) (8-2-1) 1 bar

g) (6-2-2) 1-20 Kb, 1-1 bar

h) (9-3-3) 1-20 Kb, 2-1 bar

i) (16-4-4) 2-20 Kb, 2-1 bar

j) (6-2-2) 1 bar

k) (3-1-1) 1 bar

APPENDIX IV

Alpha Particle and Fission Fragment Range Correction Calculations

The alpha particle relative ranges used to correct the ^{230}Th partitioning data were calculated from the theoretically derived equation given in Friedlander et al. (1964) and from linear interpolation of the experimental heavy ion range-energy data given in Northcliffe and Schilling (1970). The two methods yield very similar results.

For all elements (Z) heavier than O (Z=8) in the bulk compositions used, the equation given in Friedlander et al. (1964) is, with the small correction suggested:

$$1)\quad R_Z/R_{air} = 0.90 + 0.0275Z + 0.01(Z/z) + (0.06 - 0.0086Z)\ \log\ E/M$$

and for O:

$$2)\quad R_O/R_{air} = 1.00 + (0.06 - 0.0086Z)\ \log\ E/M$$

where Z is the atomic number of the target element, z is the atomic number of the incident particle (alpha z=2), E is the alpha energy (4.6875 MeV), and M is the incident particle mass (4).

The fission fragment relative ranges used to correct the ^{235}U and ^{239}Pu partitioning data were calculated from the empirical proportionality relationship given in Mory et al. (1970):

3) $R_Z = \text{constant} \cdot Z^{\frac{1}{2}}$

which is in agreement with the relative ranges calculated from the monoenergetic heavy ion range tables of Northcliffe and Schilling (1970). From this table, for ions of comparable mass (A) and energy (E) relative to fission fragments, a plot of R_Z as a function of A and E yields an array that can be fit by $R_Z = \text{constant} \cdot Z^n$ when n is allowed to vary from 0.4 to 0.6. The value of ½ is used for the corrections but the spread induced by using 0.4 and 0.6 is quadratically included in the partition coefficient errors.

The relative alpha and fission fragment ranges calculated from the above equations or taken from Northcliffe and Schilling (1970) are for pure elements; however a correction factor for compounds can easily be made using the relation (Friedlander et al., 1964):

4) $1/R_{\text{compound}} = \sum_i w_{z_i}/R_{z_i}$

where w_{z_i} is the weight fraction of element Z_i and R_{z_i} is the corresponding relative range calculated from Equation 3.

Because the partition coefficients, D, are ratios of track densities recorded on a track detector for a crystalline phase (compound) relative to the track densities recorded for the coexisting glass, the range correction that must be applied is, conveniently, just the ratio of R_{compound} for the crystal and glass:

5) $R_{\text{crystal}}/R_{\text{glass}} = (\sum_i w_{z_i}/R_{z_i})_{\text{glass}}/(\sum_i w_{z_i}/R_{z_i})_{\text{crystal}}$

The ratio $R_{crystal}/R_{glass}$ is then divided into D to give the range corrected partition coefficient which can subsequently be corrected for zoning.

Alpha Corrections

	20 Kilobars			1 Bar	
	R_{Wh}/R_{Gl}	R_{Di}/R_{Gl}	R_{Ap}/R_{Gl}	R_{Wh}/R_{Gl}	R_{Di}/R_{Gl}
Friedlander et al. (1964)	1.040	1.001	1.052	1.038	1.011
Northcliffe and Schilling (1970)	1.047	1.000	1.060	1.045	1.012

Fission Fragment Corrections

	20 Kilobars			1 Bar	
Mory et al. (1970)	R_{Wh}/R_{Gl}	R_{Di}/R_{Gl}	R_{Ap}/R_{Gl}	R_{Wh}/R_{Gl}	R_{Di}/R_{Gl}
$Z^{0.4}$	1.044	1.002	1.055	1.040	1.011
$Z^{0.5}$	1.051	1.000	1.064	1.049	1.014
$Z^{0.6}$	1.060	1.000	1.076	1.058	1.016

APPENDIX V

Trace and Minor Element Zoning Correction Calculations

The various types of zoning correction calculations used in this study vary in precision and complexity but are all derived assuming a Rayleigh-type fractionation (that is, a finite liquid reservoir), negligible diffusion in the solid phases, equilibrium partitioning at the crystal-liquid interface at all times, and a gradient-free liquid at all times (i.e., rapid diffusion and/or convection in the liquid). Furthermore, it is assumed that the partition coefficients are insensitive (variations are small compared to the errors) to variations in temperature (linear cooling), and bulk composition (as the crystalline phases nucleate and grow) for any particular synthesis experiment so that constant D values can be used in the calculations.

For the purpose of correcting for zoning, the definition of a trace element is an element that partitions in the Rayleigh manner with a well-defined D for all phases, whereas a minor element is defined as an element that may behave as a trace element in one (or more) phases but is stoichiometrically controlled in at least one other crystalline phase in the same run (such as Si in whitlockite relative to Si in diopside). In this minor element case, the D value for the trace element phase is a constant, but the stoichiometric phase D value appears to vary because, although the concentration of the element is fixed in the crystalline phase, the concentration of that element in the liquid continuously changes as crystallization proceeds. Of course, any given phase may have what appears to be components of both

stoichiometric and Rayleigh partitioning (Al and P in clinopyroxene) due to variations in partitioning with P, T, and composition, but the data generally appear to be dominated by one or the other. For the single phase experiments, the additional complications are not necessary. Because of their simpler functional form, trace element corrections will be presented first assuming only a single crystalline phase. Additional phases require introduction of D_{bulk} values; $D_{bulk}=\Sigma X_i D_i/X_f$ that only complicate the following derivations.

The basic Rayleigh fractionation equation as applied to geologic system is (Gast, 1968):

$$1) \quad C_{liq} = C_0(1-X)^{(D-1)}$$

where C_0 is the initial liquid concentration and C_{liq} is the concentration of a trace element in the coexisting liquid after X, fractional, amount of crystallization of a phase with a partition coefficient, $D = C_{crystal\text{-}rim}/C_{liq}$, where $C_{crystal\text{-}rim}$ is measured at the crystal-liquid interface. Let subscript i represent the various phases and let X_f be the final, fractional, amount of crystallization. The simplest zoning correction, for measured D values, D_m, which is always an overcorrection (see discussion below), is the crystal-rim/core ratio calculation. Using Equation 1) and the definition of D:

$$2) \quad C_{rim}/C_{core} = DC_0(1-X_f)^{(D-1)}/DC_0(1-X_0)^{(D-1)} = (1-X_f)^{(D-1)}; \text{ for } X_0=0.$$

The measured crystal actinide concentration is taken to represent the core so the measured $D_m = C_{core}/C_{liq}$. Approximating $D_m = D$, the rim/

core ratio is calculated from Equation (2), multiplied times D_m, and iterated through Equation (2) to constant value which yields the 'corrected' D value (D_1) at the crystal-liquid interface. Equation 2 in Section III-E follows directly from the above by substituting $X_{\frac{1}{2}}$ for X_0.

The next level of complexity assumes that the D_m value is the average of the concentration over the entire crystal, $\overline{C}_{xl}$, divided by C_{liq} since any measured value includes a finite volume of the crystal.

$$3)\ \overline{C}_{xl}=(1/X_f)\int_{X_0}^{X_f} DC_0(1-X)^{(D-1)}dX=(C_0/X_f)(1-(1-X_f)^D);\ \text{for } X_0 = 0$$

and therefore:

$$4)\ D_m=\overline{C}_{xl}/C_{liq} = (1-(1-X_f)^D)/X_f(1-X_f)^{(D-1)}$$

which is equation 14 in Albarede and Bottinga (1972). This can be re-arranged to give:

$$5)\ D = 1-(\ln(1+X_f(D_m-1))/\ln(1-X_f)).$$

However, measurements of the trace elements cannot be made all the way to the crystal-rim (X_f) because of alpha particle and fission range considerations, nor is the assumption that the center of the plane of the crystal analyzed is the core (X_0) necessarily true; furthermore, the assumption that the crystal nucleated on the liquidus ($X_0 = 0$) may not be valid. Consequently Equation (3) must be generalized by setting the limits of integration at X" (for X_f) and X' (for X_0) yielding:

$$6)\ D_m = ((1-X')^D-(1-X'')^D)/((X''-X')(1-X_f)^{(D-1)})$$

which cannot be simply rearranged in the manner that produced Equation (5). Additionally, X' cannot be measured so setting X' = 0 is necessary. Also, X" is in units of percent crystallized whereas the measurements are over a fraction of the total exposed area (actually a finite volume, because of range considerations) of the crystal. Therefore; for a cube with sides = a_f (a geometry resulting in overcorrection relative to other geometries), $X'/X_f = (a''/a_f)^3$ and the fractional area analyzed, q", = $(a''/a_f)^2$, so it follows that $X''/X_f = q''^{(3/2)}$ and thus $X'' = X_f q''^{(3/2)}$. Substituting the above into Equation 3) and integrating over q yields:

$$7)\ \overline{C}_{xl} = (1/q'')\int_0^{q''} DC_0(1-X_f q^{(3/2)})^{(D-1)}dq$$

and therefore:

$$8)\ D_m = (\int_0^{q''} D(1-X_f q^{(3/2)})^{(D-1)}dq)/q''(1-X_f)^{(D-1)}$$

When Equation (8) is rearranged and generalized in terms of D_{bulk}, the result is Equation (1) in Section III-C.

The 3 assumptions (Section III-C, p. 72) used to derive Equation (8) can be seen to, individually, lead to overcorrection. The assumption of each crystal nucleating at the liquidus and growing uniformly and continuously during the linear cooling produces the maximum amount of zoning. A crystal that nucleates below the liquidus will not have the

complete range of zoning and therefore the observed average trace element composition will be greater than (for $D<1$) assumed by Equation 8), leading to overcorrecting. This overcorrection also applies when $D>1$. The second assumption also assumes that the total zoning profile is measured, but if the section of the analyzed crystal does not pass through the initial nucleus, then the measured average composition is again too high as for the first assumption. The third assumption, as mentioned in Section III-C, can be best visualized by imagining a long thin crystal. Since the increments of the data contouring are of constant dimensions, in contrast to being proportional to the dimensions of the crystal, the increment in the long direction will not include the same proportion of the zoning as will the increment in the shorter dimension, with the result that the Area, A''^2, interior to the increment will have a higher average concentration than that portion of the crystal, also having area A''^2 but having the same shape as the crystal exterior, thus all three assumptions lead to the same result; the measured trace element composition will be higher than for the ideal case and will, when corrected for the ideal zoning, result in overcorrection.

The correction equations for the minor elements are dominated by mass balance considerations. Mass balance requires, for the case of only stoichiometric partitioning, that:

$$9) \quad C_{liq} = (C_o - X_f C_{xl})/(1-X_f).$$

When both types of partitioning occur for a minor element in a run containing two (or more) crystalline phases, the effects, on C_{liq} is

not the sum of Equation (1) and (9), but must be derived from first principles of mass balance and the definition of partition coefficients to yield the proper interaction of the two partitioning modes. For the assumed model of modal co-crystallization, the relative modal abundances are constant. Define this constant, $Y = X_{Raleigh}/X_f$ so $(1-Y) = X_{Stoich}/X_f$. Thus:

$$10)\ C_{liq}=(C_{st}(1-Y)/(1-D_RY)) + (C_0-(C_{st}(1-Y)/(1-D_RY)))(1-X_f)^{(D_RY-1)}$$

where C_{st} is the concentration of the element in the stoichiometric phase, D_R is the Rayleigh partition coefficient, and X_f is the total amount of crystallization.

If the change in C_{liq} with increasing crystallization is desired, then in using Equation (10), care must be taken to correct D_m to the true D value via Equation (10) in a manner analogous to Equation (2) in Section IIIE if area-volume relationship considerations are warranted.

APPENDIX VI

Redox Limited Partition Coefficient Calculations

The measured partition coefficients are expected and are observed to be functions of the fO_2 conditions of the synthesis experiments because Pu and U have multiple, stable, valence states (Th is always tetravalent). The validity of assigning a particular valence state of Pu or U to a measured D at known fO_2 can be addressed by estimating D_i (where i is a particular valence) based on the experimental conditions, measured D values (after all corrections), and the thermodynamic data.

For example, for element Z with multiple valences i and j ($i<j$) of concentration C_i and C_j in the melt, respectively, the oxidation-reduction (redox) equilibrium reaction can be written:

$$(1) \quad Z^{+i} + \tfrac{1}{4}(j-i)O_2 = Z^{+j} + \tfrac{1}{2}(j-i)O^{-2}$$

where all species are in the melt and the O^{-2} is a representation of the oxygen equilibria that is integral to the melt structure (see Morris and Haskin, 1974). Following Morris and Haskin, the equilibrium constant for this reaction in terms of mean ionic infinite-dilution activity coefficients (γ_j and γ_i in this Appendix) and mean solvent coefficients (Γ_j and Γ_i in this Appendix), is:

$$(2) \quad K_{eq} = \frac{(\gamma_j\Gamma_j)^{\frac{1}{2}(j+2)} C_j (O^{-2})^{\frac{1}{2}(j-i)}}{(\gamma_i\Gamma_i)^{\frac{1}{2}(i+2)} C_i fO_2^{\frac{1}{4}(j-i)}}$$

Since element Z is a trace element, the ratio of the infinite-dilution activity coefficients will be (approximately) unity:

$$(3)\quad K_{eq} = \frac{\Gamma_j^{\frac{1}{2}(j+2)} C_j (O^{-2})^{\frac{1}{2}(j-i)}}{\Gamma_i^{\frac{1}{2}(i+2)} D C_i f O_2^{\frac{1}{4}(j-i)}}$$

For any particular solvent (melt) composition, Z_i, Z_j, fO_2, temperature, and pressure, the ratio of the solvent coefficients and the O^{-2} concentration are constants. The constant k_{ij} is therefore defined as:

$$(4)\quad k_{ij}^{\frac{1}{2}(j-i)} = \Gamma_j^{\frac{1}{2}(j+2)} (O^{-2})^{\frac{1}{2}(j-i)} \; / \; \Gamma_i^{\frac{1}{2}(i+2)}$$

Equation (3) can be rewritten to yield:

$$(5)\quad K_{eq} = k_{ij}^{\frac{1}{2}(j-i)} C_j / C_i f O_2^{\frac{1}{4}(j-i)} = e^{-\Delta G_r^\circ / RT}$$

The measured D values are the sum of the D_i partition coefficients for the stable valence states of element Z weighted by the atomic proportions, X_i, of each valence state:

$$(6)\quad D = \sum^{i} X_i D_i$$

The atomic proportions, X_i, can be calculated from the C_i ratios calculated from Equation (5) if the values of k_{ij} are known.

Earlier experiments have shown that multivalent elements are greatly reduced in silicate melts relative to the ideal thermodynamics calculations (Johnston, 1965; Paul and Douglas, 1965) so k must be significantly greater than one.

Estimates of D_i, D_j, and k_{ij} cannot be made from measured D values at three (for the case of only two stable valence states) distinct values of fO_2 because of the observed (but not understood) fO_2 dependence of k_{ij} (Morris et al., 1974). The problem can be addressed by estimating k_{ij} or by setting limits on D_i or D_j (e.g., assume D_j = 0 at $fO_2 = 10^{-8.6}$) as was done by Benjamin et al. (1978). In order to estimate k_{ij}, data on the valence state ratio of a multivalent cation in a silicate melt at a known fO_2 are essential. Data for U have been obtained by spectroscopic means on several compositions and temperatures at several fO_2 values (Calas, 1979). For this specific case, Equations (1), (4), and (5) become, respectively:

$$(7)\quad U^{+4} + \tfrac{1}{2}O_2 = U^{+6} + O^{-2}$$

$$(8)\quad k_{46}^{U} = \Gamma_6^{\,4}(O^{-2}) \;/\; \Gamma_4^{\,3}$$

$$(9)\quad K_{eq} = k_{46}C_6 \;/\; C_4 fO_2^{\frac{1}{2}} = e^{-\Delta G^\circ_r/RT}$$

This development assumes that the ratio $(\gamma_6)^4/(\gamma_4)^3$ is approximately unity even though the U concentration used by Calas is of the order of a few weight percent. The Eu data of Morris and Haskin (1974) support this, at least to 0.10 weight percent. The discussion, in Section III-I, of the high U (3-4 weight percent) partitioning data obtained as part of this study infers that this activity coefficient ratio may vary (increase) by a factor of 1.5, a negligible difference compared with the probable errors associated with the further assumptions (see below) required for the general application of the Calas (1979) data to the

elements and partition coefficients presented in this work. Before utilizing the Calas data, the thermodynamic data for the elements of interest in this study are presented (Table VI-1). The ΔG° functions were calculated from the actinide oxide thermodynamic data of Ackermann and Chandrasekharaiah (1974) obtained at high temperature and 1 atmosphere pressure. Reaction iii data were taken from two other sources, Katz and Rabinowich (1951) and Garrels and Christ (1965). (All ΔG° values are in units of cal/mole actinide).

In Table VI-2, the log fO_2 values in equilibrium with equal amounts of the oxidized and reduced actinide (oxide) species, if $k=1$ (ideality), are calculated at temperatures representative of the 20 kilobar (1380°C) and 1 bar (1250°C) experiments (first pair of columns). The ratios of the oxidized to reduced actinide species for $k=1$, at the temperatures and fO_2 values of the experiments are also calculated (second and third pair of columns). As mentioned previously, the value of k is greater than one so the calculated fO_2 values are lower limits and the ratios at T and fO_2 are upper limits. Taken literally, Table VI-2 would result in the prediction that the actinides are all in their most oxidized valence states under all of the experimental conditions used in this study. However, the value of k is not one, and, from the partition coefficients measured in this study, more than one valence state of Pu and U must be involved to produce the differences that are observed at different fO_2 conditions (Section III-G).

For the following applications it is assumed that k_{ij} is approximately constant over the range of temperature, pressure, bulk composition, and all actinide valence states used in this study. Although the individual solvent coefficients, Γ_i, and the O^{-2} concentrations are

TABLE VI-1

All ΔG° values are in units of cal/mole actinide; T in degrees K

(See Table VI-4)

i)	$UO + \frac{1}{4}O_2 = UO_{1.5}$	$\Delta G^\circ = -65500 - T(-6.2)$		
ii)	$UO_{1.5} + \frac{1}{4}O_2 = UO_2$	$\Delta G^\circ = -72600 - T(-12.3)$		
iii)	$UO_2 + \frac{1}{4}O_2 = UO_3$	$\Delta G^\circ = -30800 - T(+12.2)$	K&R*	
		$\Delta G^\circ = -21000 - T(+19.3)$	G&C**	
iv)	$PuO + \frac{1}{4}O_2 = PuO_{1.5}$	$\Delta G^\circ = -66300 - T(-9.8)$		
v)	$PuO_{1.5} + \frac{1}{4}O_2 = PuO_2$	$\Delta G^\circ = -49200 - T(-10.7)$		
vi)	$Th + O_2 = ThO_2$	$\Delta G^\circ = -292600 - T(-43.7)$		

*Katz and Rabinowich (1951)

**Garrels and Christ (1965)

TABLE VI-2

Equilibrium Valence Ratios Calculated from Data in Table VI-1 for k=1

Reaction		log fO_2; ox/re = 1		ox/re; $fO_2 = 10^{-8.6}$		ox/re; fO_2 = 0.209	
		1653°K	1523°K	1653°K	1523°K	1653°K	1523°K
i)	U^{+3}/U^{+2}	-29.2	-32.1	1.40×10^{5}	7.63×10^{5}	1.33×10^{7}	7.29×10^{7}
ii)	U^{+4}/U^{+3}	-27.6	-30.9	5.63×10^{4}	3.71×10^{5}	5.38×10^{6}	3.54×10^{7}
iii)	U^{+6}/U^{+4}	-13.5 K&R*	-14.2	2.68×10^{2}	5.97×10^{2}	2.45×10^{6}	5.45×10^{6}
		-14.0 G&C**	-14.4	4.84×10^{2}	8.34×10^{2}	4.41×10^{6}	7.61×10^{6}
iv)	Pu^{+3}/Pu^{+2}	-26.5	-29.4	2.91×10^{4}	1.63×10^{5}	2.78×10^{6}	1.56×10^{7}
v)	Pu^{+4}/Pu^{+3}	-16.6	-18.9	1.02×10^{2}	$3.67c10^{2}$	9.78×10^{3}	3.51×10^{4}
vi)	Th^{+4}/Th^{o}	-29.1	-32.4	3.12×10^{20}	6.18×10^{23}	2.59×10^{28}	5.14×10^{31}

*Katz and Rabinowich (1951)

**Garrels and Christ (1965)

dependent on the experimental conditions (Morris and Haskin, 1974; Morris et al., 1974), it can be argued (from a limited data base) that the composite effect of the variations in experimental conditions results in a constant value for k_{ij}. For utilization of the Eu valence distribution data in Morris and Haskin (1974) and Morris et al. (1974), substituting the appropriate values into Equation (4) k_{23}^{Eu} can be calculated, which with the above assumption:

$$(10) \quad k_{23}^{Eu} = [\ \Gamma_3^{2.5}(O^{-2})^{\frac{1}{2}} / \Gamma_2^2\ ]^2$$

All further discussion of the validity of the foregoing assumption will be in terms of k.

The spectroscopic data of Calas (1979) have been used to calculate the value of k_{46}^{U} (Table VI-3) for reaction iii (Table VI-1). For all compositions, temperatures, and fO_2 conditions, the calculated value of k_{46}^{U} is nearly constant and is taken to be 2×10^5. This is the principal basis for the assumption of the constancy of k. The Eu data (referred to above) support the magnitude of k_{ij}. In comparing the Eu data for identical compositions but different temperatures (within 100-200°C), little change in k_{23}^{Eu} occurs (about a factor of two lower at higher temperatures), so k_{23} appears to be insensitive to variations in temperature. Under conditions similar to those used by Calas, the Eu data show relatively small differences in the value of k_{23}^{Eu} (factor of 3) between a diopside ($1.6\text{-}3.7 \times 10^4$) and a grossular ($4.5\text{-}9.0 \times 10^4$) melt, except at fO_2 = air. In air, k_{23}^{Eu} is a factor of seven greater than at lower ($<10^{-5}$) fO_2 values. This not easily understood since melt structure (i.e., O^{-2} concentration) should not strongly depend on

TABLE VI-3

Values of k calculated for the reaction

$UO_2 + \frac{1}{2}O_2 = UO_3$

Calas (1979)	T	fO_2	K_{46} K&R*	K_{46} G&C**	Reaction (kcal) $\Delta G°$,vii	$\Delta G°$,viii
Anorthite Melt:	1560°C,	air	1.2×10^5	2.9×10^5	-25.3	-24.0
	1565°C,	$10^{-5.9}$	2.0×10^5	4.8×10^5	-28.4	-24.8
	1560°C,	$10^{-8.5}$†	-	-	-29.4	-
Diopside Melt:	1400°C,	$10^{-6.3}$	1.1×10^5	2.0×10^5	-30.4	-22.9
Basaltic Melt:	1410°C,	10^{-6}	1.3×10^5	2.5×10^5	-30.8	-22.0
Grossular Melt:	1360°C,	10^{-6}	1.2×10^5	2.1×10^5	-30.9	-21.5

*Katz and Rabinowich (1951)

**Garrels and Christ (1965)

†No measurable U^{+6} at $fO_2 = 10^{-8.5}$

fO_2 for the compositions (Fe, Ti-free) considered. No suggestion of this occurs in the Calas data which may imply that the difference is due to Eu^{+2} since this ion is little different from Ca^{+2} whereas reduced U is mainly tetravalent and is not like any common ion (e.g., it may form anion complexes). The k_{ij} value for Eu in an anorthite melt ($3.2\text{-}5.8\times10^6$ reducing fO_2; 1.5×10^7 in air) is more than an order of magnitude larger than for the diopside or grossular melts. The bulk compositions used in this study (Appendix III) are basaltic so the general support for the magnitude of $k \sim10^5$ can be drawn from the Eu data.

Estimating k^U_{46} to be 2×10^5, the U^{+5} proportions given in Calas (1979) can be used to estimate the $\Delta G°$ of reactions vii and viii in Tables VI-3 and VI-4. As an example, if k^U_{46} equalled 10^4 or 10^6 then the calculated $\Delta G°$ values for reactions vii and viii (third and fourth column, Table VI-3) would be 5 kcal more positive or 3 kcal more negative, respectively. Note that $UO_{2.5}$ is unstable with respect to UO_2 and UO_3 at low temperatures.

The sum of reactions vii and viii yield a $\Delta G°$ (est.) of reaction for reaction iii; $\Delta G° = -40900 - T(+4.1)$ which is distinctly different from the K&R and G&C values although all three converge at about 1000°C.

Table VI-5 is a recalculation of the valence ratio-fO_2-T table (VI-2) using the value of 2×10^5 for k^U_{46} and using the rough thermodynamic data for the reactions involving U^{+5}. From Table VI-5 the proportions of each valence state of each actinide can be calculated and are listed in Table VI-6. Note that Th is always 100% Th^{+4}, unless, hypothetically, Th^{+3} or other reduced Th species, for which no thermodynamic data exist, is stabilized in silicate liquids. These

TABLE VI-4

Estimated ΔG° values for reactions involving $UO_{2.5}$

(See Table VI-1)

vii) $UO_2 + \frac{1}{4}O_2 = UO_{2.5}$ $\Delta G^\circ = +4400 - T(+17.5)$

viii) $UO_{2.5} + \frac{1}{4}O_2 = UO_3$ $\Delta G^\circ = -45300 - T(-13.4)$

actinide valence state proportions can be substituted directly into Equation (6) as is done in Section III-G. A factor of two variation in k_{46}^{U} will result in a five percent absolute change in the relative proportions of the actinide ions. This is only negligible for the dominant species.

The calculated values for the 1653°C conditions do not incorporate an allowance for a pressure effect on k_{ij}. Since k_{ij} is a measure of the interaction of the melt with multivalent elements, the reduction in viscosity (see Section III-F) at higher pressures may decrease k; therefore the equilibria at 1653°C may be shifted in favor of the more oxidized species.

TABLE VI-5

Equilibrium Valence Ratios Calculated from Data in Tables VI-1 and VI-4 for $k = 2 \times 10^5$

Reaction		$\log fO_2$; ox/re = 1		ox/re; $fO_2 = 10^{-8.6}$		ox/re; $fO_2 = 0.209$	
		1653°K	1523°K	1653°K	1523°K	1653°K	1523°K
i)	U^{+3}/U^{+2}	-18.6	-21.5	3.12×10^{2}	1.71×10^{3}	2.97×10^{4}	1.63×10^{5}
ii)	U^{+4}/U^{+3}	-17.0	-20.3	1.26×10^{2}	8.30×10^{2}	1.20×10^{4}	7.92×10^{4}
vii)	U^{+5}/U^{+4}	- 2.4	- 2.2	2.74×10^{-2}	2.44×10^{-2}	2.62	2.33
viii)	U^{+6}/U^{+5}	- 1.6	- 3.7	1.80×10^{-2}	5.84×10^{-2}	1.72	5.58
iii)	U^{+6}/U^{+4}	- 2.9 K&R*	- 3.5	1.34×10^{-3}	2.99×10^{-3}	1.23×10^{1}	2.73×10^{1}
		- 3.4 G&C**	- 3.8	2.42×10^{-3}	4.17×10^{-3}	2.21×10^{1}	3.81×10^{1}
		- 2.0 Est†	- 2.9	4.94×10^{-4}	1.43×10^{-3}	4.50	1.30×10^{1}
iv)	Pu^{+3}/Pu^{+2}	-15.9	-18.8	6.51×10^{1}	3.64×10^{2}	6.22×10^{3}	3.49×10^{4}
v)	Pu^{+4}/Pu^{+3}	- 6.0	- 8.3	2.28×10^{-1}	8.21×10^{-1}	2.19×10^{1}	7.85×10^{1}
vi)	Th^{+4}/Th^{o}	-18.5	-21.8	7.80×10^{9}	1.55×10^{13}	6.48×10^{17}	1.29×10^{21}

* Katz and Rabinowich (1951

** Garrels and Christ (1965)

† Estimated, see text in this Appendix.

TABLE VI-6

Valence State Distribution (in %) of the Actinide for $k = 2 \times 10^5$

$fO_2 = 10^{-8.6}$	U^{+2}	U^{+3}	U^{+4}	U^{+5}	U^{+6}	Pu^{+2}	Pu^{+3}	Pu^{+4}
T = 1653°K	0.0	0.8	96.5	2.6	0.0	1.2	80.4	18.3
T = 1523°K	0.0	0.1	97.4	2.4	0.1	0.2	54.8	45.0
$fO_2 = 0.209$								
T = 1653°K	0.0	0.0	12.3	32.2	55.5	0.0	4.4	95.6
T = 1523°K	0.0	0.0	6.1	14.3	79.6	0.0	1.3	98.7

APPENDIX VII

Instrumental technique for β-track mapping; Benjamin, T.M., Arndt, N.T. and Holloway, J.R. (1977) Carnegie Inst. Wash., Year. 76, 658-660.

fleet a negative anvil effect (Bell and Mao, *Year Book 69*, pp. 168-170).

Instrumental Techniques for β-Track Mapping

T. M. Benjamin, N. T. Arndt, and J. R. Holloway

The applicability of β-track radiography to partitioning in geological systems has been demonstrated by Mysen and Seitz (1975). The concentration of a radionuclide is determined by counting β tracks produced when a nuclear emulsion is exposed to a sample containing the radionuclide. Optical counting is subject to a number of limitations, the principal one being related to the size and shape of β tracks and the limited resolving power of the optical microscope. Subjective judgments must be made when using the optical counting technique. Another limitation is the restricted range of track densities that can be treated using optical methods (Mysen and Seitz, 1975). The optimum optical counting density is less than 5% of the total recording range of a nuclear emulsion. To obtain element partitioning data among phases with different trace element concentrations, two or more exposures of differing duration usually are required for each sample.

Instrumental β-track counting is an alternative technique that is not subject to the problems inherent in the optical technique. The electron microprobe or an analytical scanning electron microscope can be used to determine the β-track density by measuring the amount of silver produced by interaction of β particles with the nuclear emulsions.

The instrumental technique was applied in the investigation of the partitioning of nickel between olivine and komatiitic liquids (Arndt, this Report). Partition coefficients were determined by both optical and instrumental β-track counting and by conventional electron microprobe analysis. Ilford K-5 nuclear emulsions (Ilford Ltd., Ilford, Essex, England) were exposed to give β-track densities suitable for optical counting. The concentration of silver was measured with the electron microprobe under the following conditions: 15 kV accelerating potential, 50×10^{-9} A regulated beam current, 60-sec counting time, 20-μm spot size. Backgrounds were measured on unexposed areas of the emulsions. Integrated count rates of AgL_α radiation were obtained from areas of the emulsion corresponding to olivine and glass quenched from coexisting liquid. The partition coefficients were calculated as ratios of the background-corrected mean values of a minimum of five successive analyses of each phase. The precision of the measurements is comparable to that given by Mysen and Seitz (1975) for the optical technique. As seen in Fig. 103 (Arndt, this Report), the results of both optical and instrumental techniques are in agreement with the partition coefficients obtained by conventional electron microprobe analysis.

The range of silver concentrations that can be measured by instrumental techniques greatly exceeds the range of track densities that can be counted optically (Fig. 159). Multiple exposures of emulsions can thereby be avoided. Over the range of optical counting of track densities, silver concentration is proportional to exposure time, as shown by Holloway and Drake (1977) and in Fig. 159. When instrumental techniques are used to measure large partition coefficients, the resultant high silver concentrations must be corrected for saturation effects caused by overexposure.

To monitor the saturation effects, a single Ilford K-5 emulsion was exposed to a synthetic Fo_{92} standard containing 1600 ppm ^{62}Ni for periods ranging from 5 min to 24 hr. Analyses of silver contents in the exposed emulsion are plotted in Fig. 159. These data were obtained with the Geophysical Laboratory Jeol JSM-35 scanning electron microprobe equipped with a Tracor-Northern TN-1700 multichannel analyzer. The run conditions

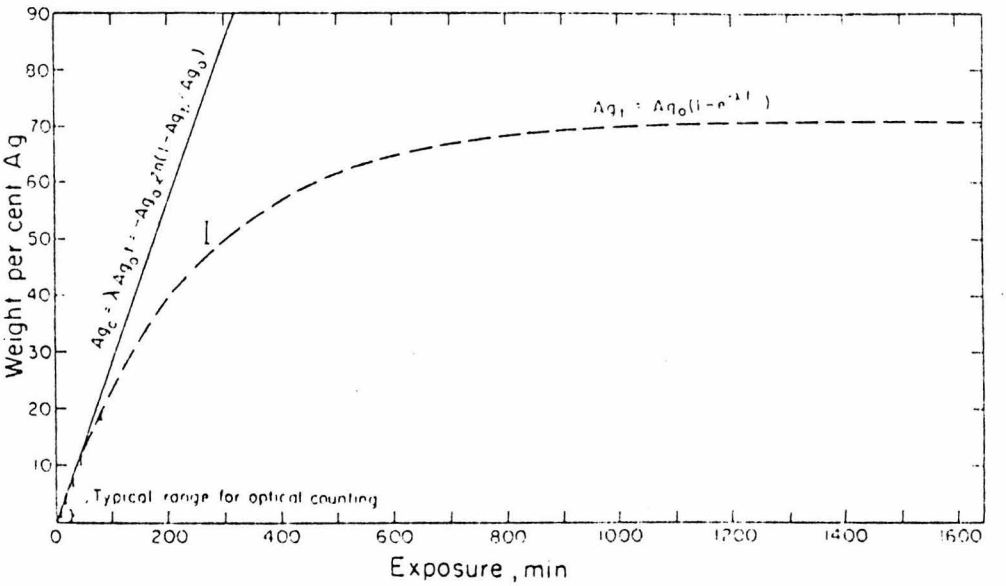

Fig. 159. Silver concentration of a single nuclear emulsion exposed from 5 to 1390 min to 1600 ppm ^{63}Ni in a synthetic olivine (Fo_{87}). Error bars are 1σ. The dashed curve is calculated from Equation 1 using values of Ag_0 = 71 wt % Ag and $\lambda = 4 \times 10^{-3}$ min^{-1}. After correction for saturation (Equation 4), all points on the dashed curve will lie on a straight line of slope λAg_0. The typical range of optical counting is shown at the lower left.

were 15 kV accelerating potential, $0.150 \pm 0.002 \times 10^{-9}$ A sample current, 50×50 μm scanned area, with 50-sec counting times integrated between 2.852 and 3.232 keV (AgL series). The background-corrected integrated counts relative to pure silver yield a count rate of 25 cps/wt % Ag. Backgrounds, measured on unexposed areas, corresponded to ~1 wt % silver.

By analogy to a similar saturation phenomenon, production of a radionuclide, a curve through the data in Fig. 159 would have the form

$$Ag_t = Ag_0(1 - e^{-\lambda t}), \qquad (1)$$

where Ag_t is the measured silver content, Ag_0 is the silver content of a saturated emulsion, λ is a constant, and t is the exposure time. The initial slope of silver production with respect to exposure time is

$$\frac{dAg_t}{dt} = \lambda Ag_0 \qquad (2)$$

from which it follows that if there were no saturation effect, the silver content at any time would plot on a straight line with a slope of λAg_0 and a silver concentration (Ag_c) related to the exposure time by the equation

$$Ag_c = \lambda Ag_0 t. \qquad (3)$$

Because saturation must eventually occur, the measured silver content (Ag_t) must be corrected from the saturation curve to the straight line described by Equation 3. Rearranging Equation 1 and substituting for t in Equation 3 results in the expression

$$Ag_c = -Ag_0 \ln (1 - Ag_t/Ag_0). \qquad (4)$$

This expression may be used to correct any measured silver value for saturation effects.

The silver-saturation value ($Ag_0 = 71.0 \pm 1.0$) is obtained by fitting the data in Fig. 159 to Equation 1. The corrected silver contents plot on the straight line of slope λAg_0 in Fig. 159, where λ =

$4.0 \pm 0.1 \times 10^{-3}$ min^{-1}. The data up to 50-min exposure time, which is ~10 times the optimum exposure time for optical counting, fall on a straight line and require little correction for saturation.

An example of the use of the instrumental technique with correction for the saturation effect is the measurement of Sm partitioning between immiscible liquids. Starting material and experimental conditions were identical with those of Watson (1976), and the partitioning of trace concentrations (25 ppm) of ^{152}Sm was determined by instrumental β-track counting. Because of the saturation effect, the measured, uncorrected partition coefficient (2.83 ± 0.24) is less than that measured by Watson (4.2 ± 0.2) with conventional electron microprobe analysis; however, the corrected value (4.38 ± 0.48) agrees within the uncertainty of the technique.

It is concluded that (1) the results obtained using instrumental β-track counting are in agreement with the results of optical β-track counting and analysis by electron microprobe; (2) the useful range of track densities that can be treated instrumentally is greater than the range of track densities that can be counted optically; (3) corrections for saturation effects can be made successfully.

Redesign of the "Shaw Apparatus" for Controlled Hydrogen Fugacity during Hydrothermal Experimentation

*J. D. Frantz, J. M. Ferry, R. K. Popp, and D. A. Hewitt**

The "Shaw apparatus" (Shaw, 1963*a*, 1967) has proved to be useful for the control of hydrogen fugacity during hydrothermal experimentation. Wones and Gilbert (1969) and Hewitt (1977*a*) used the assembly to calibrate the fayalite-magnetite-quartz oxygen buffer; Hewitt and Wones (1975) synthesized biotites of varying Fe Mg Al compositions; and Wones *et al.* (1971) determined the stability of annite. Hewitt (1977*b*) has shown, however, that the hydrogen equilibration times for the membranes are relatively slow, ranging from several days to weeks. Without special run procedures the long H_2-equilibration times can lead to erroneous results. This report presents a modification of Shaw's original apparatus that eliminates this problem with a new sample arrangement whereby equilibrium is achieved in approximately 8 hr.

In the conventional Shaw apparatus, a platinum tube filled with a solid support medium (e.g., coarse, crushed quartz) and welded closed at one end is soldered to a stainless-steel high-pressure capillary and inserted in a hydrothermal pressure vessel (Fig. 160*a*). A controlled pressure of hydrogen is imposed on the platinum tubing through the capillary, and because the platinum is permeable to hydrogen, the Pt tubing acts as a semipermeable membrane through which the partial pressure of hydrogen in the vessel is controlled. Experimental samples welded in capsules permeable to hydrogen (e.g., Pt or Ag/Pd alloys) are then placed in the pressure vessel next to the Pt membrane. The technique is used to control the fugacity of hydrogen within the experimental capsule by controlling the partial pressure of hydrogen in the pressure vessel.

A major difficulty with the method is that the hydrogen fugacity of the pressure medium in the hydrothermal vessel must reach the level imposed through the membrane before f_{H_2} in the charge reaches the desired value. The equilibration process involves the transport of a relatively large volume of hydrogen across the Pt membrane into the pressure vessel. Equilibration times can therefore be quite lengthy and are extended, as noted by Hewitt (1977*b*), by the deterioration

* Department of Geological Sciences, Virginia Polytechnic Institute and State University, Blacksburg, Virginia.

APPENDIX VIII

Laboratory studies of actinide partitioning relevant to ^{244}Pu chronometry; Benjamin, T.M., Heuser, W.R. and Burnett, D.S. (1978) Proc. 9th Lunar Planet. Sci. Conf., Geochim. Cosmochim. Suppl. 10, 1, 1393-1406. Pergamon, New York.

Proc. Lunar Planet. Sci. Conf. 9th (1978), p. 1393–1406.
Printed in the United States of America

Laboratory studies of actinide partitioning revelant to ^{244}Pu chronometry

T. BENJAMIN,*† W. R. HEUSER* and D. S. BURNETT*

*Division of Geological and Planetary Sciences
California Institute of Technology
Pasadena, California 91125

†Geophysical Laboratory
Washington, D.C. 20008

Abstract—*In situ* measurements of the crystal/liquid partitioning of Th, U and Pu among diopsidic clinopyroxene, whitlockite and liquid have been made by particle track radiography using actinide concentrations at trace levels. Measured partition coefficients (D) are corrected for actinide zoning to the crystal/liquid interface value. The D (whitlockite) satisfy criteria for equilibrium at the crystal/liquid interface, but the D(cpx) for U and Th may only be upper limits to the equilibrium values. The D(cpx) for U and Th are an order of magnitude higher for phosphate-free systems than those with 15-25% $Ca_3(PO_4)_2$; however D(cpx) values for U and Th are so low that these elements should be totally concentrated in the surface regions of any differentiating planet. At (20 Kbar, 1375°C) and (1 atm, 1270°C), the measured D(whit) are similar. The D(whit) for Th is unchanged between oxygen fugacities of 10^{-9} and air. D(whit) for U is only a factor of 1.8 lower in air than at $fO_2 = 10^{-9}$, which is surprising since U should be hexavalent in air but tetravalent at $fO_2 = 10^{-9}$. However, D(whit) for Pu is a factor of 7 lower in air, implying that trivalent Pu plays an important role in the partitioning at $fO_2 = 10^{-9}$ and, therefore, for lunar and most meteoritic conditions. Our data indicate that phosphates and, particularly, clinopyroxenes show a strong preference for trivalent over tetravalent ions, which can lead to Pu fractionation relative to U or Th. Assuming trivalent Pu, the D(cpx) values are similar to light lanthanide D values for the same ionic radius. The agreement provides some laboratory support for the proposed use of Pu/Nd for relative age measurements. Since Pu appears to be intermediate in its chemical fractionation properties between Th and Nd (at least for igneous processes) any sample with unfractionated U, Th, Nd abundances (relative to average solar system values) should be useful for Pu chronometry.

INTRODUCTION

Accurate geochronology is possible because time-dependent isotopic ratios are only slightly dependent on physical and chemical conditions. The fact that no Pu isotope except ^{244}Pu is known to be present in early solar system materials has complicated the use of its relatively rapid decay ($t_{1/2}$ = 82 m.y.) for accurate relative age determinations. Any chronological application involves ratioing a measured ^{244}Pu abundance to that of another (reference) element, X, but if any chemical fractionation has occurred between Pu and X, variations in the Pu/X ratios between two samples cannot be simply interpreted solely in terms of ^{244}Pu decay. Early measurements of ^{244}Pu in meteorites were interpreted in terms of the ratio ^{244}Pu/^{238}U, assuming that, because of the expected close chemical coherence of actinide elements, no Pu/U fractionation would occur. The well-defined Th/U

ratio of 3.8 in most meteorites and lunar rocks (Morgan and Lovering, 1968; Toksöz and Johnston, 1977) made this assumption plausible. However Podosek (1970) interpreted fission Xe data for the St. Severin chondrite as indicating that the total meteorite $^{244}Pu/^{238}U$ ratio (0.015) was less than that measured previously (0.03) in a whitlockite ($Ca_3(PO_4)_2$) separate (Wasserburg *et al.*, 1969). Crozaz (1974) found that Th was enriched relative to U in St. Severin whitlockite indicating that Pu/U fractionation was also likely. Fission track measurements on lunar minerals also suggest significant Pu/U fractionation (see e.g., Braddy *et al.*, 1975). Wasserburg *et al.* (1977) show that neither the Pu/U nor the Pu/Th ratio is constant for coexisting whitlockite and fassaitic clinopyroxene from the Angra dos Reis meteorite; however, both these workers and Lugmair and Marti (1977) found that the ratio of Pu/Nd was the same for all minerals in Angra dos Reis. Marti *et al.* (1977) found that the Pu/Nd ratio for Angra dos Reis agreed with that for an Allende coarse-grained inclusion implying that Pu and Nd were chemically very coherent and that Pu/Nd might be utilized for chronological purposes.

Since Pu no longer exists in nature and since its abundance in meteorites and lunar rocks varies because of radioactive decay as well as chemistry, laboratory studies are required for an understanding of the chemistry of Pu under meteoritic and lunar conditions. The general objectives of our laboratory studies of actinide partitioning are to define the conditions under which the actinides and light lanthanides fractionate and to then evaluate meteoritic and lunar data as to whether chronological interpretations are possible. A specific goal is to evaluate whether a constant Th/U ratio implies a constant Pu/U ratio. We believe it is possible to identify conditions and samples for which chronological information can be retrieved, although the possibility of determing applicable "chemical fractionation corrections" is still unclear. Some tentative conclusions are put forth in this paper, however, it should be recognized that the data are incomplete and many unanswered questions remain.

EXPERIMENTAL

A more thorough discussion of our experimental techniques and their reliability will be published elsewhere (Benjamin *et al.*, 1978a). Only a summary is given here.

"Whitlockite" [β-$Ca_3(PO_4)_2$ for our synthesis conditions] and diopsidic clinopyroxene were synthesized from a "haplobasaltic" composition ($2CaMgSi_2O_6 + NaAlSi_3O_8 + CaAl_2Si_2O_8$, molar) plus 25% or 15% $Ca_3(PO_4)_2$ by weight. The dried (120°C, 24 hr) starting materials were mixed and fused in a sealed Pt capsule at ~1350°C for 1–4 hr. The resultant glasses were crushed, spiked with either ~10 ppm ^{239}Pu *or* (20 ppm ^{235}U + 50 ppm ^{230}Th) and refused. The resulting glass was powdered and used as starting material for the crystal-liquid synthesis runs. For future comparison ^{151}Sm was added to the U + Th starting material. Concentrations were chosen to be at trace element levels, yet permit easy analysis by *in situ* particle track radiography techniques. Cellulose nitrate is used to detect the alpha particles from the ^{230}Th decay. The ^{239}Pu and ^{235}U are analyzed using thermal neutron induced fission tracks recorded in muscovite detectors fastened over polished sections of a synthesis run.

Crystal-liquid synthesis runs on the same starting materials have been made at 1 atm and at 20 Kbar. Liquidus temperatures will, of course, vary with pressure, but we have used different buffers to keep approximately the same oxygen fugacity at both pressures. Use of graphite crucibles in the

20 Kbar experiments sets the oxygen fugacity at $\sim 10^{-9}$ (Huebner, 1971). The same oxygen fugacity was achieved by the use of Co-CoO solid buffers for the 1 atm experiments (Robie and Waldbaum, 1968). The buffers and glass starting materials were sealed inside Pt capsules. (Inspection of the residual buffer after the experiments shows that neither Co nor CoO were depleted.) Earlier, unsealed runs of long duration (Benjamin *et al.*, 1976) acquired H_2O in uncontrolled amounts (1–10%), detectable by infrared spectrophotometry. Data from these experiments are not being considered, as they represent ill-defined conditions.

The thermal history of each run consists of heating to a super-liquidus temperature T_1 for time t_1 followed by linear cooling to a subliquidus temperature T_2 for time t_2 followed by quenching. This thermal history was chosen to produce the relatively large ($\gtrsim$50 micron) crystals required due to the finite range of the fission fragments ($\sim$10 microns) or alpha particles (15 microns) utilized for analysis. At 20 Kbar, T_1 varied between 1400 and 1450°C for t_1 = 1–16 hr.; cooling rates from 2-200°C/hr. were used; T_2 varied from 1375-1390°C with t_2 from 0–30 hr. At 1 atm, T_1 = 1285–1320°C, t_1 = 2–8 hr., cooling rates = 2–10°C/hr., T_2 = 1255–1265°C and t_2 = 1–8 hr. A complete run-by-run tabulation of the conditions will be given in a separate publication (Benjamin *et al.*, 1978a). The starting compositions with 15% $Ca_3(PO_4)_2$ have diopsidic clinopyroxene as the liquidus phase. The 25% $Ca_3(PO_4)_2$ compositions have clinopyroxene and whitlockite as co-liquidus phases at 20 Kbar and whitlockite alone at 1 atm. Small, but variable amounts ($\lesssim$2%) of apatite (Cl-rich) are observed in the 25% $Ca_3(PO_4)_2$ U + Th experiments, due to the presence of variable amounts of Cl contamination. Although somewhat unrealistic for actual rocks, we have chosen to measure clinopyroxene D values from phosphate-rich systems in order to be able to compare the clinopyroxene and whitlockite crystal-liquid partition coefficients from liquids of similar compositions.

The exposed detectors contain a track image of the distribution of radioactive material among the phases in the exposed sample. Partition coefficients (D) are calculated as the ratio of the mean track density over areas associated with mineral phases to the track density corresponding to the glass. In most cases contour maps of the crystal track density have been constructed using the actual grain dimensions and locations. From the contour maps, a more objective judgement can be made as to the interior track density of the crystal. In addition to maximizing the statistical precision for a given crystal, contouring is important because the finite range of the detected particles leads to track gradients at the crystal-melt boundries, and an objective, quantitative treatment of these gradients is necessary, particularly when the partition coefficient is small ($\lesssim$0.1). Also when D is close to 1 (0.5–1.5), there is no strong visual contrast between the crystal and glass images and an absolute system of locating the crystals is important.

Results

Table 1 shows representative electron microprobe analyses of our synthetic whitlockite and clinopyroxene. There is significant substitution of Na, Mg and Si in the whitlockite and Na and Al in the clinopyroxene.

If a run produced acceptable crystal sizes, at least two crystals (or two different regions of a single large crystal for some runs where only one large crystal was grown) were analyzed, with consistent results being obtained. The data points plotted on Fig. 1 correspond to the averages of all crystals analzyed from a given run. Table 2 gives our present best value for actinide partition coefficients (not always a simple average, as discussed below) for the different synthesis conditions investigated.

Experiments by Seitz (1973; 1974) indicate that actinide diffusion is negligible in the crystalline phases for the time scales of our experiment, but that actinide diffusion in the melt should be fast compared to crystal growth rates for cooling rates $\lesssim$600°C/hr. Consequently, actinide-zoned crystals are expected (and

Table 1. Representative electron microprobe analyses of synthetic crystals.

	(Coexisting, 20 Kbar)					
	Diopside		Whitlockite		Whitlockite (1 bar)	
	Wt.%	Cation %	Wt.%	Cation %	Wt.%	Cation %
Na_2O	1.05	1.82	0.68	1.35	0.32	0.63
MgO	15.40	20.42	3.07	4.66	3.20	4.83
Al_2O_3	6.93	7.27	0.11	0.14	BDL	—
SiO_2	52.67	46.87	0.48	0.49	0.25	0.25
CaO	24.63	23.48	49.87	54.53	50.54	54.82
FeO	BDL*	—	BDL	—	BDL	—
P_2O_5	0.16	0.12	44.87	38.78	46.01	39.43
F	BDL	—	BLD	—		
Cl	BDL	—	<0.1	—		
Total	100.90+	100.00	99.24	100.00	100.46	100.00

*BDL = Below Detection Limit (<0.03 wt.%).

+Difference between sums and totals due to <0.1 wt.% of (each) Y_2O_3, Ce_2O_3, La_2O_3, Nd_2O_3.

observed) in our experiments, but the assumption of equilibrium partitioning at the crystal-melt interface is expected to be valid for our cooling rates (2–200°C/hr). The interface (true) partition coefficient D can be obtained from an apparent partition coefficient, D_A, defined as the ratio of the average track density for the crystal to that of the glass, using Eq. 14 of Albarede and Bottinga (1972). Use of this equation requires knowledge of the fraction of the melt crystallized. This was obtained by a least squares material balance (Reid *et al.*, 1973) from microprobe analyses of the compositions of the phases crystallized, the coexisting glass and the starting materials (from super-liquidus quench runs). For runs where both whitlockite and diopside crystals were obtained, modal co-crystallization was assumed. The presence of apatite was allowed for when present.

A complication is that our interior track densities for the crystals give only an approximation to D_A (usually within 10%), even when obtained by the contouring technique described above. This is because (1) the presence of track gradients from the surrounding glass (due to the finite range of the particles) prevents us from measuring right up to the crystal/glass interface (graphical extrapolation of the interior profiles to the interface is not accurate), (2) a 3-dimensional average of the track density is required for a rigorous calculation of D_A and (3) the plane of the sample section will, in general, not pass through the center of the crystal. The errors associated with items (1)–(3) will tend to cancel, although there will probably be a net tendency to undercorrect slightly. We have adopted an error in the corrected D value equal to ½ of the zoning correction. Although arbitrary, this should be a conservative error estimate. Errors from the microprobe analyses used to make the zoning correction are unimportant. Despite the uncertainties it should be emphasized that application of the zoning correction leads to more

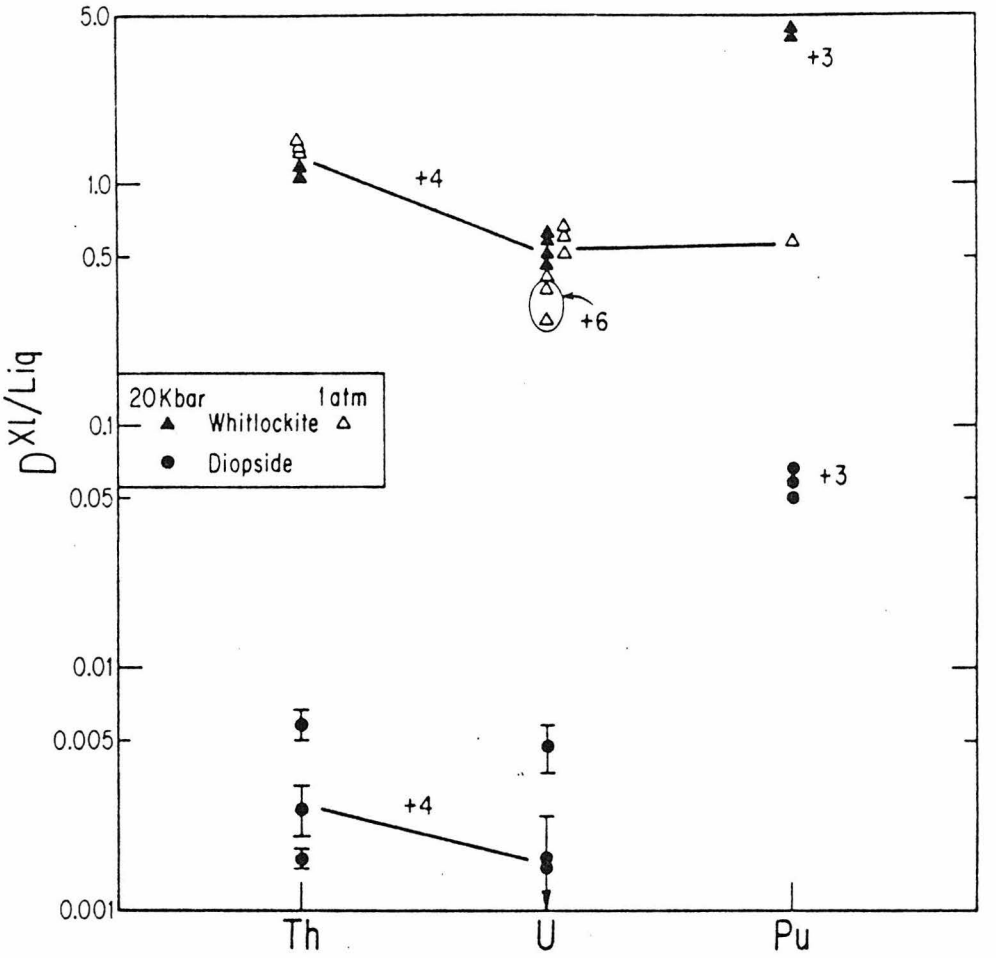

Fig. 1. Experimental actinide crystal/liquid partition coefficients, $D^{Xl/Liq}$, are plotted in order of increasing atomic number. Data points are the average of all crystals from a given synthesis run. Data for both high (200°C/hr) and low cooling rate (≤3°C/hr) experiments are plotted. Except possibly for the highest D(cpx) for U and Th, no differences can be seen. In general, the partition coefficients for whitlockite are much higher than those for diopsidic clinopyroxene. Tentative valence state assignments for the various experimental conditions (see text) are indicated. The "+3" symbols for Pu imply only that the observed D value is dominated by the presence of Pu^{+3}. The measured D values at $fO_2 = 10^{-9}$ are only lower limits to the Pu^{+3} partition coefficients. Similarly, the 1 atmosphere D_{Pu}(whit) is an upper limit for the Pu^{+4} partition coefficient. A relatively smooth "D-pattern" (solid line) for the tetravalent actinides is observed. However, for natural (low) fO_2 conditions trivalent Pu will be important for $fO_2 \leq 10^{-9}$, whereas U and Th will probably remain tetravalent.

reliable D values. In most cases the internal variation in the corrected D values is smaller than for the uncorrected values. Moreover, if D is not large (≲5) and if the amount of crystallization of the initial liquid is small, then the difference

Table 2. Actinide crystal-liquid partition coefficients (a).

	P = 20 Kbar			P = 1 atm	
	$fO_2 = 10^{-9}$ cpx/liq	$fO_2 = 10^{-9}$ cpx/liq	$fO_2 = 10^{-9}$ whit/liq	$fO_2 = 10^{-9}$ whit/liq	fO_2 = air whit/liq
(P_2O_5)	[6.9]	[0]	[10.5]	[10.5]	[10.5]
Th	≤0.0019	0.027(b)	1.26 ± .04	1.36 ± .05	1.40 ± .05
U	≤0.0018	0.017(b)	0.67 ± .07	0.50 ± .05	0.36 ± .03
Pu	0.06 ± .01	—	4.3 ± 0.3	—	0.59 ± .04

(a) Entries are corrected for actinide zoning (see text) and represent our best values for the equilibrium interface crystal-liquid partition coefficients. Small systematic corrections for the relative ranges of fission fragments in the various phases have not been applied. P_2O_5 contents (weight percent) are those of the starting materials.

(b) Preliminary values, uncorrected for zoning.

between D_A and the true partition coefficient is small. In the one atmosphere whitlockite experiments, the zoning corrections are only a few percent and a straight average of the corrected D values is tabulated in Table 2. For Th in whitlockite, for which the D values are close to 1, negligible zoning is expected, so Table 2 again just represents the average of the corrected, measured, Th-whitlockite values. Many of the 20 Kbar runs, in order to grow large crystals, have fairly large amounts of crystallization (up to 48%). In these cases, relatively large zoning corrections (up to 30%) lead to relatively large errors (Table 2). The D values differ slightly from those in Benjamin *et al.* (1978b), where the uncorrected values were given.

The existence of equilibrium at the crystal-liquid interface is still essentially an assumption. However, it is quite likely that most disequilibrium effects would not be reproducible from crystal to crystal or from run to run or upon variation in experimental conditions. Consequently we have invested considerable time in evaluating our analytical errors in order that reproducibility can by quantitatively assessed. We propose four consistency tests for equilibrium: (a) reproducibility of D values among crystals (ideally of different sizes) within a run and between runs, (b) reproducibility of minor element D values, (c) results independent of cooling rate, (d) no actinide zoning in glass. We feel that it is conceivable that the above are sufficient criteria for interface equilibration, although more work is needed to establish this conclusion. A complete comparison of our data with respect to these criteria will be given in Benjamin *et al.* (1978a). (A tabulation of our minor element partition data was included in Benjamin *et al.*, 1978b.) We only summarize the conclusions here. Overall, our whitlockite data satisfy these criteria well, although one 200°C/hr. cooling rate experiment produced high and variable Si content in the whitlockite. Another high cooling rate experiment produced relatively high P_2O_5 concentrations in clinopyroxene and also resulted in the highest clinopyroxene D(Th) and D(U) (shown in Fig. 1). The D(Th) and D(U) for clinopyroxene are very sensitive to the presence of submicroscopic

liquid inclusions; 0.2% glass in the interior of the crystals will double the measured D. Consequently, only results with cooling rates $\lesssim 5°C/hr.$ have been utilized on constructing Table 1, although for generality all runs have been plotted on Fig. 1. The D(cpx) for U and Th are quite low and difficult to measure; nevertheless there is scatter well beyond our analytical error (compare Fig. 1), and we may not be measuring equilibrium partition coefficients for U and Th in clinopyroxene (i.e., criterion (a) above is not satisfied). Consideration of possible mechanisms for disequilibrium (some types of defect substitution, rapid crystal growth, etc.) as well as possible analytical sources for the variability indicates that our results should be regarded as upper limits. Consequently, our lowest measured results are given as upper limits in Table 2 for U and Th partitioning into clinopyroxene. However, these D values are so low that for any practical application, they can be considered to be zero. The similarity of D_{Th} and D_U in Table 2 for clinopyroxene is perhaps somewhat misleading in that we have always observed $D_{Th} > D_U$. The run tabulated in Table 2 happens to have the lowest D_{Th}/D_U. In strong contrast to U and Th, the D_{Pu}(cpx) values are 30 times higher and satisfy the above equilibrium criteria. The value given in Table 2 is from our best run. Two other runs give values about 25% higher but with larger errors.

Although it is not possible to vary pressure, temperature and amount of crystallization independently, Table 1 shows that for $fO_2 = 10^{-9}$ the changes in conditions between the 1 atm and 20 Kbar experiments produced relatively small changes in D_U (whitlockite) and D_{Th} (whitlockite). The changes that are observed are small and only significant at the 1σ levels. Conceivably, pressure and temperature variations have approximately cancelled between the (1 atm, 1270°C) and (20 Kbar, 1375°C) experiments. However, it is more plausible to conclude that the D (whitlockite) are relatively insensitive to temperature and pressure over the range of our experimental conditions.

As a test of the effect of liquid composition, particularly the large P_2O_5 content in our melts, a measurement of D(cpx) for U and Th was made with a P_2O_5-free composition with all other components having the same relative concentrations as our phosphate-rich compositions. The temperature range of crystallization was 1515 to 1450°C. In this case much larger D values were obtained, $0.027 = D_{Th}$ and $0.017 = D_U$, an increase of slightly more than a factor of 10 from the phosphate-rich system. The presence of P_2O_5 must stabilize the tetravalent actinides in the liquid, presumably by some form of complexing. Clinopyroxene crystallization from a low P_2O_5 liquid is probably more realistic for comparison with actual rocks. However, despite the large change, the D values are still quite small and effectively zero for most petrological purposes.

Only the tetravalent state of Th has appreciable stability; however Pu and U compounds in the +3, +4 and +6 valence states have been characterized. Consequently, the partitioning behavior of the actinides is expected to depend on oxygen fugacity. Free energy data indicate that the pure actinide oxides would be primarily tetravalent at $fO_2 = 10^{-9}$ (Ackermann and Chandrasekharaiah, 1974), but that U should be oxidized to the +6 state in air. Thus, as expected, Table 1

shows that D_{Th}(whitlockite) is the same in air as at $fO_2 = 10^{-9}$. Somewhat surprisingly, D_U(whitlockite) is only slightly lower in air (presumably U^{+6}) than at $fO_2 = 10^{-9}$ (tetravalent U). Conceivably most of the U has remained tetravalent even in air due to stabilization of lower valence states in the melt.

The interesting result of our air runs is the D_{Pu}(whit), which is a factor of 7–8 lower than the $fO_2 = 10^{-9}$ value at 20 Kbar. (The small changes seen for D_{Th}(whit) and D_U(whit) between 1 atmosphere and 20 Kbar show that it is fair to compare the D_{Pu} values at 20 Kbar and 1 atmosphere.) We interpret this large difference as due to the changes in the Pu^{+4}/Pu^{+3} ratio such that the partitioning of Pu in whitlockite is dominated by the presence of Pu^{+3} at $fO_2 = 10^{-9}$ (and lower). Our data do not permit rigorous calculation of trivalent and tetravalent D_{Pu} or of C_4/C_3 for any phase (where C_i is the concentration of Pu^{+i}). However, in general, the large change in D_{Pu}(whit) means either (1) the trivalent Pu partition coefficient, D_3(whit), is large or (2) C_4/C_3 in the liquid is low at $fO_2 = 10^{-9}$. In either case the effect of Pu^{+3} has been to produce large differences in the partitioning of Pu relative to U or Th in our experiments at $fO_2 = 10^{-9}$ and similar large differences should be present at the lower oxygen fugacities characteristic of meteorites and lunar rocks. Quantitatively, our data do set the following limits: D_4(whit) ≤ 0.6; D_3(whit) ≥ 4; D_3 (cpx) ≥ 0.06, where D_i refers to the Pu^{+i} partition coefficient.

As an illustration of the qualitative statements made above, it is useful to consider the broad constraints which can be set by our present data. We assume that D_4(Pu,cpx) $\leq D_{Th}$(cpx) $\simeq 0.002$, since the measured clinopyroxene partition coefficients tend to decrease in going from Th to U. Minimum values of C_4/C_3 in the liquid ($fO_2 = 10^{-9}$) of around 0.02–0.05 can be set by the requirement that D_4(whit) ≥ 0. (The range depends on assumptions about the temperature dependence of the activity coefficients in the liquid). Thus our data are compatible with Pu being predominantly trivalent in the liquid at $fO_2 = 10^{-9}$. However, if D_3(whit) is very large, then C_4/C_3 can be very large also, showing that our data do not *require* that Pu be primarily trivalent in the liquid at $fO_2 = 10^{-9}$. There are only a few reported values of trace element partition coefficients in the literature greater than about 15. If we take D_3(whit) ≤ 15, then $C_4/C_3 \leq 3$ in the liquid at $fO_2 = 10^{-9}$ and D_3(cpx) ≤ 0.2. If D_3(whit) is allowed to be arbitrarily large, then there are no constraints on C_4/C_3 or D_3(cpx). However, extremely large D_3 values (300 for whitlockite, 5 for clinopyroxene) are required for the assumption of ideal solution to be valid. Measurements for other oxygen fugacities can yield tighter constraints. Similar stabilization of trivalent relative to tetravalent Ce have been reported for glasses by Johnston (1965) and by Paul and Douglas (1965).

Morris *et al.* (1974) show that oxygen equilibration between liquid and gas phases is relatively rapid. This argues against the possibility that the differences in our air and $fO_2 = 10^{-9}$ experiments reflect disequilibrium between the melt and buffer oxygen fugacities.

Tentative valence assignments have been entered on Fig. 1. The +3 symbols for Pu are to be regarded as indicating that the observed (total) D_{Pu} value is

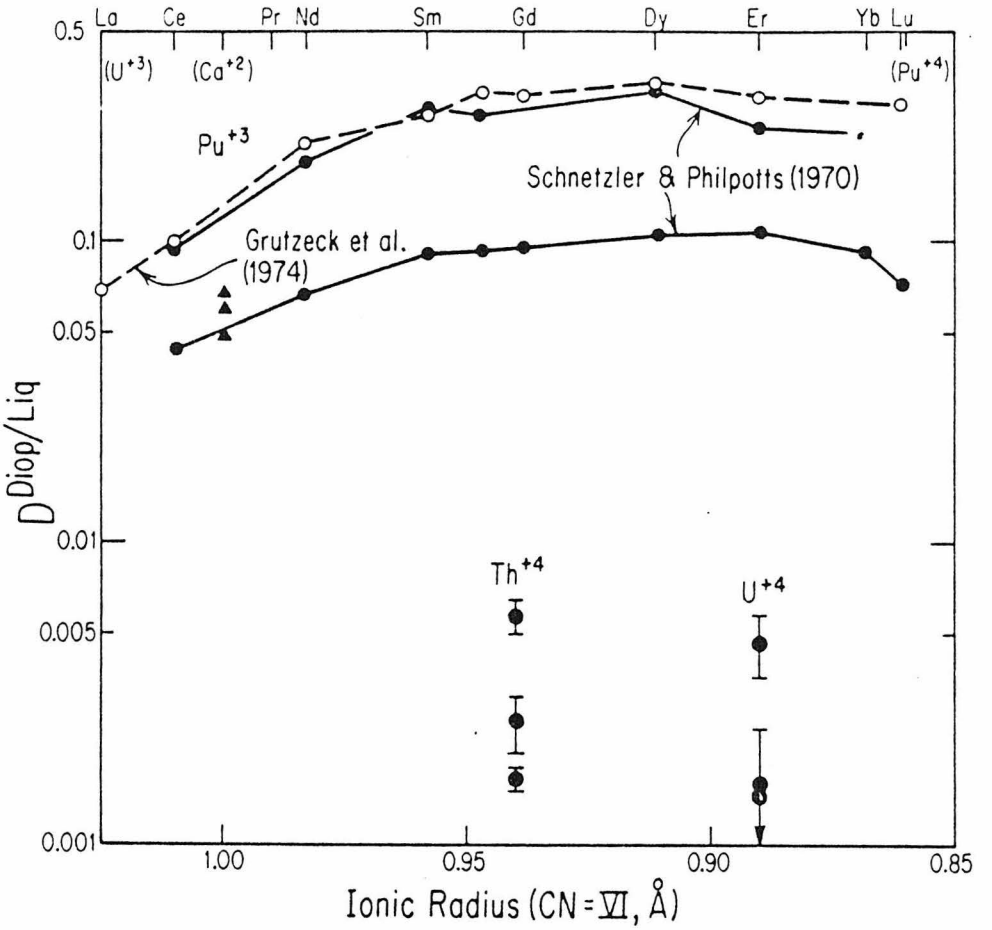

Fig. 2. The actinide (this work) and lanthanide (literature) partition coefficients for diopsidic clinopyroxene are compared as a function of ionic radius. The dashed line connects the lanthanide D values for synthetic diopsides as measured by Grutzeck *et al.* (1974). The solid lines connect two D patterns for natural diopside phenocryst-matrix samples by Schnetzler and Philpotts (1970). The ionic radii (6-fold co-ordination) are taken from Shannon, (1976). No appreciable differences would result for other choices of ionic or crystal radii, although 8-fold coordination radii would be more appropriate for the M2 site in diopside. Data points are plotted assuming trivalent Pu and tetravalent U and Th for our measurements at $fO_2 = 10^{-9}$. For reference the ionic radius locations of U^{+3}, Pu^{+4} and Ca^{+2} are indicated on the upper scale. Clinopyroxene shows a strong preference for partitioning trivalent, as opposed to tetravalent ions, presumably because of easier charge compensation. The similarity in D values between Pu^{+3} and light lanthanides gives support to the use of Pu/Nd for chronology purposes.

dominated by the presence of Pu^{+3} at $fO_2 = 10^{-9}$. We assume U and Th are tetravalent under all conditions. The much larger D_{Pu} values at $fO_2 = 10^{-9}$ for both clinopyroxene and whitlockite compared to U and Th can now be under-

stood as the effect of Pu^{+3}. Even considering 0.6 to be only an upper limit for D_4(Pu, whit) a relatively smooth "partition coefficient pattern" is suggested for the tetravalent actinides. However, it should be emphasized that the relevant pattern for either clinopyroxene or whitlockite relative to liquid in a meteorite or lunar rock (low fO_2) would have the large positive "Pu anomaly". By analogy with the large variations for Eu^{+2}/Eu^{+3} in glasses reported by Morris and Haskin (1974) the Pu^{+3}/Pu^{+4} ratio at a given fO_2 is expected to depend on melt composition. Nevertheless, since lunar and most meteoritic oxygen fugacities at similar temperatures were much lower than 10^{-9}, it appears certain that trivalent Pu is important for meteoritic/lunar conditions, as was previously proposed by Boynton (1977).

Figure 2 compares our actinide clinopyroxene partition coefficients with those of the lanthanides when plotted as a function of ionic radius. When our results for $fO_2 = 10^{-9}$ are plotted at the position of Pu^{+3} there is a reasonable correspondence with the lanthanide partition coefficient pattern, particularly with one of the two patterns obtained from natural phenocryst-matrix partition coefficients by Schnetzler and Philpotts (1970) for low-Fe, high-Ca pyroxenes. Diopsidic clinopyroxene is seen to strongly exclude tetravalent ions in favor of trivalent ions even for the same ionic radius. The data shown in Fig. 2 provide some laboratory support for the proposed chemical coherence of Pu and light lanthanides.

DISCUSSION

Our results provide a plausible mechanism to explain the observed fractionations of Pu and U, as discussed in the introduction, a mechanism analogous to the well-known Eu anomaly in lunar rocks. If a significant fraction of the Pu is trivalent, whereas U and Th remain tetravalent under meteoritic/lunar conditions, important trace element bearing phases such as clinopyroxene and phosphates are shown by our data to have a much greater tendency to accept trivalent, as opposed to tetravalent ions. This preference defines a potentially important fractionation mechanism, and may also apply to other forms of fractionation than crystal/liquid (e.g., metamorphic re-equilibration or gas-solid). The possibility of trivalent U cannot be ruled out at present for $fO_2 \leq 10^{-9}$. For samples with trivalent U, similar partitioning might be expected for Pu and U, but both Pu and U would be distinct from Th, which should be tetravalent under all conditions. Given the several documented examples of Pu/U fractionation in meteorites, significant amounts of trivalent U seem less likely.

Despite the large difference in D values between Pu and U or Th, it should be emphasized that the D(cpx) values for the actinides are all quite low. Unless source regions for igneous rocks exist with $P_2O_5 \gtrsim 0.1\%$, any reasonable degree of partial melting will almost quantitatively concentrate the actinides in the liquid phase, and no fractionation will result. In particular, unless future work (e.g., with Fe-bearing systems) produces much higher D(cpx) values for U and Th, it appears very difficult for these elements not to be quantitatively concentrated

near the surface of a differentiating planet. Consequently, our results provide an experimental basis for the commonly-made assumption that a planetary heat-flow measurement can be equated to the total U content of a planet (e.g., Keihm and Langseth, 1977, for the moon).

It is unlikely that Pu^{+3} will show a factor of 10 increase in D(cpx) as was observed for U and Th in a phosphate-free, as compared to a phosphate-rich, system. However, if a large increase should be observed, then the possibility of Pu/U and Pu/Th fractionation during partial melting will have to be reconsidered. A large increase would complicate Pu/Nd chronology. However, by analogy with our Th and U results on P_2O_5 free systems, some increase in D_{Pu} (cpx) is expected for natural clinopyroxenes, and we tentatively adopt D_{Pu} (cpx) ≈ 0.1 in the following discussion.

Although liquids produced by partial melting of more than ~5 percent would be expected to show little actinide fractionation, the residual solid will be very depleted in U and Th compared to Pu. In particular, clinopyroxene cumulates should have anomalously high Pu/U ratios. Any direct sampling of a residue from near-surface partial melting would yield very fractionated material with respect to Pu/U, but relatively unfractionated Th/U and Pu/Nd ratios. For such samples reasonably accurate relative D values are needed to calculate the fractionated ratios. A liquid produced by remelting of such residues will have relatively unfractionated abundances because the remelting tends to cancel the fractionations produced by the initial partial melting.

Many examples of igneous rocks with fractionated Th/U ratios are known (including the lunar Apollo 17 high-Ti basalts) in spite of the difficulty indicated by our laboratory measurements. This appears to be most readily accomplished by the effect of phosphates or, conceivably, by other minerals not included in our present studies. Specifically, the model proposed by Laul and Fruchter (1976) for the origin of the fractionated Th/U ratios in Apollo 17 high-Ti mare basalts by partial melting of a residual cumulate from the initial lunar differentiation, appears unlikely to us because these authors assumed $D_U(cpx) > D_{Th}(cpx)$ whereas our experiments (Fig. 1) show $D_{Th} \geq D_U$ for clinopyroxene and, for our phosphate-free composition, $D_{Th}/D_U \simeq 1.6$ for clinopyroxene.

It is worth emphasizing that partition coefficients depend on bulk composition and temperature and that we do not yet have a sufficient data base to evaluate the effects of those parameters. This makes development of quantitative models premature. Nevertheless, taking our present partition coefficients as generally applicable, the best way to fractionate Pu from U and Th in igneous processes is by late-stage near-surface fractional crystallization processes, particularly if some phosphate has crystallized. Detailed discussion of models will not be given here. But, to consider an arbitrary example, if the last 3% of a magma is lost after 30% clinopyroxene, 1% phosphate and 66% inert minerals have crystallized, the residual solid will have a Pu/U ratio higher than the initial magma by a factor of 2.6. Assuming D(Nd)/D(Pu)=2 (Fig. 2), the Pu/Nd ratio will be about 82% of that in the initial magma, and an age calculated from the ratio would be low by about 30 m.y. This error would be acceptable in some, but not all,

chronologic applications. Further, D(Nd)/D(Pu) may be much closer to unity in many systems than our assumed value of 2, and (based on ionic radii, Fig. 2) Pr or Ce may be preferrable to Nd (Boynton, 1977). Regardless of whether we adopt D(Th) ≅ D(U) for clinopyroxene, or D(Th) ≃ 1.6 D(U), as suggested by our phosphate-free measurement (Table 2), the (Th/U) ratio is increased in the residual solid by about a factor of 1.5–2. In this example a fractionated (Th/U) would be a clue as to the presence of appreciable Pu/U fractionation. Mixing of this late-stage liquid with an unfractionated rock could lead to low (Pu/U) and low (Th/U) ratios.

Our actinide partitioning results, coupled with literature D values for rare earths, indicate a simple criterion for assessing Pu fractionation. For clinopyroxene a sequence of D values is defined, $D(U) \leq D(Th) < D(Pu) \leq D(Nd)$, such that Pu is bracketed between Nd and the other actinides. The D(whit) for Gd of Green *et al.* (1971) suggest $D(Nd) \simeq D(Pu^{+3})$ for whitlockite so that this "bracketing" relationship may be valid for all important minerals. More work is clearly needed to test this hypothesis; however, if true, then any sample with solar system relative abundances (i.e., unfractionated) of U, Th and Nd can be safely assumed to have an unfractionated *whole rock* Pu abundance, relative to any of these elements. Many achondritic meteorites, including Angra dos Reis (Wasserburg *et al.*, 1977) appear to satisfy this criterion. In general, rare earth, U and Th measurements on the same specimen are needed for a good test. The bracketing criterion is, of course, plausible even without our measurements. For example, it has been used previously by Grossman and Ganapathy (1976). Our contribution has been to show that Pu is intermediate in its chemical properties compared to U, Th and Nd. The "bracketing theorem" would not be valid if this were not so.

Acknowledgments—The original techniques for the 20Kbar experiments were developed by M. Seitz. We wish to acknowledge the support of Peter Bell and the Carnegie Geophysical Laboratory in performing the 20Kbar experiments. We have benefited from critical reviews of the manuscript by W. Boynton, D. Lindstrom and J. Shirck. This work was supported by NASA Grant NSG-7202.

REFERENCES

Ackermann R. J. and Chandrasekharaiah M. S. (1974) Systematic thermodynamic properties of actinide metal-oxygen systems at high temperatures. p. 3–26. IAEA (International Atomic Energy Agency), Vienna.

Albarede F. and Bottinga Y. (1972) Kinetic disequilibrium in trace element partitioning between phenocrysts and host lava. *Geochim. Cosmochim. Acta* 36, 141–156.

Benjamin T. M., Burnett D. S. and Seitz M. G. (1976) Experimental plutonium, thorium, and uranium partition coefficients with application to meteoritic assemblages. *Carnegie Inst. Wash., Year.* 75, 684–687.

Benjamin T. M., Burnett D. S., Seitz M. G. and Heuser W. R. (1978a) Laboratory partitioning of Pu, U, and Th between whitlockite, diopsidic clinopyroxene and anhydrous melt at 20Kbar. To be submitted to *Geochim. Cosmochim. Acta.*

Benjamin T. M., Heuser R. and Burnett D. S. (1978b) Solar system actinide abundances: I. Laboratory partitioning between whitlockite, diopsidic clinopyroxene and anhydrous melt (abstract). In *Lunar and Planetary Science IX*, p. 70–72. Lunar Planetary Institute, Houston.

Boynton W. V. (1977) Fractionation of Th, U, Pu and Cm in the early history of the solar system: Implications for dating techniques (abstract). In *Lunar Science VIII*, p. 136–138. The Lunar Science Institute, Houston.

Braddy D., Hutcheon I. D. and Price P. B. (1975) Crystal chemistry of Pu and U and concordant fission track ages of lunar zircons and whitlockites. *Proc. Lunar Sci. Conf. 6th*, p. 3587–3600.

Crozaz G. (1974) U, Th, and extinct ^{244}Pu in the phosphates of the St. Severin meteorite. *Earth Planet. Sci. Lett.* **23**, 146–169.

Green D. H., Ringwood A. E., Ware N. B., Hibberson W. O., Major A. and Kiss E. (1971) Experimental petrology and petrogenesis of Apollo 12 basalts. *Proc. Lunar Sci. Conf. 2nd*, p. 601–615.

Grossman L. and Ganapathy R. (1976) Trace elements in the Allende meteorite—I. Coarse-grained, Ca-rich inclusions. *Geochim. Cosmochim. Acta* **40**, 331–344.

Grutzeck M., Kridelbaugh S. and Weill D. (1974) The distribution of Sr and REE between diopside and silicate liquid. *Geophys. Res. Lett.* **1**, 273–275.

Huebner J. S. (1971) Buffering techniques for hydrostatic systems at elevated pressures. In *Research Techniques for High Pressure and High Temperature* (G. C. Ulmer, ed.), p. 123–177. Springer Verlag, N.Y.

Johnston W. D. (1965) Oxidation-reduction equilibria in molten Na_2O-$2SiO_2$ glass. *J. Amer. Ceram. Soc.* **48**, 184–190.

Keihm S. J. and Langseth M. G. (1977) Lunar thermal regime to 300 Km. *Proc. Lunar Sci. Conf. 8th*, p. 499–514.

Laul J. C. and Fruchter J. S. (1976) Thorium and uranium variations in Apollo 17 basalts, and K-U systematics. *Proc. Lunar Sci. Conf. 7th*, p. 1545–1559.

Lugmair G. W. and Marti K. (1977) Sm-Nd-Pu timepieces in the Angra Dos Reis meteorite. *Earth Planet. Sci. Lett.* **35**, 273–284.

Marti K., Lugmair G. W. and Scheinin N. B. (1977) Sm-Nd-Pu systematics in the early solar system (abstract). In *Lunar Science VIII*, p. 619–621. The Lunar Science Institute, Houston.

Morgan J. W. and Lovering J. F. (1968) Uranium and thorium abundances in chondritic meteorites. *Talanta* **15**, 1079–1095.

Morris R. V. and Haskin L. A. (1974) EPR measurement of the effect of glass composition on the oxidation states of europium. *Geochim. Cosmochim. Acta* **38**, 1435–1445.

Morris R. V., Haskin L. A., Biggar G. M. and O'Hara M. J. (1974) Measurement of the effects of temperature and partial pressure of oxygen on the oxidation states of europium in silicate glasses. *Geochim. Cosmochim. Acta* **38**, 1447–1459.

Paul A. and Douglas R. W. (1965) Cerous-Ceric equilibrium in binary alkali borate and alkali silicate glasses. *Phys. Chem. Glasses* **6**, 212–215.

Podosek F. A. (1970) The abundance of ^{244}Pu in the early solar system. *Earth Planet. Sci. Lett.* **8**, 183–187.

Reid M. J., Gancarz A. J. and Albee A. L. (1973) Constrained least-squares analysis of petrologic problems with an application to lunar sample 12040. *Earth Planet. Sci. Lett.* **17**, 433–445.

Robie R. A. and Waldbaum D. R. (1968) Thermodynamic properties of minerals and related substances at 298.15°K (25°C) and one atmosphere (1.013 bars) and at high temperatures. *U. S. Geol. Survey Bull. 1259*. 256 pp.

Schnetzler C. C. and Philpotts J. A. (1970) Partition coefficients of rare-earth elements between igneous matrix material and rock-forming mineral phenocrysts—II. *Geochim. Cosmochim. Acta* **34**, 331–340.

Seitz M. G. (1973) Uranium and thorium diffusion in diopside and fluorapatite. *Carnegie Inst. Wash., Yearb.* **72**, 586–588.

Seitz M. G. (1974) Promotion of kinetic disequilibrium of trace thorium. *Carnegie Inst. Wash., Yearb.* **73**, 551–553.

Shannon R. D. (1976) Revised effective ionic radii and systematic studies of interatomic distances in halides and chalcogenides. *Acta Crystallogr.* **A32**, 751–767.

Tokosöz M. N. and Johnston D. H. (1977) The evolution of the moon and the terrestrial planets. In *The Soviet-American Conference on Cosmochemistry of the Moon and Planets*, p. 295–328. NASA SP-370. Washington, D. C.

Wasserburg G. J., Huneke J. C. and Burnett D. S. (1969) Correlation between fission tracks and fission type xenon in meteoritic whitlockite. *J. Geophys. Res.* **74**, 4221–4232.

Wasserburg G. J., Tera F., Papanastassiou D. A. and Huneke J. C. (1977) Isotopic and chemical investigations on Angra Dos Reis. *Earth Planet. Sci. Lett.* **35**, 294–316.

APPENDIX IX

Laboratory partitioning studies testing the validity of ^{244}Pu-rare earth chronology (Abstract); Benjamin, T.M., Jones, J.H. and Burnett, D.S. (1979) In Lunar Planet. Sci. X, 1, 98-100. Lunar Planet. Inst., Houston.

LABORATORY PARTITIONING STUDIES TESTING THE VALIDITY OF ^{244}Pu-RARE EARTH CHRONOLOGY. T.M. Benjamin, J.H. Jones and D.S. Burnett, Div. of Geol. & Planet. Sci.; Calif. Inst. of Tech.; Pasadena, Calif. 91125

It is well-established that age differences between most meteorites are, at best, barely resolvable with traditional geochronological techniques based on the decay of long-lived ($\gtrsim 10^9$ yr) nuclei. However, relative age measurements with much higher time resolution are possible utilizing measurements of the decay products of short lived ($\lesssim 10^8$ yr) nuclei (1). The nuclei ^{129}I and ^{244}Pu are potentially most useful for this purpose because the decay products (Xe isotopes) are clearly recognized in a wide variety of meteorites. Relative ages from both ^{129}I and ^{244}Pu are potentially complementary but may not be internally consistent at present (2). We are attempting to understand the chemical fractionations of Pu relative to other actinide and lanthanide elements because only ^{244}Pu was present in meteorites, and relative ages between two meteorites must be calculated by assuming that differences in the ratio of ^{244}Pu to some other nuclide, e.g. ^{238}U, reflect only the decay of ^{244}Pu and not chemical fractionation. Several studies (3,4,5) show that significant fractionations of Pu, U and Th can occur; however actinide and lanthanide data on mineral separates from the Angra dos Reis achondrite (5,6) and from an Allende coarse-grained white inclusion (7) indicated that the ratio Pu/Nd might be relatively invariant. Boynton (8) proposed that the coherence of Pu and light rare earths could be explained if Pu were trivalent under meteoritic redox conditions. The importance of trivalent Pu and similar partitioning properties of Pu and light rare earths are supported by our previous experimental studies (4). Our present studies are focussed on a direct comparison of Pu and light rare earth (specifically Sm) partitioning on the same synthetic crystal-melt systems.

A starting composition of 25% Ab-25% An-50% Di (molar), to which about 7ppm ^{239}Pu and 50ppm ^{151}Sm (^{151}Sm/Total Sm=0.97) were added, has diopsidic clinopyroxene as the liquidus phase. A second composition, made by adding 25% $Ca_3(PO_4)_2$ by weight to the above, has $Ca_3(PO_4)_2$ as the liquidus phase. Pu and Sm crystal-liquid partition coefficients (D) can be measured for the same crystal by fission track and ^{151}Sm beta radiography, respectively. Crystals were grown at 1 atmosphere and $fO_2=10^{-9}$ or air by slow cooling from initial temperatures of (1276, 1330°C) to (1210, 1250°C) for (clinopyroxene, $Ca_3(PO_4)_2$) using cooling rates of 1.5-10 deg/hr. Microprobe analyses of the synthesis products show ~10% crystallization. Pu radiography is described in (4). Beta radiography (9) was done by microprobe counting of Ag L-alpha X-rays (10) on nuclear emulsions (Ilford K5, 25 micron) exposed to polished sections of our synthesis products (15kV; 5 nAmp current; semiconductor detector). Although most background appears to arise from brehmstrahlung on the organic constituents of the emulsion, interpolated manual background corrections (20 to 50%) were made for each spectrum to allow for possible Ag brehmstrahlung contributions. A small (<5%) correction is made for ^{239}Pu alpha background. For our 30 micron spot size and counting times (50 sec), volatilization of the emulsion organic constituents is not significant ($\lesssim$1% increase in Ag counting rate). Exposure times are chosen to give Ag counting rates in a range ($\lesssim$15% Ag metal counting rates) where rates and ^{151}Sm content were shown to be proportional. Emulsion "fading" during exposure (loss of Ag) was found to be ~6%/day and thus negligible for our total exposure times ($\lesssim$6 hr). Multiple exposures for different times on the same slide are used to measure D values differing greatly from 1. We have occasionally observed "radiationless" developing (i.e. Ag formed by chemical or physical mechanisms) which only occurs over regions of the emulsion exposed to our samples. Control of the clamping pressure during exposure of the sample to emulsion appears to alleviate this effect, but it is a poten-

tially serious source of error. For this reason and also as a test of equilibrium partitioning (4), we have gone to considerable lengths to demonstrate reproducibility of our results and to estimate our statistical errors independent of the scatter in the results. Statistical errors in the Ag X-ray counting rates are not given by the number of observed counts but instead by fluctuations in the number of beta tracks in the area analyzed by the microprobe beam. Based on the measured spread in a large number (42) of analyses of an exposure of a homogeneous ^{151}Sm glass, we expect repeated analyses of a sample having a counting rate, R (expressed in % of Ag metal counting rate), with a beam spot of diameter, d (in microns), to show a standard deviation (in %) given by $2.2x10^4/(R^{\frac{1}{2}}d^2)$. To be acceptable, the scatter in the observed data must be compatible with this error estimate.

Figure 1 shows a point by point display of our D_{Sm}(cpx) data with horizontal rows of points representing independent analyses of a given grain. The data represent both different points on a grain from a single exposure and the analysis of the same point on different emulsion slides. Results for different synthesis runs are also distinguished. The expected standard deviation calculated from the above equation is shown at the top of the figure and does a reasonably good job of describing the observed scatter. Consequently our D_{Sm} (cpx) data appear quite reproducible, corresponding to a value of 0.35±.02. Correction for zoning (4) would increase this to about 0.36. Our D_{Sm}(cpx), at trace concentration levels, are slightly higher than 0.26 and 0.32 reported by Grutzeck et al. (11) for similar compositions using percent levels of Sm_2O_3. The differences are in the same sense, but smaller, than the "Henry's Law" deviations reported by Mysen (12) for Sm in orthopyroxene. However, our results are preliminary.

The Ag counting rates for $Ca_3(PO_4)_2$ crystals from 3 different synthesis runs show standard deviations ranging from 10 to 19%, consistently higher than the predicted 9%, although counting rates for co-existing glass were compatible with the expected range for only statistical errors. Also, the average values for the runs: 7.2±0.5, 9.8±1.0 and 6.2±0.5 do not agree well. Consequently, our $D_{Sm}(Ca_3(PO_4)_2)$ are not well determined at present. Nevertheless strong Sm partitioning into $Ca_3(PO_4)_2$ is indicated with a measured D ~8±2 which, when corrected for zoning (4) will reduce to about 6. This result is somewhat higher than the D_{Gd} of about 3.5 measured for a diopside-$Ca_3(PO_4)_2$ composition by Green et al. (13) using percent levels of Gd_2O_3.

In our previous study of actinide partitioning (4) we found $D_{Pu}(Ca_3(PO_4)_2)$= 3.4 for $fO_2=10^{-9}$ and $D_{Pu}(Ca_3(PO_4)_2)$=0.5 in air, reflecting the importance of trivalent Pu under more reducing conditions. The $D_{Pu}(Ca_3(PO_4)_2)$ in our recent samples have not been particularly reproducible, but show values intermediate between 0.5 and 4, suggesting that we have not been achieving redox equilibrium in our recent runs. This interpretation can be checked in future work, but there was no evidence for this effect in the original results. Consequently, $D_{Pu}(Ca_3PO_4)$=3.4 should still be a good value for reducing conditions. Although possibly also affected by redox equilibration problems, our best estimate of D_{Pu}(cpx) is 0.15 for $fO_2=10^{-9}$ and (P,T)=(1 atm, 1276°C). This is 3 times higher than the 0.05 result in (4), reflecting primarily the absence of P_2O_5 in our present pyroxene synthesis runs. A similar, but larger (x10), reduction in D(cpx) for U and Th in P_2O_5-rich melts was observed previously (4).

Table 1 summarizes our best estimates of actinide and Sm partition coefficients at $fO_2=10^{-9}$ based on the results of (4) and the present study. Possible effects of variations in (P,T) between our 1 atmosphere and 20Kbar experiments have been neglected. Using the D_{Sm}/D_{Nd} from (11) and assuming $D_{Sm}=D_{Nd}$ for $Ca_3(PO_4)_2$, we infer D_{Pu}/D_{Nd}=0.53 and 0.48 for clinopyroxene and whitlockite respectively. Although our results suggest Pr or Ce might be a better refer-

100

Pu-Rare earth partitioning

T.M. Benjamin

ence element for ^{244}Pu chronology, in practice, the differences in D values we have measured would result in relatively little fractionation for many plausible igneous fractionation processes (see (4) for some specific models). Thus our present results support the proposed use of $^{244}Pu/Nd$ for early solar system chronology. From Pu/Nd chronology it thus appears, surprisingly, that the age differences between the formation of Allende coarse-grained inclusions and the highly-evolved igneous cumulate, Angra dos Reis was less than 25 m.y., in agreement with model age differences from initial $^{87}Sr/^{86}Sr$ (3,5).

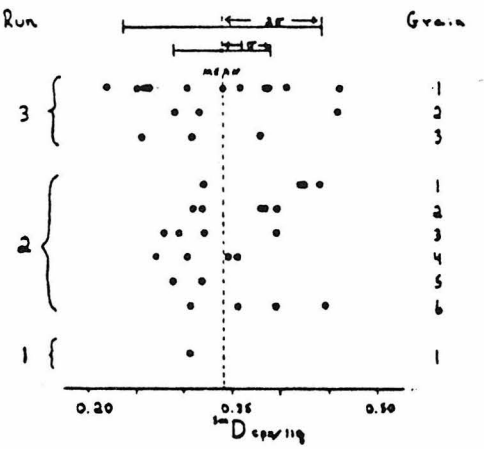

Fig. 1. Individual analyses of $D_{Sm}(cpx)$ show a spread consistent with independently calculated error estimates (σ= 0.05, see text, σ mean=0.02).

References. (1) Wetherill,G.W. (1975) Ann. Rev. Nuc. Sci. 25, 283. (2) Gray,C.M., Papanastassiou, D.A. and Wasserburg,G.J. (1973) Icarus 20, 213-239. (3) Crozaz,G. (1974) E.P.S.L. 23, 164-169. (4) Benjamin, T.M., Heuser,W.R. and Burnett,D.S. (In press, 9th L.P.S.C. Proc.); also subm. to Geochim. Cosmochim. (5) Wasserburg,G.J., Tera, F., Papanastassiou,D.A. and Huneke,J.C. (1977) E.P.S.L. 35, 294-316. (6) Lugmair, G.W. and Marti, K. (1977) E.P.S.L. 35, 273-284. (7) Marti,K. Lugmair, G.W. and Scheinin,N.G. (1977) Lunar Sci. VIII, 619-621. (8) Boynton, W.V. (1978) E.P.S.L. 40, 63-70. (9) Mysen,B.O. and Seitz,M.G. (1975) J. G.R. 80, 2627-2635. (10) Holloway, J.R. and Drake,M.J. (1977) Geochim. Cosmochim. 41, 1395-1397. (11) Grutzeck,M., Kridelbaugh,S. and Weill, D. (1974) Geophy. Res. Lett. 1, 273-275. (12) Mysen,B.O. (1978) Geochim. Cosmochim. 42, 871-886. (13) Green, D.H., Ringwood,A.E., Ware,N.G. Hibberson,W.O., Major,A. and Kiss,E. (1971) Proc. 2nd L.S.C., vol. 1, 601-615.

Table 1. Best values for actinide-Sm crystal-liquid partition coefficients

	Th	U	Pu	Sm	
D(cpx)	0.03	0.02	0.15	0.36	(25%Ab+25%An+50%Di) = H
D(cpx)	0.002	0.002	0.05	-	85%H+15%$Ca_3(PO_4)_2$
D($Ca_3(PO_4)_2$)	1.2	0.52	3.4	6	75%H+25%$Ca_3(PO_4)_2$